

DIPLOMARBEIT

Ein Multiskalenansatz zur Poisson-Nernst-Planck Gleichung

(A Multiscale Approach to the
Poisson-Nernst-Planck Equation)

Angefertigt am
Institut für Numerische Simulation

Vorgelegt der
Mathematisch-Naturwissenschaftlichen Fakultät der
Rheinischen Friedrich-Wilhelms-Universität Bonn

Juli 2010

Christian P. T. Neuen

Aus
Bonn

Illud in his obsignatum quoque rebus habere
convenit et memori mandatum mente tenere,
nil esse, in promptu quorum natura videtur,
quod genere ex uno consistat principiorum,
nec quicquam quod non permixto semine constet.
et quod cumque magis vis multas possidet in se
atque potestates, ita plurima principiorum
in sese genera ac varias docet esse figuras.

Lucretius, De rerum natura, 55 v. Chr.

Hierbei muss man auch dies als festversiegelt betrachten
Und in die Seele geprägt mit zähem Gedächtnis bewahren,
Dass kein einziges Ding, daß Wesen sich offen bekundet,
Nur aus einerlei Art der Urelemente bestehe,
Keines auch sei, das nicht stets aus gemischten Atomen sich bildet;
Ja, je mehr es in sich an Kräften und Wirkungen herbergt,
Desto größere Menge von Arten der Urelemente
Zeigt sich hierin vereint und desto verschiednere Formung.

(Übersetzung: Hermann Diels, 1924)

Contents

Einführung	1
Zusammenfassung	5
0.1 Moleküldynamik	5
0.2 Herleitung der makroskopischen Modellgleichung mittels Multiskalenansatz	5
0.3 Das Poisson-Nernst-Planck Gleichungssystem	8
0.4 Numerische Experimente	9
0.5 Schlussbemerkungen	10
1 Introduction	13
2 Molecular Dynamics	17
2.1 The Schrödinger Equation	17
2.2 Deriving Classical Molecular Dynamics	19
2.3 Classical Molecular Dynamics	20
2.4 Theory of Statistical Physics	29
3 Multiscaling: Obtaining the Macroscopic Equation	33
3.1 Ionic Migration without Multiscaling	33
3.2 Multiscale Methods – an Overview	35
3.3 The Method of Averaging and the Continuity Equation	37
3.4 Diffusion	39
3.5 The Convective Term	47
3.6 Compiling the Extended Nernst-Planck Equation	54
3.7 Additional Reactive Contributions	54
4 The Poisson-Nernst-Planck System	57
4.1 Nondimensionalization	57
4.2 A Review of System Discretizations	59
4.3 Definitions	60
4.4 Weak Formulation of the Extended Nernst-Planck Equation	61
4.5 Time Discretization and the Coupled Poisson-Nernst-Planck System	66
4.6 Convergence	68

5	Numerical Experiments	73
5.1	The Finite Element Library Deal II	73
5.2	Molecular Dynamics and Multiscaling of Ethylene Carbonate	74
5.3	Transporting Defects in a Solution	84
5.4	Ionic Migration in a Battery System	87
5.5	Multiple Species with the Incorporation of a Reaction Term	93
6	Concluding Remarks	97
6.1	Future Prospects	98
A	Homogenization	101
B	Existence and Uniqueness of a Solution to the decoupled Nernst-Planck Equation	107
	Bibliography	113

Einführung

Die Kombination von Diffusion und Konvektion durch poröse Materialien mit variierender Struktur ist ein Vorgang, der in vielen verschiedenen Bereichen der Natur- und Ingenieurwissenschaften herausragende Bedeutung besitzt.

In der Biologie und Medizin wird der Durchgang von Ionen durch Zellmembranen untersucht um Vorgänge in Organismen zu verstehen und in der Fortführung neue Medikamente zu entwickeln oder bestehende zu verbessern. In der Geologie betrachtet man Fluidbewegungen durch Gestein oder andere poröse Bodenstrukturen, Vorgänge die bei der Förderung oder Lagerung von Bodenschätzen wie Erdöl oder Erdgas wesentlichen Einfluss auf den Erfolg des Unternehmens haben. Die gleichen Modelle sind anwendbar, wenn Öl oder andere flüssige Chemikalien ungewollt austreten und im Boden versickern. Die Eingrenzung oder Vorhersage der Ausbreitung der Kontamination und der damit eventuell einhergehenden Schädigung von Trinkwasserquellen können von lebenswichtiger Bedeutung sein. In den Materialwissenschaften beobachtet man, dass sich in Abhängigkeit von Ionenauswaschungen gewisse Eigenschaften von Materialien ändern. Insbesondere ist bekannt, dass die Stabilität von Mörtel und Zement durch die Auswaschung von Calcium herabgesetzt wird. Gewisse Chemikalien, wie sie zum Beispiel in saurem Regen enthalten sind, fördern diesen Verfall. In Anbetracht der weitreichenden Verwendung dieser Materialien in der Konstruktion von Brücken, Flughäfen, Wohngebäuden und zahllosen anderen großen und kleinen Projekten auf der ganzen Welt ist das Verständnis der Ionenmigration, als Schlüssel auf dem Weg zum Schutz dieser Strukturen vor dem Verfall, von unschätzbarem Wert. Im Gebiet der Elektrotechnik hat die Erforschung von Ionenmigration eine ebenso hohe Bedeutung. Batterien und Akkumulatoren funktionieren auf Basis dieses Vorganges. Bereits jetzt sind diese aus unserer Gesellschaft nicht mehr wegzudenken, sie machen die Nutzung von Handys, Laptops und anderen mobilen Elektronischen Geräten erst möglich. Neue Verkehrskonzepte sehen für die Zukunft die Umstellung der Energiequellen des motorisierten Individualverkehrs von fossilen Brennstoffen auf elektrische Speicher vor. Bereits jetzt gibt es erste Prototypen von Batteriebetriebenen Autos. Diese unterliegen allerdings noch starken Einschränkungen in der bereitgestellten Leistung und Kapazität, so dass mit ihrer jetzigen Leistungsfähigkeit die beschriebene Umstellung nicht durchführbar ist. Die Erforschung neuer Materialien und Konstruktionen ist somit unabdingbar, um die Vision von der flächendeckenden Verwendung von Elektrogetriebenen Fahrzeugen realisieren zu können.

Es ist ganz natürlich, dass für einen Prozess mit derartig vielfältigen und bedeutenden Anwendungen mathematische Modelle entwickelt werden, und es ist die Aufgabe der Numerischen Mathematik, mit diesen Modellen Vorhersagen über das Verhalten solcher Prozesse unter

gegebenen Randbedingungen zu treffen. Zwar kann die numerische Simulation die Durchführung von Experimenten auf dem Weg zum fertigen Produkt nicht völlig ersetzen aber das Zusammenspiel von guten Modellen und leistungsfähigen mathematischen Verfahren kann allerdings als Indikator für das qualitative Verhalten eines Systems dienen, und so bei der Entscheidung einen Prototyp zu produzieren oder zu verwerfen zur Ersparnis von Zeit und Kosten führen.

Wir werden uns bei der Entwicklung und Herleitung unserer numerischen Methode auf die Ionenmigration konzentrieren und Anwendungen im Bereich der Zementartigen Materialien und vor allem der Batterien in den Fokus unserer Aufmerksamkeit rücken.

Ionenmigration wird vom gekoppelten System der Poisson-Nernst-Planck Gleichungen beschrieben, die diffusive und konvektive Beiträge zur Änderung der ionischen Konzentration beinhalten. In Abhängigkeit von der Systemkonfiguration, die simuliert werden soll, variieren die Koeffizienten dieser Gleichung in hohem Maße, ebenso wie die Randbedingungen, die an die Gleichung angelegt werden. Im Normalfall werden diese Werte durch vorherige Experimente in ähnlichen Systemen bereitgestellt, die Simulation wird dann genutzt, um Vorhersagen in Abhängigkeit von kleinen Variationen der Startbedingungen zu machen.

Wenn man nun jedoch Vorhersagen über das Verhalten eines Systems machen möchte, bevor ein entsprechender Prototyp existiert, sei dies im Bereich neuartiger Zement-Mischungen oder im Bereich der Elektrolyte oder Membranen von Batterien, so ist es aus offensichtlichen Gründen nicht möglich, die benötigten Simulationsparameter auf diesem Weg zu erhalten. Aus diesem Grund muss eine alternative Methode herangezogen werden, um die Koeffizientenfunktionen und Randbedingungen der Poisson-Nernst-Planck Gleichung bereitzustellen. Eine Möglichkeit ist, die Aufmerksamkeit auf eine kleinere, der bisherigen Beschreibung zugrunde liegende Skala zu richten, nämlich auf die Atome und Moleküle, aus denen sich das System zusammensetzt. Indem wir ihr Verhalten auf Grundlage der fundamentalen Kräfte zwischen ihnen simulieren, werden wir unabhängig von experimentellen Abschätzungen der makroskopischen Eigenschaften der Materialien und beziehen die vollständigen und grundlegenden Materialeigenschaften in unsere Berechnungen ein.

Es ist jedoch nicht praktikabel, die Simulation des vollständigen makroskopischen Systems auf molekularer Ebene zu implementieren, da es erforderlich wäre, das Verhalten von einer Anzahl von Atomen in der Größenordnung von Avogadros Konstante ($6.022 \cdot 10^{23}$) zu bestimmen. Die Vielzahl der entsprechenden Freiheitsgrade würde jegliche Speicher- und Rechenzeitkapazitäten, die man heutzutage und in absehbarer Zukunft bereitstellen könnte, überlasten.

Nichtsdestotrotz ist es möglich die Vorteile eines Ansatzes an der atomaren Struktur zu nutzen, ohne das vollständige System auf dieser Skala simulieren zu müssen. Indem man beide bereits erwähnten Skalen der Simulation in Betracht zieht und kombiniert, ist es möglich, eine Simulationsroutine zu konstruieren, die eine angemessene Komplexität aufweist, so dass die Berechnung mit angemessenem Aufwand an Ressourcen durchgeführt werden kann. Gleichzeitig können Vorhersagen auf Basis von atomarem Verhalten gemacht werden, ohne dass man gezwungen wäre, den Umweg über die experimentelle Beschaffung von Daten zu gehen. Um dies zu erreichen, werden wir einem Multiskalenansatz folgen, dessen grundlegende Rechnungen das Verhalten von Atomen und Molekülen beschreiben. Die Resultate der Simulationen

auf dieser Skala werden gemittelt, um die Koeffizienten zu bilden, die benötigt werden, um das Poisson-Nernst-Planck (PNP) Gleichungssystem zu bilden, welches dann für Vorhersagen auf der makroskopischen Skala herangezogen wird. Dabei werden für unterschiedliche Material- oder Strukturregionen auf der makroskopischen Skala entsprechend getrennte MD Simulationen und Mittelungen durchgeführt.

Von den Simulationen auf der atomaren Ebene, die typischerweise im Längenbereich von einigen Ångstrom oder Nanometern (10^{-10} bzw. 10^{-9} m) durchgeführt werden, muss das Verfahren auf Systeme bis hin zu sichtbarer Größenordnung skalieren, mit typischen Längen von Millimetern und Zentimetern (10^{-3} bzw. 10^{-2} m). Darüber hinaus werden auch Größenordnungen von Mikrometern (10^{-6} m) im Durchführbarkeitsbereich des Verfahrens liegen.

Im Zuge dieser Arbeit werden wir das von uns entwickelte Verfahren testen und seine Anwendbarkeit demonstrieren.

Bezüglich der Simulation atomarer Systeme können wir uns auf die bereits geleistete Arbeit von Jan Hamaekers und Ralf Wildenhues stützen, die die *TREMOLO* Moleküldynamik Simulationssoftware am INS der Universität Bonn implementiert haben. Im Zuge der Programmierung des numerischen Lösers für die Poisson-Nernst-Planck Gleichung wurde die deal.II-Programmbibliothek verwendet.

Wir geben hier kurz die eigenständigen Beiträge dieser Arbeit wieder:

- Erweiterung der bisherigen Einstein-Relation für den Diffusionskoeffizienten, um konvektive Korrekturen zu berücksichtigen.
- Implementierung besagter Korrektur in der *TREMOLO* Simulationssoftware.
- Implementierung einer Messroutine für das chemische Potential.
- Formulierung eines stabilen, linearen Operators für das nichtlineare, gekoppelte Poisson-Nernst-Planck-Gleichungssystem.
- Implementierung eines adaptiven Finite Element Lösers für das erweiterte, zeitabhängige, gekoppelte Poisson-Nernst-Planck-Gleichungssystem in zwei und drei Raumdimensionen.

Danksagung

An dieser Stelle möchte ich all denen danken, die diese Arbeit möglich gemacht haben. Allen voran stehen meine Eltern Doris und Klaus, die die Grundlagen gelegt haben, noch bevor ich überhaupt angefangen habe, daran zu arbeiten. Nicht nur dadurch, dass sie mir ein sorgenfreies Studium ermöglicht haben, sondern auch durch ihre Förderung und Erziehung in allen anderen Belangen. Ohne sie wäre ich heute nicht der Mensch, der ich bin. Dieser Dank erweitert sich auch auf meine Schwestern Susanne und Britta. Ich kann keine höhere Wertschätzung zum Ausdruck bringen, als zu sagen, dass sie mir Familie sind.

Von größter Bedeutung für diese Arbeit war Professor Dr. Griebel, dem ich einerseits für das grossartige und spannende Thema danke, aber auch für die Freiheit, die ich in seiner

Bearbeitung genossen habe und die Hilfestellungen, die ich erhielt, wenn ich auf Probleme stiess. Ebenso danke ich Herrn Professor Dr. Schweitzer für die Übernahme der Zweitkorrektur.

Mein Dank gilt auch allen Mitarbeitern im INS, die in allen Belangen immer ansprechbar und auch ansonsten gute Kollegen sind. Darunter ist besonders Frederik Heber hervorzuheben, dessen Zeit mir jederzeit für fruchtbare Diskussionen zur Verfügung stand. Ihm und Ralf Wildenhues danke ich auch für die aufbauenden Gespräche in den Momenten, in denen ich nur Probleme und keine Lösungen gesehen habe. Darüber hinaus danke ich ihnen, sowie Jan Hamaekers und Elena Görtz für das Korrekturlesen meiner Arbeit. Besonderer Dank geht auch an Christian Feuersänger für seine Entwicklung und Hilfestellungen zum *pgfplots*-Paket, mit dem nahezu alle Graphen in dieser Arbeit erstellt wurden.

Bedanken möchte ich mich auch bei der Studienstiftung des Deutschen Volkes, deren Förderung mich seit dem ersten Semester begleitet und mit vielen interessanten Menschen in Kontakt gebracht hat. Sie hat mein Studium über das Fachliche hinaus bereichert.

Als letztes, aber nicht am geringsten danke ich meinen Freunden, im Studium und außerhalb, in der Nähe und in der Ferne. Ohne sie würde das Leben abseits des Schreibtisches kaum halb so viel Vergnügen bereiten.

Zusammenfassung

Wir werden hier nun kurz auf Deutsch den Inhalt der auf Englisch abgefassten Arbeit zusammenfassen. Dabei skizzieren wir die Herleitungen der wichtigsten Resultate. Detaillierte Berechnungen und Erläuterungen finden sich im englischen Hauptteil ab Kapitel 2.

0.1 Moleküldynamik

Zunächst beschreiben wir den Zugang zur moleküldynamischen Simulation, indem wir auf die Annahme der Gültigkeit der Newtonschen Bewegungsgleichungen, die Integration derselben über die Zeit und die Randbedingungen der Simulationen eingehen. Dabei behandeln wir auch die Berechnung einiger Potentiale, die Ensembles, in denen die Berechnungen stattfinden und wenden uns dem Fehler zu, dem diese Berechnungen unterliegen. Der wichtigste Punkt dieses Kapitels ist aber die Einführung des Phasenraumes. Dies ist ein abstrakter, hochdimensionaler Raum, in welchem wir ein vollständiges atomares System als einzigen Punkt mit den Koordinaten aller seiner Freiheitsgrade betrachten. Die Menge der Punkte, deren Koordinaten ein gleiches Ensemble ausmachen, nennen wir die virtuelle Gesamtheit dieses Ensembles. Makroskopische physikalische Variablen entsprechen nun dem Mittelwert der korrespondierenden Messungen der Freiheitsgrade über die virtuelle Gesamtheit, dies nennen wir das Ensemblemittel. Die Moleküldynamik (MD) berechnet für ein System in einem Ensemble eine Trajektorie in der virtuellen Gesamtheit. Wir zitieren die Ergodenhypothese, die besagt, dass der zeitliche Mittelwert der Messungen entlang der berechneten Trajektorie gegen das Ensemblemittel konvergiert. Es ist diese Aussage, die es uns ermöglicht, die Moleküldynamik zur Berechnung der makroskopischen Zustandsgrößen heranzuziehen.

0.2 Herleitung der makroskopischen Modellgleichung mittels Multiskalenansatz

In diesem Kapitel führen wir die Multiskalenmethode ein, welche die Ergebnisse auf der Molekülebene auf die Makroebene überträgt. In diesem Zusammenhang leiten wir auch die makroskopische Gleichung zur Modellierung von Ionenmigration her. Daher diskutieren wir zunächst Vor- und Nachteile verschiedener Ansätze zur Behandlung von Ionenmigration ohne Multiskaleneinflüsse, wobei wir auch Modelle präsentieren, die nicht zum Poisson-Nernst-Planck Gleichungssystem führen. Ebenso analysieren wir verschieden Multiskalenzugänge auf

ihre Eignung für den Einsatz im Bereich der Ionenmigration, unter denen wir uns für die Methode der Mittelung entscheiden.

Im Zuge der Untersuchung der zeitlichen Änderung der Konzentration leiten wir die Kontinuitätsgleichung her

$$\frac{\partial c}{\partial t} = -\nabla \cdot \vec{J}, \quad (0.1)$$

und unterteilen den Partikelfluss \vec{J} in diffusive und konvektive Anteile,

$$\vec{J}(x) = \underbrace{\frac{1}{|B_r(x)|} \int_{B_r(x)} \sum_{p: x_p \in \Omega} \delta(x - x_p) (\vec{v}_p - \langle v \rangle) dx}_{\text{Diffusion}} \quad (0.2)$$

$$+ \underbrace{\frac{1}{|B_r(x)|} \int_{B_r(x)} \sum_{p: x_p \in \Omega} \delta(x - x_p) \langle v \rangle dx}_{\text{Konvektion}} \quad (0.3)$$

die wir einzeln untersuchen.

$$J_{\text{diff}} = -\frac{1}{6} \frac{l^2}{\delta t} \nabla c = -D \nabla c \quad (0.4)$$

ist der diffusive Anteil des Ionenflusses, wobei

$$D = \frac{1}{6} \frac{l^2}{\delta t}. \quad (0.5)$$

die Formel für den Diffusionskoeffizienten ist. Dieser wird aus MD Simulationen heraus traditionell mittels der mittleren quadratische Verschiebung (engl.: Mean Square Displacement) gemessen. Die Messung modifizieren wir dahingehend, dass sie konvektive Beiträge herausfiltert, und so nur tatsächlich zufällige Bewegungen misst:

$$\langle L^2(t) \rangle = \frac{1}{n} \sum_{i=0}^n (r_i(t) - \langle r(t) \rangle)^2 \quad (0.6)$$

Unter Verwendung dieser Größe ergibt sich für den Diffusionskoeffizienten somit

$$\frac{1}{6} \left\langle \frac{\partial \langle L^2(t) \rangle}{\partial t} \right\rangle = \frac{1}{6T} \int_0^T \frac{\partial \langle L^2(t) \rangle}{\partial t} dt \quad (0.7)$$

$$= \frac{1}{6T} \langle L^2(T) \rangle. \quad (0.8)$$

Umstellungen der Formel führen auf eine analytisch äquivalente, auf Grund der unterschiedlichen Berechnung numerisch aber unterschiedliche Methode zur Berechnung des Diffusi-

onskoeffizienten, nämlich die der Geschwindigkeits-Autokorrelation (engl.: Velocity Auto Correlation). Auch für diese führen wir unsere Korrektur durch und erhalten:

$$D = \frac{1}{3} \lim_{t \rightarrow \infty} \int_0^t \langle v(t - \tau)v(0) \rangle - \langle v(t - \tau) \rangle \langle v(0) \rangle d\tau. \quad (0.9)$$

Wir zeigen ferner, dass die Konvergenz der Formel eng an die Erfüllung der Ergodenhypothese geknüpft ist. Nach der Behandlung der Diffusion wenden wir uns dem konvektiven Anteil des Partikelflusses zu, den wir zunächst allgemein über die Einstein-Smoluchowski Relation mit dem Diffusionskoeffizienten in Verbindung bringen. Die Ursachen der Konvektion teilen wir ein weiteres Mal auf, nämlich in die Beiträge des elektrischen Feldes und die des chemischen Potentials. Im Falle des elektrischen Feldes führen wir den gewöhnlichen physikalischen Zusammenhang zwischen elektrodynamischen Kräften mit der Einstein-Smoluchowski Gleichung zusammen und finden die nichtlineare Kopplung der verschiedenen Ionenspezies untereinander. Das elektrische Potential erfüllt

$$-\Delta\Phi = \frac{F}{\varepsilon_0\varepsilon_r} \sum_i z_i c_i(x), \quad (0.10)$$

womit sich der Flussbeitrag aus

$$\vec{J}_e = -D \frac{z \cdot e}{k_B T} \nabla\Phi \cdot c \quad (0.11)$$

errechnet. Für die Herleitung des Beitrages des chemischen Potentials μ zur Ionenmigration betrachten wir die Minimierung der freien Helmholtzenergie, um

$$\vec{J}_{chem} = -\nabla\mu \cdot \frac{D}{k_B T} c \quad (0.12)$$

zu erhalten. Die Messung dieser Größe aus klassischen Merkmalen thermodynamischer Systeme ist nicht möglich, so dass wir die folgende Integrationsformel über mehrere Partikelkonzentrationen (und damit auch mehrere MD Simulationen) nutzen:

$$\frac{\mu}{k_B T} = \ln(n_0 \Lambda^3) + \left(\frac{pV}{Nk_B T} - 1 \right) + \int_{n_0}^n \left(\frac{pV}{Nk_B T} - 1 \right) \frac{dn'}{n'}, \quad (0.13)$$

Die genannten Beiträge zum Partikelfluss fassen wir zusammen, um die erweiterte Nernst-

Planck Gleichung zu erhalten:

$$\frac{\partial c}{\partial t} = -\nabla \cdot \vec{J} \quad (0.14)$$

$$= -\nabla \cdot (\vec{J}_{diff} + \vec{J}_e + \vec{J}_{chem}) \quad (0.15)$$

$$= -\nabla \cdot \left(-D\nabla c - D \frac{ze}{k_B T} \nabla \Phi c - \nabla \mu \frac{D}{k_B T} c \right) \quad (0.16)$$

$$= \nabla \cdot \left(D \left(\nabla c + \frac{z \cdot e \nabla \Phi + \nabla \mu}{k_B T} c \right) \right). \quad (0.17)$$

Unter bestimmten Voraussetzungen kann dieser Gleichung noch ein Reaktionsterm hinzugefügt werden, so dass wir in der Gesamtheit folgendes gekoppeltes Gleichungssystem zur Ionenmigration erhalten:

$$\begin{aligned} \frac{\partial c_i}{\partial t} &= \nabla \cdot \left[D_i \left(\nabla c_i + \frac{z_i \cdot e \nabla \Phi + \nabla \mu_i}{k_B T} c_i \right) \right] + K_i(x) c_i(x) \\ -\Delta \Phi &= \sum_i q_i c_i(x). \end{aligned} \quad (0.18)$$

0.3 Das Poisson-Nernst-Planck Gleichungssystem

Wir leiten nun über in die Behandlung des makroskopischen **Poisson-Nernst-Planck** (PNP) Gleichungssystems. Zunächst führen wir eine Skalenanalyse und Entdimensionalisierung der PNP durch. Dabei stellen wir fest, dass in physikalischen Rechnungen die Kopplungskonstante zwischen den verschiedenen ionischen Spezies eine Größe von $O(10^{16})$ in Abhängigkeit von der Gebietsgröße erreichen kann. Des Weiteren etablieren wir eine Abschätzung für die Zeitschrittweite des Systems in Abhängigkeit von der Gebietsgröße. Bevor wir zu unserer eigenen Diskretisierung übergehen, skizzieren wir einige andere Ansätze, das PNP System zu diskretisieren. Unser eigener Ansatz macht sich die Methode der Finiten Elemente zunutze und mit dieser etablieren wir die schwache, voll implizite Formulierung der entkoppelten PNP, ohne zunächst auf die Zeitdiskretisierung einzugehen. Diese Vorarbeit genügt aber für eine Diskussion der mathematischen Umsetzung physikalisch sinnvoller Randbedingungen. Dabei wird die Einbettung in eine equilibrierte Umgebung durch Dirichlet Randbedingungen beschrieben, während die Kontrolle von Flüssen über den Rand des Gebietes mittels Robin- bzw. von-Neumann Randbedingungen erfolgt. Nach der Etablierung der Randbedingungen wenden wir uns der Implementierung der Zeitabhängigkeit zu. Es hat sich herausgestellt, dass die Verwendung der implizienten Formulierung in der Konzentration mit explizitem elektrischem Potential zwar zu kleinen, schnell lösbaren Systemen einerseits, aber auch zur Einführung einer instabilen Kopplung führt. Eine semi-explizite Behandlung des nicht-linearen Konvektionsterm, wobei das elektrische Feld implizit und die Konzentration explizit behandelt wird, führt zu

einem stabilen Zeitprogressionsoperator der folgenden Gestalt:

$$\begin{pmatrix} I - \nabla D_1 \nabla & 0 & \dots & -\frac{z_1 F}{RT} [Du_1^n \Delta + D(\nabla u_1^n) \nabla] \\ \vdots & \ddots & & \vdots \\ 0 & \dots & I - \nabla D_k \nabla & -\frac{z_k F}{RT} [Du_k^n \Delta + D(\nabla u_k^n) \nabla] \\ z_1 Id & \dots & z_k Id & \frac{\varepsilon_0 \varepsilon_r}{F} \Delta \end{pmatrix} \cdot \begin{pmatrix} u_1^{n+1} \\ \vdots \\ u_k^{n+1} \\ \Phi^{n+1} \end{pmatrix} = \begin{pmatrix} u_1^n + g_1 \\ \vdots \\ u_k^n + g_k \\ 0 \end{pmatrix}, \quad (0.19)$$

welcher allerdings soeben eingeführte schwache Formulierung und Randbedingungen vermissen lässt. Mit den Abkürzungen

$$\mathcal{J}(u, v) = \int_{\Omega} uv \, dx, \quad (0.20)$$

$$\mathcal{D}_i(u, v) = \int_{\Omega} D_i \nabla u \nabla v \, dx, \quad (0.21)$$

$$\mathcal{B}_i(\phi, v) = \int_{\Omega} \frac{z_i F}{RT} [D_i u^n \Delta \phi + D_i (\nabla u^n) \nabla \phi] v \, dx, \quad (0.22)$$

$$\mathcal{P}(\phi, \psi) = \int_{\Omega} \frac{\varepsilon_0 \varepsilon_r}{F} \nabla \phi \nabla \psi \, dx, \quad (0.23)$$

$$\mathcal{F}_i(v) = \int_{\Omega} u_i^n v \, dx, \quad (0.24)$$

$$\mathcal{G}_i(v) = \int_{\partial \Omega} g_i v \, dx. \quad (0.25)$$

liest sich die schwache Formulierung, inklusive der Behandlung von Randbedingungen, als

$$\sum_{i=1}^k \sum_j [(\mathcal{J}(u_i, v_{ij}) + \mathcal{D}_i(u_i, v_{ij}) - \mathcal{B}_i(\Phi, v_{ij}) + z_i \mathcal{J}(u_i, \phi_j)) + \mathcal{P}(\Phi, \phi_j)] = \sum_{i=1}^k \sum_j \mathcal{F}_i(v_{ij}) + \mathcal{G}(v_{ij}), \quad (0.26)$$

wobei der Index i die verschiedenen Ionen Spezies und der Index j die Testfunktionen durchläuft. Wir beenden das Kapitel mit einer kurzen Diskussion von Konvergenz und Adaptivität.

0.4 Numerische Experimente

Nach den theoretischen Vorbereitungen widmen wir uns in diesem Kapitel der Durchführung von numerischen Experimenten. Da wir uns zur Umsetzung des Finite Element Lösers der deal.II Bibliothek bedient haben, leiten wir das Kapitel mit einer Beschreibung der Funk-

tionalitäten ein, die wir aus dieser Bibliothek verwenden, bevor wir uns den tatsächlichen Simulationsergebnissen zuwenden. Wir beginnen die numerischen Experimente mit den Simulationen auf der atomaren Skala. In traditionellen Konvektionsbereinigten Testensembles stellen wir die Gleichwertigkeit unserer neuartigen Messmethode für den Diffusionskoeffizient fest, sowie im Falle von Ensembles, die einen Konvektionsterm enthalten, die klare Überlegenheit der neuartigen Methode. Wir gehen dann zu einem realistischen Fall über, messen die Diffusion sowie das chemische Potential von Li^+ und BF_4^- Ionen in der Elektrolyt-Substanz Ethylen-carbonat und diskutieren die erhaltenen Werte. Für die Verifizierung der Ergebnisse unseres PNP-Lösers existieren leider keine standardisierten Testfälle mit bekannten Lösungen. Daher demonstrieren wir zunächst die Fähigkeit, Konzentrationsdefekte zu transportieren. Danach wenden wir uns einem Beispiel zu, das eine Batterie modelliert, vergleichen Schlüsselcharakteristiken der Lösung mit den Resultaten anderer Arbeiten und führen Konvergenzuntersuchungen durch. Zu guter Letzt zeigen wir die weitergehenden Fähigkeit unseres Lösers, indem wir Störungen in unsere Geometrie einbringen, die mit den bisherigen eindimensionalen Lösern so nicht behandelbar sind.

0.5 Schlussbemerkungen

In dieser Arbeit haben wir einen leistungsfähigen Multiskalenlöser für das Poisson-Nernst-Planck Gleichungssystem zur Modellierung von Ionenmigration erarbeitet. Im Zuge dieser Arbeit haben wir traditionelle Messmethoden für Diffusionskoeffizienten aus moleküldynamischen Simulationen verbessert und eine bereits bekannte Methode zur Messung des chemischen Potentials implementiert. Des Weiteren wurde ein linearer Operator für das nicht-lineare gekoppelte PNP System entwickelt, der ungeachtet der starken nicht-linearen Kopplung durch die Poisson-Gleichung eine stabile Integration in der Zeit erlaubt.

Die durchgeführten numerischen Experimente haben gezeigt, dass die modifizierte Messmethode des Diffusionskoeffizienten dem traditionellen Verfahren überlegen ist.

Für unseren neuen PNP Löser haben wir auf Grund der fehlenden Benchmark Probleme eine Vielzahl von Simulationen durchgeführt. Dabei zeigte der Löser erwartetes Verhalten und reproduzierte charakteristische Eigenschaften der jeweiligen Systeme. Zusätzlich haben wir demonstriert, dass unser Löser auch weitergehende Einsatzmöglichkeiten hat, als bisher bekannte Verfahren. Zusammenfassend stellen wir fest, dass unser Multiskalen-Verfahren auf allen zugehörigen Leveln erfolgreich arbeitet und das Potential hat, durch qualitativ hochwertige Vorhersagen über das Verhalten neuer Materialien und Strukturen im Bereich der Batterien und amorphen Materialien zur Lösung der dortigen technologischen Herausforderungen beizutragen.

0.5.1 Ausblick

Die eingeschränkte Genauigkeit der Messungen moleküldynamischen Simulation sind im wesentlichen eine Folge der geringen Zahl von Ionen, denen eine große Zahl von Molekülen des Umgebungsmaterials gegenübersteht, die die Beschränkungen der Systemgröße bestimmen. Genauere Simulationsergebnisse wären daher nach der Bereitstellung von leistungsfähigeren Parallelrechnern möglich. Ebenso ist die Genauigkeit der Simulationsergebnisse von korrekten

Parametern der intramolekularen Potentiale abhängig, deren Bereitstellung in den Aufgabenbereich der theoretischen Chemie fällt.

Im Bereich unseres PNP Löser wird es notwendig sein, die durch die systembedingte, nicht divergenzfreie Konvektion hervorgerufenen Massenverluste zu beheben. Ein weiterer Forschungsbereich eröffnet sich in der Behandlung der Randbedingungen. Kurzfristig ist eine makroskopische Modellierung in Abhängigkeit des lokalen Potentialgradienten ein vielversprechender Ansatz. In Anbetracht der hohen Bedeutung, die das Elektroden-Elektrolyt-Interface auf die Leistung von Batterien hat, sollte aber langfristig auch hier die Entwicklung von Multiskalenmethoden ins Auge gefasst werden.

Chapter 1

Introduction

The combination of diffusion and convection through porous media or membranes with varying structure is a procedure which is of significant relevance in many different areas of science and engineering.

In biology and medicine, research is carried out on the permeation of ions through cell membranes in order to understand activity in organisms and in extension develop new medical treatments or improve existing ones. In geology there is attention on the motion of fluids through rocks and other porous soil structures, as those are relevant in the extraction or storing of oil or gas resources and have significant impact on the success of such ventures. The same models apply, when oil or other liquid chemicals leak and seep into natural soil. The restriction or prediction of the contamination and the corresponding possible infection of reservoirs of potable water can be of vital importance. In material science the change of mechanical properties due to the leaching of ions out of material matrices is investigated. For example it is known that the stability of mortar and cementitious materials in general deteriorates with the leaching of calcium. Certain chemicals, such as those contained in acitic rain, boost this deterioration. In light of extensive use of those materials in the construction of bridges, airports, residential buildings and numerous other large and smaller building projects throughout the world, the comprehension of ion migration as a key to finding protective measures of those structures from decay is of immense value. In the field of electrical engineering the research of ion migration has equivalent significance. Batteries and accumulators function on the basis of this process. Even today our society can hardly function without them as they enable the use of cell phones, notebooks and other mobile electronic devices. New concepts for traffic systems envision the change of the primary energy source for motorized individual transportation to change from fossil fuels to electrical storage devices. First prototypes of battery powered cars already exist, however they are still subject to severe limitations in the accessible power and capacity so that the envisioned change can not be implemented on their current performance. Thus the invention of new materials and structural layouts is required prior to the realization of the vision of common use of electric vehicles.

It is only natural that mathematical models are developed for a process with such diverse applications and it is the task of numerical mathematics to use those models to analyse, describe and – if possible – predict the behavior of such processes under given conditions. While numerical simulation is not able to completely remove the need for experiments on

the path to a finished product but the combination of well adjusted models and powerful mathematical methods can serve as an indicator for the qualitative behavior of a system and thus save time and resources on a decision whether to produce a prototype or not.

In the creation and derivation of our numerical method we will focus on ionic migration and keep applications in the fields of cementitious materials and batteries in the center of our attention.

Ionic migration is described by the system of the Poisson-Nernst-Planck (PNP) equations, which takes into account diffusive and advective contributions to the change in molecular concentration and under certain conditions allows treatment of reactive contributions as well. Depending on the system or layout to be simulated, the values of the coefficients of this equation differ greatly, as do the boundary conditions to be applied. Generally those values are obtained from prior experimentation in such a system, the simulation then predicting the behavior of the system depending on variations of the starting conditions.

However, if we wish to make prediction about the performance of a new system layout prior to the existence of a prototype, let that be that of a new composition of concrete or of a battery's electrolyte or membrane, this method of obtaining simulation parameters is for obvious reasons impossible. Consequently, different paths need to be taken, as the coefficients and boundary conditions required in the PNP equation are not known. One way to achieve that goal is to go down in scale, to the atoms and molecules making up the system. By simulating their behavior and relying on the more fundamental forces among them, one becomes independent of knowing experimental approximations of macroscopic properties of an electrolyte or membrane and encompasses the full properties of the natural material behavior.

It is however infeasible to implement simulations on a molecular level for the whole macroscopic system, e.g. a battery, since one would be required to simulate the behavior of a number of atoms on the scale of Avogadro's number. Such a system would easily overstrain any memory and computing time capacity one could provide due to the complexity of the problem. Nevertheless, an approach via the molecular structure is not completely in vain. By thinking in scopes of both scales mentioned before, it is possible to construct a simulation routine which has a reasonable computational complexity so that it can be performed within very reasonable limits of resources. At the same time it generates predictions on the basis of the actual molecular behavior, bypassing the need to obtain experimental data beforehand. In order to do this, one has to perform a multiscaling (or upscaling) approach, using initial computations on the behavior of atoms and molecules. The results obtained there can then be statistically averaged and used to supply those coefficients, which are required in order to run the simulation of the Poisson-Nernst-Planck equation System (PNP), which then predicts the macroscopic behavior of the system. For different material or structural regions of the macroscopic domain corresponding separate MD simulations and upscaling computations will be performed.

Between our calculations on the atomic scale, which typically range over distances of Ångstrom and nanometers (10^{-10} and 10^{-9} m respectively), the procedure is required to scale to applications as large as the visual range, which typically have a size in the range of millimeters and centimeters (10^{-3} and 10^{-2} m respectively), although applications on scales of micrometers (10^{-6} m) will be within the capabilities of the algorithm as well. In the course of this work we will test our developed method and demonstrate its applicability.

For the simulation of the atomistic systems we can rely on the work done by Jan Hamaekers and Ralf Wildenhues, who have implemented the *TREMOLLO* molecular simulation software package at the INS of the university of Bonn. For the implementation of the numerical solver for the Poisson-Nernst-Planck equation system the deal.II program library was used.

We present a short overview of the contributions established by this work:

- Extension of the Einstein relation for the Diffusion coefficient to correct for convective behavior.
- Implementation of said correction into the *TREMOLLO* software.
- Implementation of a measuring routine for the chemical potential.
- Producing a stable, linearized operator for the non-linear, fully coupled Poisson-Nernst-Planck equation system
- Implementation of an adaptive finite element solver for the extended, time-dependent, coupled Poisson-Nernst-Planck equation system in two and three space dimensions.

Chapter 2

Molecular Dynamics

When turning to the simulation of atomic or molecular systems respectively, one would naively expect those simulations to employ the results and equations of quantum mechanics. Since the physical scales are so small, quantum effects should produce a significant contribution to the behavior of a system. However, in reality, full quantum mechanical calculations are hardly ever used for systems of interesting size, due to the fact that such computations are immensely time-consuming. Nevertheless, simulations on a molecular scale are not in vain, since classical mechanics combined with empirical potentials capture part of the quantum mechanical nature and enable calculations of sufficient accuracy at reasonable costs in computing time [Gri04, Fre02, Hab95].

In the first section we will thus motivate and deduce the jump from molecular dynamics based on quantum mechanics to the those based on pseudo physical potentials. Afterwards, we will give a review of the mechanics of classical many-body systems and some numerical techniques used for the simulation of such systems, before we mention thermodynamics in form of many particle physics and the phase space, whose concept is fundamental in the validation of the measurement procedures used in the **Molecular Dynamics (MD)** simulations.

Since the goal of this chapter is the introduction of MD rather than a complete derivation of the latter from quantum mechanics, the reader is referred to standard literature for detailed remarks on that topic, for example [Sch]. For the transition from the Schrödinger equation to molecular dynamics (MD) we shall follow the work in [Gri04], where the interested reader can find a much more detailed derivation, as we provided it in the scope of this work.

2.1 The Schrödinger Equation

For a system of N nuclei and K electrons, let

$$\Psi = \Psi(R_1, \dots, R_N, r_1, \dots, r_K, t) \quad (2.1)$$

be its wave function with R_i and r_i being the coordinates in real space of the nuclei and electrons, respectively. Naturally, the wave function needs to satisfy the time dependent

Schrödinger equation

$$i\hbar \frac{\partial \Psi(R, r, t)}{\partial t} = H\Psi(R, r, t), \quad (2.2)$$

where i is the imaginary unit and H the Hamilton operator of the system. Ignoring spin and relativistic effects, as well as assuming the nuclei and electrons to be point masses, this Hamilton operator takes the form

$$\begin{aligned} H(R, r) = & \underbrace{-\frac{\hbar^2}{2m_e} \sum_{k=1}^K \Delta_{r_k}}_{T_e} \quad \underbrace{-\frac{\hbar^2}{2} \sum_{k=1}^N \frac{1}{M_k} \Delta_{R_k}}_{T_n} \\ & + \underbrace{\frac{e^2}{4\pi\epsilon_0} \sum_{k<l}^K \frac{1}{\|r_k - r_l\|}}_{V_{ee}} \quad + \underbrace{\frac{e^2}{4\pi\epsilon_0} \sum_{k<l}^N \frac{Z_k Z_l}{\|R_k - R_l\|}}_{V_{nn}} \\ & - \underbrace{\frac{e^2}{4\pi\epsilon_0} \sum_{k=1}^K \sum_{l=1}^N \frac{Z_l}{\|r_k - R_l\|}}_{V_{en}}. \end{aligned} \quad (2.3)$$

Here, e is the elementary charge of an electron and m_j its mass. Equivalently, M_k denotes the mass of the k^{th} nucleus and Z_k its respective charge number and $\hbar = \frac{h}{2\pi}$ with h being Planck's constant.

For ease of use shorthands for the operators have been introduced, with T_e and T_n being the operators of kinetic energy for the electrons and nuclei, respectively, and V_{en} , V_{nn} and V_{ee} being the operators for the potential energy (in terms of the Coulomb potential) between and among the electrons and nuclei. We will later reference this decomposition. First it should be noticed though that the Hamiltonian operator above has no explicit time dependency, which allows for a separation ansatz for the wave function:

$$\Psi(R, r, t) = \Psi'(R, r) \cdot f(t). \quad (2.4)$$

For ease of use we will drop the prime and simply refer to Ψ from now on. Inserting the above ansatz into the Schrödinger equation leads to a separation into two decoupled equations:

$$i\hbar \frac{1}{f(t)} \frac{df(t)}{dt} = \frac{1}{\Psi(R, r)} H\Psi(R, r) \quad (2.5)$$

$$\Rightarrow i\hbar \frac{1}{f(t)} \frac{df(t)}{dt} = E \quad (2.6)$$

$$H\Psi(R, r) = E\Psi(R, r) \quad (2.7)$$

Since the solution of (2.6) is well known to be

$$f(t) = c \cdot \exp\left(\frac{-iEt}{\hbar}\right), \quad (2.8)$$

we can use the stationary Schrödinger equation (2.7) as an eigenvalue equation to each energy eigenvalue E_n to produce the eigenfunctions Ψ_n .¹ Since a variation in E yields different functions f_n as well, we write down a formal solution for the wave equation in dependency on different eigenvalues E_n and the unknown eigenfunctions Ψ_n :

$$\Psi(R,r,t) = \sum_n c_n \exp\left(\frac{-iE_n t}{\hbar}\right) \Psi_n(R,r) \quad (2.9)$$

with the weights $c_n = \int \Psi_n^*(R,r) \Psi(R,r) dRdr$.

2.2 Deriving Classical Molecular Dynamics

We now return our attention to the previously introduced Hamilton operator and its decomposition. We call upon the Born-Oppenheimer approximation, which states that due to the substantial mass difference of nuclei and electrons it is reasonable to assume that the latter follow the movement of the former instantaneously and assume a new configuration in dependence of the new nuclei positions. Thus we intend to separate the treatment of the electrons from those of the nuclei and therefore introduce the electronic Hamilton operator

$$H_e = T_e + V_{ee} + V_{nn} + V_{ne}. \quad (2.10)$$

This operator takes into account all parameters which have an influence on the state of the electrons. Solving their respective wave function would yield a potential field, to which we then couple the motion of the nuclei via Newton's laws, as the gradient of the potential determines the force acting on the nuclei. While decoupling the computation of nuclei and electron states reduces the complexity of the problem, finding the electron wave function still dominates the problem and limits the number of particles that can be treated this way. In response to this problem one ignores those calculations and assumes all electrons to be in an averaged state with respect to their nucleus at all times. Then the field in which the nuclei move only depends on their own positions and the averaged state chosen for the nuclei. The choice of the electron behavior is expressed by effective force fields, which are chosen for the particles in the system. The force fields used do not necessarily express actual physical interaction, but are fitted so that the resulting force terms reproduce the behavior of the physical systems.

¹ The index n denotes eigenvalues and functions of the Hamilton Operator (possibly accounting for multiplicity). Proof of the discreteness of the spectrum of eigenvalues and -functions can be found in standard literature such as [Sch].

2.3 Classical Molecular Dynamics

In the previous section we have derived molecular dynamics by following the classical mechanical equations from Newton's laws for the nuclei, assuming all electron configurations to be in the ground state at all times. We thus have to solve the following equation, assuming a time independent conservative field¹:

$$m_j \ddot{x}_j = F_j = -\nabla V_{tot}(r_{ij}) \quad (2.11)$$

for each atom, indexed by j , where m_j is the mass of the atom, x_j its position, F_j the force on the particle, V is the potential, which is a function of the relative positions r_{ij} of (potentially) all other atoms.

Some simple and common potentials are:

The Coulomb potential

$$V(r_{ij}) = \frac{1}{4\pi\epsilon_0} \frac{q_i q_j}{r_{ij}} \hat{r}_{ij}, \quad (2.12)$$

with the dielectric constant ϵ_0 and particle charges q_i .

The van der Waals potential

$$V(r_{ij}) = -a \left(\frac{1}{r_{ij}} \right)^6, \quad (2.13)$$

where a is a parameter depending on the properties of the particle type, e.g. its ionization energy.

The general Lennard-Jones potential

$$V(r_{ij}) = \alpha \epsilon \left[\left(\frac{\sigma}{r_{ij}} \right)^n - \left(\frac{\sigma}{r_{ij}} \right)^m \right] \quad m < n, \quad (2.14)$$

where $\alpha = \frac{1}{n-m} \left(\frac{n^n}{m^m} \right)^{\frac{1}{n-m}}$ and σ and ϵ are parameters to the potential. Specifically ϵ is the minimum of the potential well, whereas σ is its root. A choice often seen are $m = 6$ and $n = 12$, where $m = 6$ quite obviously corresponds to the van der Waals potential and $n = 12$ models a strong repulsive force of the nuclei-nuclei interaction, though choosing $n = 12 = 2 \cdot m$ is an arbitrary decision for mathematical simplicity.

Those simple potentials only model non-bonded interaction and thus non-bonded forces between pairs of particles. One does not need too much imagination to conclude that for simulations to depict reality more elaborate potentials are required, which, for example, take into account bond angles, that is to say potentials, relying on multiple atom positions simultaneously to be calculated. Nevertheless, those simple potentials are sufficient to present us with a large computational complexity, since the force on each particle is dependent on all other relative

¹ The time independence refers only to direct variable dependence, via the time dependence of the particle coordinates the field does change with time.

particle positions, $O(N^2)$ operations would be required.¹ This severely limits the number of particles which can be simulated efficiently.

2.3.1 Time Integration via Störmer-Verlet

Up to this point we have not yet mentioned how the equations of motion are actually solved. Since the simulation is to be performed with a computer, the equations need to be discretized. That is, instead of searching for a continuous solution, one attempts to approximate it at discrete points in time. In this particular instance a discretized second difference scheme of (2.11)

$$m_i \frac{1}{\delta t^2} (\vec{x}_i^{n+1} - 2\vec{x}_i^n + \vec{x}_i^{n-1}) = \frac{\vec{F}_i^n}{m_i}, \quad (2.15)$$

for which past positions (and velocities) are known, can be transformed into the following equation:

$$\vec{x}_i^{n+1} = 2\vec{x}_i^n - \vec{x}_i^{n-1} + \delta t^2 \cdot \frac{\vec{F}_i^n}{m_i}, \quad (2.16)$$

which allows to update the positions. When one is interested in the velocities of the particles, e.g. for the computation of the kinetic energy, one is required to calculate them separately in this scheme:

$$\vec{v}_i^n = \frac{\vec{x}_i^{n+1} - \vec{x}_i^{n-1}}{2\delta t}. \quad (2.17)$$

The approximation in equation (2.16) might not be entirely suitable, as it is prone to numerical instability. Since the time step δt is by nature of the scheme of very small magnitude. The multiplication of δt^2 to the force term, which is added to the positions, whose scale does not depend on the time, might differ by orders of magnitude, implying the possibilities of severe rounding errors.

In response to this problem alternative formulations have been developed, which are equivalent in exact arithmetic, but less susceptible to rounding errors. A popular reformulation is the so called Velocity-Störmer-Verlet algorithm. We observe that

$$\vec{x}_i^{n+1} = \vec{x}_i^n + \delta t \vec{v}_i^n + \frac{\vec{F}_i^n \cdot \delta t^2}{2m_i}, \quad (2.18)$$

which is the standard integration result from classical physics of motion. This time we need the velocities prior to the update of the positions, so we need to express v_i^{n+1} in terms of old

¹ Taking into account Newtons third law: $F_{ij} = -F_{ji}$ allows for a speedup of approximately $\frac{1}{2}$, nevertheless it is only a constant leaving the asymptotic behavior unchanged.

velocities and forces. Starting by expanding the old expression from (2.17):

$$\vec{v}_i^n = \frac{\vec{x}_i^{m+1} - \vec{x}_i^{m-1}}{2\delta t} = \frac{\vec{x}_i^m - \vec{x}_i^{m-1}}{\delta t} + \frac{\vec{F}_i^n}{2m_i} \delta t \quad (2.19)$$

and adding the same expression with updated time

$$\vec{v}_i^{n+1} + \vec{v}_i^n = \frac{\vec{x}_i^{m+1} - \vec{x}_i^{m-1}}{\delta t} + \frac{\vec{F}_i^{n+1} + \vec{F}_i^n}{2m_i} \delta t \quad (2.20)$$

it is possible to achieve the following by immediately subtracting (2.17)¹

$$\vec{v}_i^{n+1} = \vec{v}_i^n + \frac{\vec{F}_i^{n+1} + \vec{F}_i^n}{2m_i} \delta t. \quad (2.21)$$

Since within each sum there is at least one term whose power of δt deviates by at most one, this algorithm (Calculation of forces, 2.21 and 2.18) is numerically stable and has the advantage that the velocities of the particles are generated along the simulation at the same temporal nodes as the positions, enabling the calculation of the systems total energy as the sum of kinetic and potential energy without extra effort.

Additionally the trajectories generated by this scheme are time reversible and symplectic, a property which will be properly discussed with the introduction of the phase space in section 2.4.2.

It is quite obvious that the calculations presented above need to be performed for each particle, scaling with $O(N)$. This is a natural lower bound for the complexity of any MD algorithm. The calculation of the forces incorporated has not yet been discussed in detail, however in the above sections we have hinted that even for simple inter-particle potentials the complexity scales with $O(N^2)$ when evaluated naively.

2.3.2 Boundaries to the Simulation

After having discussed the interactions between the particles themselves, it is equally important to consider the boundary conditions containing the domain, where one can choose among free, hard, periodic or heated wall boundaries. When dealing with more than one space dimension one might also consider settings in which the boundary conditions vary in the different dimensional directions. It comes as no surprise that on the small scale of particles the choice makes a substantial difference in the results of the simulation, as free boundary conditions would practically imply that all particles on the rim of the simulated structure would behave as if they were on the surface of the material, whereas periodic boundary conditions would imply the presence of bulk material in all directions. Hard walls are more difficult to relate to relevant examples, although they can be interpreted as forming the boundaries of a potential well, which is either infinite or exhibits potential barrier whose energy exceeds that of

¹ The same result can be obtained by using the integration of the classical equations of motion using the average force value between the two timesteps.

the particles by several orders of magnitude.

The difference, which the boundary conditions make for the whole sample, becomes apparent when considering the regular numbers of particles in molecular simulations ranging from a few thousand to a million particles. Those making up the surface account for 49% in the case of 10^3 particles a number that goes down to 'just' 6% in the case of 10^6 particles. Systems in physical reality are made up of particles in the order of Avogadro's number ($6.023 \cdot 10^{23}$), where the surface to bulk ratio is in the order of 10^{-16} . Thus, in simulations, the number of particles experiencing surface effects is still exceptionally large. In order to simulate bulk material, periodic boundary conditions are generally the more appropriate choice for a physical model. However there are configurations, for which the other boundary conditions have their merits as well. Since the hard and free boundaries are trivial and heated walls have no application in the context of this thesis, we commence with the description of periodic boundary conditions only.

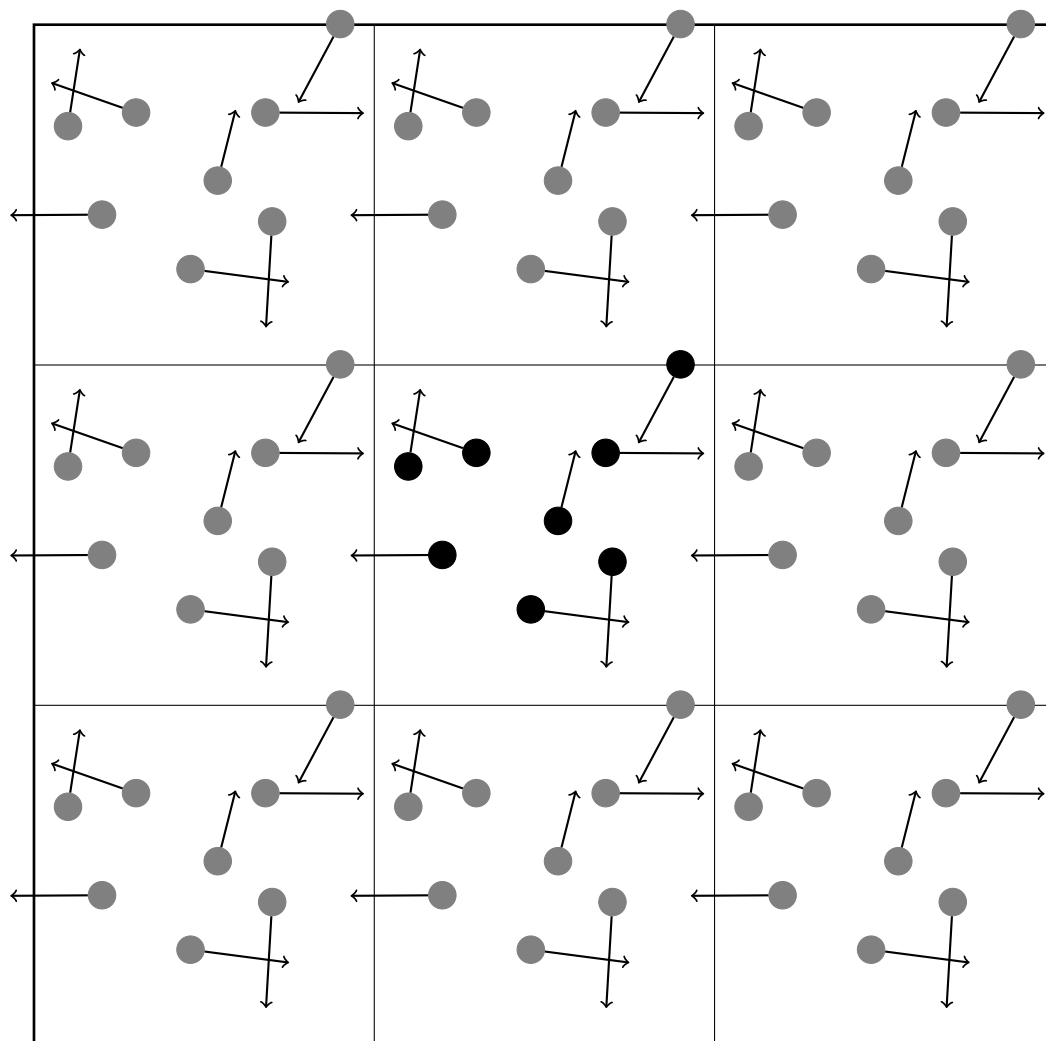


Figure 2.1: Periodic cells.

For periodic boundary conditions the periodic shifts of particles need to be included in the calculation as well,

$$m_j \ddot{\vec{x}}_j = F_j = \nabla V_{tot,j}(\vec{r}_{ij}) = \nabla \sum_{i=1\dots N, \vec{n} \in \mathbb{Z}^3} V(\vec{r}_{ij} + \vec{n}L) \quad (2.22)$$

where \vec{n} is a vector of integers. (The sum needs to exclude $i=j$ in the case of $\vec{n} = 0$, to avoid singularities in the potential). This equation suggests that periodic boundary conditions require the evaluation of an infinite sum, rendering this composition quite expensive to deal with. First molecular dynamics simulations actually approximated this sum [Woo57], whereas modern implementations of molecular dynamics truncate it generally even before iterating over periodic cells at all: As described in the following section, a cutoff distance can be chosen under certain conditions, limiting the number of periodic images to be taken into account. Specifically, a cutoff radius smaller than half of the boxlength would prevent a particle from being taken into account with more than one image, which is the usual approach. But even if it were not so, the cutoff would reduce the infinite sum to a finite one.

2.3.3 Evaluation of Potentials and Cutoff Distance

In the previous section we suggested the use of a cutoff radius to cope with infinite sums. Since this introduces an error in the computation of the particle movement, we will discuss various truncation methods and their respective effect on the error in this section. The basic idea is that for particle interactions based on “fast vanishing” potentials the contributions of particles far away are so marginal that they can be omitted safely. If one were to imagine a cutoff distance r_c and ignored all contributions beyond this radius, one would be left with an easily computable sum and a systematic error. In order to account for this error the following equation should be observed:

$$V_{tot,j} = \sum_{i, r_{ij} < r_c} V(r_{ij}) + \frac{N\rho}{2} \int_{r_c}^{\infty} V(r) 4\pi r^2 dr \quad (2.23)$$

where ρ is the averaged particle density. It is apparent that the integral in the above equation converges if $V(r)$ decreases more rapidly than r^{-3} . Then a sensible choice of r_c allows to decrease the error into marginality.¹

There is more than one way to implement said truncations. While the easiest and most obvious is a simple cut at r_c setting the potential to zero afterwards:

$$V_{Cut}(r) = \begin{cases} V(r) & r \leq r_c \\ 0 & r > r_c \end{cases}, \quad (2.24)$$

¹ Note that equation 2.23 itself and this requirement are valid for 3 dimensions. In different settings the requirements for truncation need to be adjusted to potentials decreasing faster than r^{-d} for d space dimensions.

it is obvious that this introduces a discontinuity in the potential. In response, various other methods of truncation have been introduced, among those are the minimum image convention, the truncation with shift and the truncation with continuous extension. The minimum image convention means that all particles in the test cell are included in the calculation of the potential at least once, with their nearest image in the periodic representation. Since this is not a spherical cutoff its use is discouraged, despite the fact that the simulated potential would be continuous. [Fre02]. Truncating the potential and shifting it by the value at the cutoff

$$V_{Cut}(r) = \begin{cases} V(r) - V(r_c) & r \leq r_c \\ 0 & r > r_c \end{cases}, \quad (2.25)$$

is again an instance with continuous effective field. The shift in the nearfield potential does change the simulated potential energy and pressure, so that any measure of those quantities would require correction. More problematic is the discontinuity of the first derivative, as the forces used for the motion equations are equal to the gradient of the potential. Thus unwanted impulsive forces appear and in a dynamic simulation energy would no longer be conserved.¹

This is taken into account in the final example, the truncation with continuous extension. In this implementation a function is fitted to the potential at the point of the cutoff radius, which conserves continuity in the potential and the forces, and then vanishes again continuously and differentially after some larger, 'final' cutoff radius. An example of this can be found in section 3.7.3 of [Gri04].

One should note that there are some important potentials which do not satisfy the stated requirement of vanishing fast enough, such as the Coulomb potential (2.12). In order to work efficiently with those potentials other techniques are required, which often adopt a strategy of separating the potential in a long- and short-range term. The splitting should be done in a way resulting in a short range term which satisfies the above requirements, while the long-range term should be smooth enough to allow for fast interpolation of the combined potential of all particles on the complete domain. This potential interpolation can then be differentiated and the resulting force field can be evaluated at the particle positions. As we will not go further into detail here, we refer the reader to [Gri04] for a more detailed description of the procedures which can be used.

We also would like to mention that the above methods can be used for dealing with the previously mentioned general complexity of the atomic simulations as well. Since we have introduced a cutoff radius on most potentials, particle interaction is now highly localized. By using sophisticated particle management, such as the linked cell method or Verlet lists, one is now able to restrict force calculations for a given particle to its neighbours. Assuming a bounded, homogeneous distribution of particles in the domain, this leads to a computational complexity of $O(N)$, instead of the previous $O(N^2)$.

¹ This problem becomes in those cases academic where a closed expression for the force is used, which could be cut off without the need for differentiation.

2.3.4 Ensembles and Thermostats

As for any imaginable type of numerical simulation it is naturally important to discuss the starting conditions for the simulated system, which are generally called ensembles in molecular dynamics, where the term ensemble not only applies to the initial setting, but also to the fixed degrees of freedom related to macroscopic statistical quantities¹. When starting naively, one would create a simulation cell with fixed side lengths and shape in which a fixed number of particles would be set, which would then be supplied with initial velocities². This naive approach is a valid ensemble, denoted as the microcanonical ensemble or NVE ensemble (= **N**umber of particles, **V**olume, (total) **E**nergy), where the abbreviated properties of the system remain constant throughout the simulation. Other ensembles are the NVT (**N**umber of particles, **V**olume, **T**emperature/kinetic energy) (canonical) ensemble or the NPT (**N**umber of particles, **P**ressure, **T**emperature/kinetic energy) ensemble, which both have the property that the temperature (kinetic energy E_{kin}) of the sample is to be fixed whereas the total energy (consisting of the sum of kinetic and potential energy) may now vary. The NPT ensemble additionally allows the deformation of the simulation cell, while in return the pressure on the outer walls remains constant. Since the ensembles employed in this thesis require T to be fixed, the proper setup of thermostats shall be discussed in this section.

Thermostats may be imagined as an infinite, virtual heat bath in contact with the simulated system, which leads to an energy exchange and the system changing its temperature towards the one of the heat bath. In the simulation procedure there is no bath of course, but a reference temperature, which the system is bound to approach via various means.

From thermodynamics the relation

$$E_{kin} = \frac{3N}{2}k_B T \quad (2.26)$$

is known, tying the temperature to the kinetic energy distributed among the degrees of freedom of the particles³. Solving for T and replacing the kinetic energy by its definition we obtain

$$T = \frac{2}{3Nk_B} E_{kin} = \frac{2}{3Nk_B} \sum_{i=1}^N \frac{m_i}{2} \vec{v}_i^2. \quad (2.27)$$

This equation suggests to control the temperature in a simulation by scaling the velocities \vec{v}_i of the particles. Several well known thermostats, by Berendsen or Nosé and Hoover are based on a manipulation of the particle velocities. Those manipulations vary from a simple scaling of the velocities outside of the general updating procedure to the inclusion of a friction term in the integration algorithm.

¹ The term “ensemble” extends to settings of non-dynamic, Monte-Carlo type of molecular simulations.

² Note that a velocity of 0 (eg. the velocities are not set by any means) is also a velocity in the physical interpretation.

³ This expression is valid for particles without spatial extension (point-like particles such as atoms in the present model), since otherwise rotation and vibration within the particle would have to be counted towards the degrees of freedom.

Velocity Scaling

An implementation of a thermostat as introduced by Berendsen [Ber84] is a direct scaling of the velocities

$$\vec{v}_i^n := \beta \vec{v}_i^{n-1} \quad (2.28)$$

outside of the regular update of the velocities in the integration procedure. In order to achieve an immediate shift to the desired temperature, the scaling factor needs to be chosen as

$$\beta := \sqrt{\frac{T^D}{T(t)}} = \sqrt{\frac{E_{kin}^D}{E_{kin}}}, \quad (2.29)$$

where the superscript D denotes the desired temperature (or kinetic energy). One might decide that the subsequent changes in the energy of the system after this scaling are too drastic and wish for a dampened scaling. Choosing a parameter $\gamma \in [0, 1]$, one uses

$$\beta_\gamma := \sqrt{1 + \gamma \left(\frac{T^D}{T(t)} - 1 \right)}. \quad (2.30)$$

It is apparent that the extremal choices of γ either lead to the absence of scaling ($\gamma = 0$) or again to 2.29 ($\gamma = 1$).

Friction in the Equations of Motion

We will now have a look at a different approach to the control of temperature, the so-called Nosé-Hoover thermostat, implemented via a friction-like term added to the force in the integration. The continuous equation takes the form

$$m_i \dot{\vec{v}}_i = \vec{F}_i - \xi m_i \vec{v}_i, \quad (2.31)$$

with \vec{F}_i the regular physical force and ξ a friction constant, so that similar to macroscopic mechanical systems the change of velocity depends on its own magnitude. It is quite obvious that a positive choice of ξ leads to a monotone decrease in total energy, whereas a negative choice implies an increase in total energy. Assuming one wants to maintain the temperature and kinetic energy at a constant level, one would compute

$$\begin{aligned} 0 &= \frac{dE_{kin}}{dt} = \sum_{i=1}^N m_i \vec{v}_i \cdot \dot{\vec{v}}_i = \sum_{i=1}^N \vec{v}_i \cdot (\vec{F}_i - \xi m_i \vec{v}_i) \\ &= - \sum_{i=1}^N \vec{v}_i \cdot (\nabla_{x_i} V + \xi m_i \vec{v}_i) = - \left(\frac{dV}{dt} + \xi \sum_{i=1}^N m_i \vec{v}_i^2 \right) \\ &= - \left(\frac{dV}{dt} + \xi 2 \cdot E_{kin} \right), \end{aligned} \quad (2.32)$$

showing that the change in kinetic energy is the negative change of potential energy (which usually would account for the conservation of energy) minus frictional losses. Solving for ξ then results in

$$\xi = -\frac{\frac{dV}{dt}}{2E_{kin}(t)}, \quad (2.33)$$

which results in the energy transformed from kinetic to potential type (or vice versa) being made up for by the frictional term. This thermostat would be rendered useless if it were not able to react to a change in energy. In order to achieve just that, ξ is tied to the deviation from the target temperature T^D by the following ordinary differential equation:

$$\frac{d\xi}{dt} = \frac{\sum_{i=1}^N m_i \vec{v}_i^2 - 3Nk_B T^D}{M}, \quad (2.34)$$

where the parameter $M \in \mathbb{R}^+$ is a fictitious mass, determining the strength of the coupling between the simulated system and the virtual heat bath. The above description demands that the changing friction constant is taken care of via an additional integration.

2.3.5 Error of Extended Integration

When the discrete algorithm was presented, it was hinted that the calculations performed do not match the exact trajectories. However, no qualitative estimate of the error progression has been given, which will be the subject of this section.

We define

$$\begin{pmatrix} x^{n+1} \\ v^{n+1} \end{pmatrix} = \Theta(x^n, v^n, \delta t) = \begin{pmatrix} \Theta_1(x^n, v^n, \delta t) \\ \Theta_2(x^n, v^n, \delta t) \end{pmatrix} \quad (2.35)$$

to be the numerical approximation of the exact expression

$$\Phi(x^n, v^n, \delta t) := \begin{pmatrix} x(t_n + \delta t) \\ v(t_n + \delta t) \end{pmatrix}, \quad (2.36)$$

where x^n and v^n are the coordinates and velocities at timestep t_n and δt is the size of the timestep. The following assumptions shall hold for the numerical scheme:

- It is of order m , which means

$$\|x^{n+1} - x(t_n + \delta t)\| = O(\delta t^{m+1}), \quad (2.37)$$

$$\|v^{n+1} - v(t_n + \delta t)\| = O(\delta t^{m+1}). \quad (2.38)$$

- Θ is Lipschitz continuous with respect to the time variable with Lipschitz constant M , meaning that for all $t_1 \neq t_2$

$$\|\Theta(x, v, t_1) - \Theta(x, v, t_2)\| < M \cdot \|t_1 - t_2\| \quad (2.39)$$

While those assumptions guarantee tight control over the error in any one time step, the result for a long-term simulation (that is multiple timesteps) takes the following form:

$$\|x^n - x(t_{end})\| \leq C \cdot \delta t^m \cdot \frac{e^{M(t_{end}-t_0)} - 1}{M}. \quad (2.40)$$

This suggests that even small perturbations can cause significant changes in the simulation by being exponentially increased over time. Independent from any choice for the order of accuracy m for the individual timesteps or the time refinement δt the error rises above any set error mark, when the simulations run sufficiently long. In fact, it can be shown via trivial examples that the estimate is sharp [Gri04]. Therefore, it is futile to perform MD simulations for the sake of extracting trajectories; they will almost certainly deviate strongly from those in the real world. The above results seems to call the utility of MD simulations into question. However, while the trajectories for the particles are inaccurate, one can still obtain results from the observation of conserved values and their average over the duration of the simulation. This is possible under the assumption that the used scheme for the MD simulation is symplectic and can be regarded as a perturbation of the exact differential equation or more precisely that the numerical operator is a perturbation of the exact operator. Then the numerical trajectories are exact solutions to this perturbed operator and its conserved quantities remain constant on its trajectories. As a sidenote, it is generally not possible to compute the perturbed operator, thus foregoing the possibility to verify that the conserved quantities are again approximations of the conserved quantities of the exact system to be simulated.

2.4 Theory of Statistical Physics

In the above paragraphs classical mechanics and Newton's laws have been established as the fundamental principle behind molecular dynamics as they are known today. However, when doing actual computations, it is, as mentioned before, almost never feasible to compute the whole system. Thus one will restrict oneself to samples of the structure. In cases where the matter at hand has a regular structure, such as crystals or other solids, one such sample could be an excellent representation of the whole. When dealing with amorphous materials, such as fluids, one sample will certainly not be an exact image of all possible portions of the system. It is then that one should put some thought into thermodynamics and the connection between macroscopic properties and statistical mechanics, which we present in this section. The so called phase space – and how it connects to the various ensembles – is of interest, as it allows for judging the quality of approximation of one sample with respect to all possible samples.

2.4.1 Thermodynamical Quantities and Statistical Mechanics

When dealing with material samples consisting of particles ranging in the order of magnitude of Avogadro's number, one is rarely interested in the individual behavior of the particles at all. One rather makes the assumption that the individual behavior of a particle, the states of its corresponding degrees of freedom, do not influence the behavior of the complete system as a whole. Moreover, one assumes that when the system is in an equilibrium, its properties are

reproducible (equilibrium hypothesis). Furthermore, the equilibrium state can be characterized by a finite (and actually quite small) set of physical quantities, such as particle number, volume and temperature (NVT ensemble) or particle number, volume and energy (NVE). The equilibrium point of the system is characterized by the fact that those quantities are constant in time. Said quantities correspond to averages over the whole set of microscopic degrees of freedom, i.e. the state of the particles. This is where the classical, phenomenological thermodynamics give way to statistical physics, which link the macroscopic properties to the behavior of the individual particles.

2.4.2 The Phase Space

The phase space is an abstract multidimensional space in which each point represents a different state of the system. When dealing with mechanical particle systems in three dimensions containing n particles, we can describe the system at this point in time completely by giving the location

$$\vec{x}_i = \begin{pmatrix} x_i^1 \\ x_i^2 \\ x_i^3 \end{pmatrix} \quad (2.41)$$

and impulse

$$m_i \dot{\vec{x}}_i = m_i \begin{pmatrix} \dot{x}_i^1 \\ \dot{x}_i^2 \\ \dot{x}_i^3 \end{pmatrix} = m_i \begin{pmatrix} v_i^1 \\ v_i^2 \\ v_i^3 \end{pmatrix} = m_i \vec{v}_i = \vec{p}_i \quad (2.42)$$

of each particle. Considering the individual particles as components of a single system, we unite this information into a $6n$ -dimensional vector $(\vec{x}_1(t), \dots, \vec{x}_n(t), \vec{p}_1(t), \dots, \vec{p}_n(t))$. The system state is then a point in a corresponding $6n$ -dimensional vector space which is called the phase space or Γ space. Each point in this space represents a snapshot of a system state at a given time. We now consider the set of all points which represent systems with the same macroscopic quantities, e.g. have the same temperature, volume and, of course, particle number. This set is called the *virtual entirety*¹.

When we now wish to find other macroscopic values, it is necessary to average them over this virtual entirety, taking into account that the system states might have a different probability of being occupied. To obtain a macroscopic variable \mathcal{A} , which is dependent on the location and impulse of the particles, let f be the probability density of all states in the phase space and Γ be the virtual entirety within the phase space. We now take the *ensemble average* over the virtual entirety of admissible states

$$\langle \mathcal{A} \rangle = \frac{\int_{\Gamma} \mathcal{A}(\vec{x}, \vec{p}) f(\vec{x}, \vec{p}) d\vec{x} d\vec{p}}{\int_{\Gamma} f(\vec{x}, \vec{p}) d\vec{x} d\vec{p}}. \quad (2.43)$$

¹ Virtual entirety is the authors translation of the German phrase *virtuelle Gesamtheit*, which does not seem to be used with the same enthusiasm in English literature.

However, for most systems the probability density of the phase space and the distribution of the virtual entirety is unknown. Remembering the equilibrium hypothesis in section 2.4.1, an equilibrated system retains its macroscopic physical quantities, meaning it remains within its virtual entirety over time. A multi-particle system satisfies said assumptions when its Hamiltonian is not explicitly time dependent. When observing a trajectory of some starting state, it will, while running through different states, still belong to the same entirety, thus sampling a variety of system states describing the same system¹. It is this trajectory which is modeled by an MD simulation and whose average we use to predict the behavior of the sample.

With the trajectory of the system at hand, we observe the time average of the macroscopic quantity

$$\langle \mathcal{A} \rangle_\tau = \frac{1}{\tau} \int_{t_0}^{t_0+\tau} \mathcal{A}(\vec{x}(t), \vec{p}(t)) dt. \quad (2.44)$$

The ergodic hypothesis [Gri04, Hab95] now states that for $\tau \rightarrow \infty$ the ensemble and time average coincide. This implies the independence of the time average of the starting configuration of the system, as well as that in the course of time the trajectory occupies any state of the virtual entirety with a probability corresponding to its contribution to the ensemble average.

However, in a numerical simulation we are unable to compute the exact trajectory but are bound to use an approximation. In order to guarantee that the approximated trajectory does not leave the virtual entirety, we demand that integration scheme which extends the trajectory is symplectic. That means, that the trajectories created by the scheme satisfy the Liouville theorem, which demands that the phase space volume encompassed between neighboring trajectories is constant [Tuc99].

¹ Often the viewpoint is taken, that the virtual entirety resembles different systems in different states, which is fitting for a Monte Carlo simulation approach. Molecular dynamics however observe one system undergoing changes in its microstate.

Chapter 3

Multiscaling: Obtaining the Macroscopic Equation

Since the goal of this thesis is an accurate description and prediction of ionic migration behavior, it is a natural task to give a rigorous derivation of the model used to determine those descriptions or predictions. With good reason many authors begin their derivation on the level of ionic concentration, deriving their formulas empirically from prior observed behavior of ionic migration. However, we reasoned in our introduction that we intend to begin on a smaller scale. Nevertheless, we will outline other approaches to ionic migration for comparison. We will then give an overview of the available multiscaling methods, describing the advantages and disadvantages of each method for our approach. More rigor and detail will be used in the description of a variant of the method of averaging, which not only allows scaling between the micro and macro scale, but in addition allows the derivation of the continuity equation and as a result of the Nernst-Planck equation directly from the atomic scale. To begin with, we assume only the validity of the particle motion for the atoms and molecules, which assemble the solution of the ions to be described.

With the continuity equation for ions in a solution at hand, we investigate the contributions of diffusive and convective behavior of the particles to this equation, meaning contributions by random and directed movement of the particles. Combining the findings of this chapter will result in the macroscopic equation, as well as in the methods required to determine its coefficients from the simulations on the nanoscale.

We end this chapter by a digression into the implementation of reactive contributions.

3.1 Ionic Migration without Multiscaling

In this section we briefly present approaches to model ionic migration which do not stem from direct observation of the molecular movement. While each of them has its merits, we will find that neither will be able to satisfy our demand – as described in detail in the introduction – of being able to predict macroscopic behavior without prior knowledge of macroscopic properties of the materials in use.

3.1.1 Ionic Migration from Macroscopic Transport

As stated in the introduction, equations which govern ionic migration are often derived from macroscopic properties of the materials involved. In these cases the diffusive and convective behavior of ions in a solution is assumed as a fact, without consideration for the actual ionic behavior. When the macroscopic material possesses properties, which contribute to the ionic transport on a scale which is by magnitudes larger than the properties of the atomic behavior, this approach is particularly sensible. Examples for those settings include non-stationary solvents, which by themselves possess macroscopic convection and diffusion, so that the solvated ions are expected to move along with the solvent. One can then approach the migration problem by describing the ionic motion by the equations governing the motion of its solvent, resulting, for example, in the need to solve the Navier-Stokes equation. However, besides being inapplicable in our case due to our focus on stationary solvents, approaching the ionic migration via the motion of its solvent has been found to lack accuracy [Cho09].

3.1.2 Fitting the Model

Some researchers begin with the Nernst-Planck model of ionic migration, arguing that the system of differential equations is a valid model of the macroscopic physics. Since in the course of our extensive derivation of the macroscopic equation this will become apparent as well, we will not discuss this matter in this subsection. From the Nernst-Planck system, a lot of different approaches are taken towards numerical results. More often than expected the parameters of the model are chosen and fitted until the simulation shows the behavior which is expected from experimental results (e.g. [Pan05]). Additionally, restricting assumptions are often placed on the ion species handled with the model. Some authors consider single species behavior only [Kra08], only allow species with identical charge [Nos07, Kra08] or demand (local) electroneutrality [Pan05, Kra08]. Either restriction is obviously a severe hindrance for simulations depicting realistic setups. While in [Kra08] a model is presented only for two monovalent species, the authors refer to tests on multiple species with non-monovalent charges, whose results validate the electroneutrality assumption. The model found in [Nos07] holds onto the restrictions of monovalence but differs from the others by introducing a concentration dependence of the diffusion coefficient on the ionic concentration. This dependence is – as the equations – derived from phenomenological data.

3.1.3 Treating Migration with a Reaction Model

We now describe an approach which in derivation bears some resemblance to our derivation of the Poisson-Nernst-Planck system as it models the equation on proposed atomic behavior and with additional consideration of statistical physics. It is proposed that one needs to take not only the distribution of the ions into account but also their surroundings. The dependency relations are not obtained by observing behavior of the ions on the nanoscale but due to phenomenological correlations with local concentration, frictional coefficient and temperature. While the initial approach via Fick's first law is similar to our upscaling to the continuity equation, the derivation then deviates severely, as the state dependence of the diffusion coefficients is connected with the chemical potential/the chemical activity, which is used to introduce a dependence on the local

concentration. In essence, this introduces a convection element into the model as well, even though this is not explicitly stated in the paper. While the ionic flux is dependent on both terms and it is generally possible to interconnect them, we caution against blindly adopting such a step, for reasons which we will become clear in our following derivation, particularly in section 3.5.3. Furthermore, the diffusion process is modeled as a (chemical) reaction taking place between adjacent cells, which is essentially different from any model of the ionic migration via differential equations. The reactions (in the context of this reference this means actual reactions as well as diffusive and convective movements) are then executed strictly sequentially, where the succession is determined by the probabilistic Gillespie's algorithm [Gil77]. This method uses the timescale of the respective reactions to assemble a global queue of events, which are then executed sequentially. (In the paper cited, the global queue of Gillespie's original algorithm is exchanged for cell-dependent queues.)

3.1.4 Poisson-Nernst-Planck System from the Langevin Equations

The last approach to ionic migration, which we will present here, takes the behavior of individual molecules into account. However, instead of *calculating* the individual activity of all particles, those of the solvent and the solute alike, the derivations proceed with *assumptions* on a relation between solute and solvent and use stochastic differential equations to obtain the ionic behavior. This includes assumptions on the time scale of the respective motions and their dampening, which are dependent on the materials used, primarily the solvent. Using those assumptions, the memory-less Langevin equations are used to derive a coupled Poisson-Nernst-Planck system. In this setting, particles are treated as a corresponding probability distribution in order to extend the model to regions with extremely low concentrations down to cases in which very few ions assemble as a single queue within a channel. While this approach is very powerful in this particular setting, it cannot be extended to high concentration solutions or even channels which permit multiple ion queues. Those shortcomings make this approach unsuitable for the problems which we consider, even if we were willing to make the assumptions on the relation of solute and solvent without verification on the atomic scale. [Sch01]

3.2 Multiscale Methods – an Overview

After having discussed several approaches to ionic migration which do not use multiscale, we now face the task of scaling up from the atomic scale to the macroscopic scale. Again, we outline some approaches which can be found in the literature before describing in detail the method used in this work. While there is a huge quantity of upscaling methods available, we need to bear in mind that the scale from which our upscaling originates is the atomic scale, which a priori does not provide us with continuous functions. Thus, the set of methods available to us is restricted. Nevertheless, we will give some more consideration to the method of homogenization. Even though it does not provide us with the ability to interconnect the discrete, atomic level to the continuous one, we will discuss specific problems in which the method of homogenization might add value to our computations.

3.2.1 Adaptive Resolution Simulation Scheme

The first method presented is an upscaling method specifically intended for upscaling from an all-atom MD level to a so called *coarse-grained* MD simulation. The method aims at reducing the degrees of freedom of a molecular dynamics simulation to those which are relevant for the physical behavior. This is achieved by combining a collection of atoms with a specific pattern into macromolecules, which, with effective potentials, can interact in an MD simulation among themselves and those atoms which have not been treated in this way. The effective potential is determined by measuring the contribution of the potentials of all atoms within a molecule in application to its new mesoscale representation. The transition is comparable to a phase transition in the material, as certain degrees of freedom are restricted, in this case those which are intramolecular. As a result the energy of the sample fluctuates and thermodynamical equilibrium cannot be assured. In fact, changes in pressure and density are reported to occur regularly. Another restriction of the method is the dependence on the shape of the molecules. In the original introduction [Pra05] and the follow-up paper [Pra06] it has only been demonstrated on tetrahedral and spherical molecules. In fact, the method as it is should not be expected to produce sensible results for arbitrary molecules, as a macromolecules orientation in space can influence its interactions. Taking care of such contributions via a multipole-like extension of the potential function might be sensible, but has – to our knowledge – not yet been attempted.

While this method reduces the number of degrees of freedom of the system, it apparently has flaws, which would be relevant to our application. Furthermore, the reduction in the degrees of freedom is generally not sufficient, as the new scope is on the molecular instead of the atomic level. Recalling, that a complete system of interest has particles in the magnitude of Avogadro's number, the remaining complexity would still not allow for reasonable simulations.

3.2.2 The Bridging Scale Method

The **Bridging Scale Method** (BSM) is specifically designed for the upscaling from the molecular to the continuum level and thus, at first glance, seems ideal for our needs. However, one soon finds that the setting for which the method was developed differs in essential aspects from our problem, and several requirements of the method are not met. In particular, the scheme was developed to couple spatially separate atomic and continuum simulations where the interface is rigid, i.e. the atoms on the interface are neither exchanged nor interchanged. This essentially restricts the method to solids or similar static structures such as nanotubes. The parameters to be transported across the scales are similarly limited, e.g. to the physical force and displacement respectively. In the MD system, the aforementioned static interface atoms are referred to as *ghost atoms*, which are tied to the displacement and physical force of the bulk material to establish the interface towards the continuous domain. In return, a technique called *time history kernel* is used to extrapolate the fine scale displacement of these ghost atoms in order to interface with the discrete scale. This requires the use of inverse Fourier- and Laplace transforms. [Tan06, Liu, Dre08, Far07]

3.2.3 Homogenization

Prior to introducing our upscaling method, we will present another multiscale approach. The homogenization theory is different from the previously introduced methods in the sense that it does not allow upscaling from a discrete (atomic) level, but it is used as a scaling mechanism between two continuous levels. It is thus of no use in the initial upscaling from the MD simulations. However, after those upscalings are complete, there are certain circumstances in which a homogenization-like approach might add to the the validity of our computations and this shall be outlined here. Homogenization is a technique used in cases in which coefficient functions of a partial differential equation oscillate rapidly on a periodic or semi-periodic domain. By analyzing the behavior of the solution on the periodic cells, one is able construct effective, non-oscillating coefficients for the bulk domain. When we deal with structures whose characteristic features have length scales which fit into an MD simulation cell, the method of homogenization would be of no use to us, as we have resolved all structural information. Should we encounter a material however, which undergoes a change on a length scale larger than an MD simulation domain ($\tilde{5}$ -10nm), we are bound to perform simulations on each of the two characteristic samples and either simulate our macroscale with a refinement which resolves the appropriate length scale, or we need to average over the obtained values. It is the latter case in which the homogenization procedure might prove helpful. However, the theory of homogenization does place certain requirements on the solution and coefficient functions, which are not always fulfilled. The most notable clash between the requirements of the homogenization procedure and the physical reality occurs when we intend to average over a domain which contains regions in which the coefficient functions are zero. While the averaging computations can still be performed, it is no longer possible to guarantee that the results from the homogenized equation are the limit of the results of the oscillating equation. Since on the other hand such a convergence is not out of the question and might be proved, we will present the required averaging computations in the appendix A.

3.3 The Method of Averaging and the Continuity Equation

Due to the shortcomings of the previously described methods, we turn towards the so called method of averaging [Sal98], which will provide us with the means to transform a discrete system into a continuous one, exchanging the notion of individual particle positions for one of particle concentration. The potency of the method becomes apparent right from the beginning, when basic manipulations on the averaging integral yield the well known continuity equation.

For an instructive derivation of the method, we introduce a discrete concentration function¹

$$\tilde{c}(x) = \sum_{p: x_p \in \Omega} \delta(x - x_p) \quad (3.1)$$

¹ In order to be precise, one should in this case avoid the term “function” in favor of the term “distribution” as only after integration we obtain a function from $\mathbb{R}^3 \rightarrow \mathbb{R}$ in the traditional sense. The delta distribution is defined to be the unique distribution with the property $\int \delta(x - x_0) f(x) dx = f(x_0)$

where Ω denotes the whole domain of the particles and x_p is the location of particle p . This allows to put forth the following definition of concentration:

$$c(x) = \frac{1}{|B_r(x)|} \int_{B_r(x)} \tilde{c}(x') dx' \quad (3.2)$$

where $B_r(x)$ is a topological sphere of radius r around the point x . The choice of r needs to reflect the physical reality at that point: On the one hand being much larger than the average distance between particles in the vicinity, on the other hand being sufficiently small, so that the resulting function $c(x)$ would not exhibit significant different values at points x_1 and x_2 with $|x_1 - x_2| \leq r$.

We will now use the above method to derive the well known continuity equation (for now ignoring possible contributions by chemical reactions within the system). Applying the time derivative to (3.2), we obtain

$$\frac{\partial c}{\partial t} = \frac{\partial}{\partial t} \frac{1}{|B_r(x)|} \int_{B_r(x)} \sum_{p: x_p \in \Omega} \delta(\tilde{x} - x_p) d\tilde{x} \quad (3.3)$$

We substitute $x' = \tilde{x} - x$. It should be noted that $\frac{1}{|B_r(x)|} = \frac{1}{|B_r(y)|}$ for all x and y , since the volume of the ball is constant, only its position changes. This allows for commutation with the differentials:

$$= \frac{\partial}{\partial t} \frac{1}{|B_r(0)|} \int_{B_r(0)} \sum_{p: x_p \in \Omega} \delta(x + x' - x_p) dx' \quad (3.4)$$

$$= \frac{1}{|B_r(0)|} \int_{B_r(0)} \sum_{p: x_p \in \Omega} \frac{\partial}{\partial t} \delta(x + x' - x_p) dx' \quad (3.5)$$

$$= \frac{1}{|B_r(0)|} \int_{B_r(0)} \sum_{p: x_p \in \Omega} \sum_{i=1}^3 \frac{\partial \delta(x + x' - x_p)}{\partial x_p^i} \frac{\partial x_p^i}{\partial t} dx' \quad (3.6)$$

$$= \frac{1}{|B_r(0)|} \int_{B_r(0)} \sum_{p: x_p \in \Omega} \sum_{i=1}^3 (-1) \frac{\partial \delta(x + x' - x_p)}{\partial x^i} \frac{\partial x_p^i}{\partial t} dx' \quad (3.7)$$

$$= - \sum_{i=1}^3 \frac{\partial}{\partial x^i} \frac{1}{|B_r(0)|} \int_{B_r(x)} \sum_{p: x_p \in \Omega} \delta(x + x' - x_p) \frac{\partial x_p^i}{\partial t} dx' \quad (3.8)$$

$$= - \nabla \frac{1}{|B_r(0)|} \int_{B_r(0)} \sum_{p: x_p \in \Omega} \delta(x + x' - x_p) \frac{\partial \vec{x}_p}{\partial t} dx' \quad (3.9)$$

$$= - \nabla \frac{1}{|B_r(x)|} \int_{B_r(x)} \sum_{p: x_p \in \Omega} \delta(\tilde{x} - x_p) \frac{\partial \vec{x}_p}{\partial t} d\tilde{x} \quad (3.10)$$

$$= - \nabla \vec{J}, \quad (3.11)$$

where \vec{J} is called the flux of the particles, their averaged movement throughout the domain.¹

As stated above, this equation ignores the possibility of particles being created or removed within the domain without crossing its boundary, as might be a result from a chemical reaction. In this case, the net reaction rate needs to be added to the change of concentration, which leads to

$$\frac{\partial c}{\partial t} = -\nabla \vec{J} + R, \quad (3.12)$$

where R is the reaction rate. The task is now to obtain the contributions to the molecular flux \vec{J} and the reaction rate R as they appear in ionic migration.

In order to distinguish the contributions to the flux, we consider its definition, where we separate the velocity of each particle into an average part and individual, random movement.

$$\vec{J} = \frac{1}{|B_r(x)|} \int_{B_r(x)} \sum_{p: x_p \in \Omega} \delta(x - x_p) \frac{\partial \vec{x}_p}{\partial t} dx \quad (3.13)$$

$$= \frac{1}{|B_r(x)|} \int_{B_r(x)} \sum_{p: x_p \in \Omega} \delta(x - x_p) \vec{v}_p dx \quad (3.14)$$

$$= \frac{1}{|B_r(x)|} \int_{B_r(x)} \sum_{p: x_p \in \Omega} \delta(x - x_p) (\vec{v}_p - \langle v \rangle + \langle v \rangle) dx \quad (3.15)$$

$$= \frac{1}{|B_r(x)|} \int_{B_r(x)} \sum_{p: x_p \in \Omega} \delta(x - x_p) (\vec{v}_p - \langle v \rangle) dx \quad (3.16)$$

$$\underbrace{\hspace{10em}}_{\text{diffusion}} + \underbrace{\frac{1}{|B_r(x)|} \int_{B_r(x)} \sum_{p: x_p \in \Omega} \delta(x - x_p) \langle v \rangle dx}_{\text{convection}}. \quad (3.17)$$

We observe that the expression can be split into two parts, the first of which contains solely the random movement of the particles, called *diffusion*, whereas the latter contains the mean value of the movement, called *convection*. While this splitting is trivially obtained, it is fundamental for the following derivations, which could not be performed on the closed expression.

3.4 Diffusion

We begin our derivation of the flux by relating the random, undirected movement of the molecules (their diffusion) to a contribution to the molecular flux.

¹ Note that the popular proof of the continuity equation, by applying Gauss's theorem (sometimes also known as the divergence theorem) to the integral over the flux along the boundary of the domain, is infeasible in this setting, since the boundary is a domain of measure zero with respect to the positions of the individual particles.

While poetic descriptions of diffusive behavior go back as far as the first century BC [Carhr], its discovery is generally attributed to Robert Brown in 1827, whose findings resulted in physicists giving attention to the matter and connecting the macroscopic observations to molecular and atomic movement, among them the notable works of Einstein at the beginning of the 20th century [Ein06].

In section 2.3.4 it was established that at non-zero temperatures, particles have a characteristic non-zero kinetic energy, which translates into a characteristic velocity. In the absence of (intra-atomic) forces, such as structural bonds or fields in the substance, this motion could be expected to continue indefinitely. However, due to the sheer number of particles present in any reasonable amount of material (under standard conditions, one liter of H₂ contains $2.8 \cdot 10^{22}$ particles, so in general we are dealing with magnitudes on the order of Avogadro's number), collisions between particles are bound to happen, resulting in the application of force even in ideal gases or fluids. Knowing that no structural deformation of the particles will occur¹, we can assume all collisions to be completely elastic, so that the sum of the momenta of the particles is preserved.

These ongoing collisions among themselves, to which the particles are subjected, reorient their directions and disperse them. This dispersion results in a random, statistical movement of the particles, even in presence of an external force field, which would encourage a preferred direction of motion in space. This random component in the movement of particles is called Brownian motion and will be discussed in the forthcoming section. We call particular attention to the fact that we improve upon the form used in the literature by considering simultaneous convective contributions to the movement of the particles and removing those contributions from the diffusion calculation.

3.4.1 Derivation of Brownian Motion as the Source of Diffusion

Since we intend to derive our equations from first principles, we cannot follow Einstein's fundamental derivation in [Ein06], since he draws from the concept of osmotic pressure and friction. Instead, we will look at a specific, discretized example of particle movement in order to obtain a connection of the flux of particles with Brownian motion.

Let Ω_1 and Ω_2 be two cubic cells with edge length l which share one face Γ . Let Ω_i contain n_i particles, each with a velocity v_i of common magnitude v (see figure 3.1). This simplification does keep the orientation of the particles random, which is decisive for the phenomenon. Nevertheless we will allow for random velocities in 3.4.2. For now, we fix a time step δt such that $\delta t \cdot v = \sqrt{3}l$. This ensures that all particles within the box pass through one of its faces within one timestep. A particle will then cross the interface Γ during δt when its movement is oriented in the "correct" direction. To obtain the average probability $P(\Gamma)$ for a particle to cross Γ , we average the solid angle $\omega(\vec{x})$ of Γ from the point \vec{x} over all points in the cell Ω_i

¹ The kinetic energies achieved by molecular motion in everyday matter are far below those used by particle accelerators, where destruction of the particles may take place. Although chemical reactions between colliding particles might occur, this will not be taken into account at this time, but discussed in a later section.

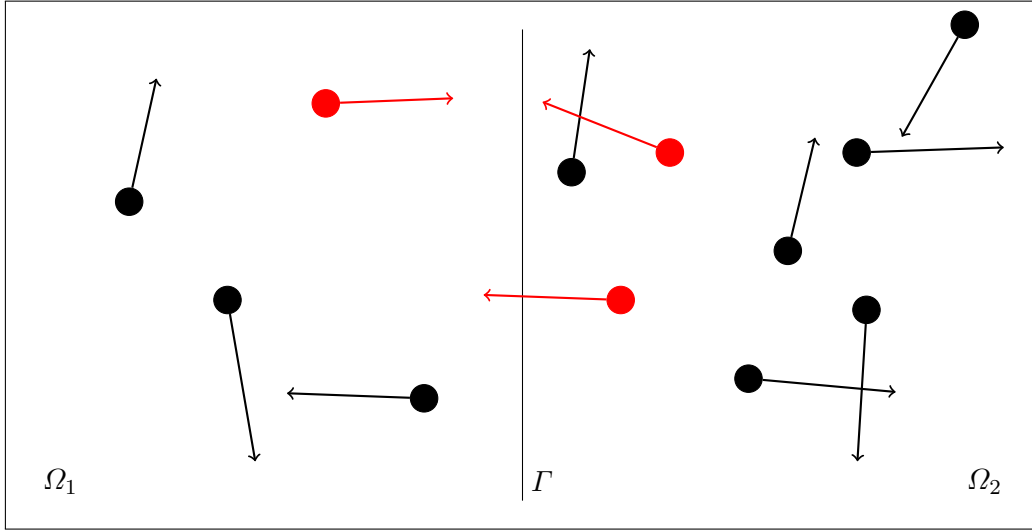


Figure 3.1: Exemplification of a diffusion process. Notice that the right cell contains twice as many particles as the left one, and on average twice as many particles will cross the interface from right to left as the other way around.

and divide by the full solid angle 4π . This results in the formula

$$P(\Gamma) = \frac{1}{|\Omega_i|} \int_{\Omega_i} \frac{\omega(\vec{x})}{4\pi} d\vec{x} = \frac{1}{|\Omega_i|} \frac{1}{4\pi} \int_{\Omega_i} \int_{\Gamma} \frac{(\vec{x} - \vec{y})\vec{n}}{|\vec{x} - \vec{y}|^3} d\vec{y} d\vec{x} \quad (3.18)$$

where \vec{n} is the normal vector of Γ . Executing the integration results in a probability factor of $\frac{1}{6}$.

It is then apparent that the particle flux across Γ in direction from Ω_1 to Ω_2 will be

$$J_1 = P(\Gamma)vn_1 = \frac{1}{6} \frac{l}{\delta t} n_1 \quad (3.19)$$

and equivalently $J_2 = \frac{1}{6} \frac{l}{\delta t} n_2$ in the other direction. The cumulated flux of particles across Γ is then

$$J_{tot} = \frac{1}{6} \frac{l}{\delta t} (n_1 - n_2). \quad (3.20)$$

Now using the aforementioned technique of averaging over those two cells (for now allowing integration over cubes instead of spheres), we obtain a difference in concentration rather than in particles: $\frac{1}{6} \frac{l}{\delta t} (c_1 - c_2)$. This in turn allows us to express the difference in terms of the discrete gradient: $c_1 - c_2 \simeq -l \cdot \nabla c \Leftrightarrow \frac{c_1 - c_2}{l} \simeq -\nabla c$. The negative sign stems from the fact that the gradient always points in the direction of the steepest ascent and the particles will on average move in the direction of descending concentration. Thus we have the expression

$$J_{diff} = -\frac{1}{6} \frac{l^2}{\delta t} \nabla c = -D \nabla c \quad (3.21)$$

for the flux J across the face Γ , where we have introduced the diffusion coefficient D , depending on the mean distance of the particles travelled during the time interval δt :

$$D = \frac{1}{6} \frac{l^2}{\delta t}. \quad (3.22)$$

3.4.2 Mean Square Distance

In the previous section we have derived a connection between the movement of particles and the flux of their concentration in a trivial example. In order to apply this to more complex systems, the term $\frac{l^2}{\delta t}$ will need to be reviewed, since the particles cannot be expected to move at the same speed, so the mean distance between collisions will be different. In order to average over the individual particles' square displacement, we define the averaging operator

$$\langle X \rangle_k = \frac{1}{n} \sum_{i=0}^n X(k_i). \quad (3.23)$$

When in the future omitting k in the notation, we always refer to the averaging over the number of particles. Furthermore, we define the variable

$$r_i(t) = x_i(t) - x_i(0), \quad (3.24)$$

expressing the position change undergone by a particle i after the time t has passed. While we are interested in the mean motion of an indexed particle set with n particles over time, it is fruitless to regard the mean displacement

$$\langle r(t) \rangle = \frac{1}{n} \sum_{i=0}^n (r_i(t)) \quad (3.25)$$

since at the present we are interested in the contribution induced by random movement. The above relation will give zero in the absence of an outer force and otherwise will give an approximation of the corresponding convective term in the presence of one.

The general mean square distance, which is direction independent, reads as

$$\langle r^2(t) \rangle = \frac{1}{n} \sum_{i=0}^n (r_i(t))^2, \quad (3.26)$$

resulting in the following formula for the diffusion coefficient:

$$D = \frac{1}{6} \frac{\langle r^2(t) \rangle}{t}. \quad (3.27)$$

It is here that we deviate from the known derivation of the Einstein relation, which is restricted to this form of the mean square displacement. However, when there is an additional directed component present during the measurement, it is necessary to correct for this convection induced movement, which might taint the results. Obtaining the undirected mobility of the

particles can easily be achieved by subtracting the mean displacement (3.25) before squaring in (3.26), resulting in

$$\langle L^2(t) \rangle = \frac{1}{n} \sum_{i=0}^n (r_i(t) - \langle r(t) \rangle)^2. \quad (3.28)$$

In this equation we measure in fact the variance of the variable “distance traveled”, which will later enable the use of standard error estimation techniques for variance expressions. From this variance we can compute the diffusion over the time interval t

$$D = \frac{1}{6} \frac{\langle L^2(t) \rangle}{t}. \quad (3.29)$$

We take note of the following analytic equivalences for $T = N \cdot \delta t$:

$$\frac{1}{6} \frac{\langle L^2(T) \rangle}{T} = \frac{1}{6} \frac{\langle L^2(T) \rangle - 0}{T} \quad (3.30)$$

$$= \frac{1}{6} \frac{\langle L^2(T) \rangle - \langle L^2(0) \rangle}{T} \quad (3.31)$$

$$= \frac{1}{6} \frac{\langle L^2(T) \rangle - \langle L^2(0) \rangle}{N \cdot \delta t} \quad (3.32)$$

$$= \frac{1}{6N} \sum_{i=1}^N \frac{\langle L^2(i \cdot \delta t) \rangle - \langle L^2((i-1) \cdot \delta t) \rangle}{\delta t} \quad (3.33)$$

$$\xrightarrow{\delta t \searrow 0} \frac{1}{6} \left\langle \frac{\partial \langle L^2(t) \rangle}{\partial t} \right\rangle_t, \quad (3.34)$$

where in (3.33) we expand the telescopic sum. In the context of a continuous average, the above reads

$$\frac{1}{6} \left\langle \frac{\partial \langle L^2(t) \rangle}{\partial t} \right\rangle_t = \frac{1}{6T} \int_0^T \frac{\partial \langle L^2(t) \rangle}{\partial t} dt \quad (3.35)$$

$$= \frac{1}{6T} \int_0^T d \langle L^2(t) \rangle \quad (3.36)$$

$$= \frac{1}{6T} \langle L^2(T) \rangle. \quad (3.37)$$

Those results are significant since our initial derivation relates the diffusion coefficient to one single time step. Since measuring at a single time is prone to statistical errors, averaging over several data points is a general method to obtain more accurate results. For this particular problem we have thus demonstrated that applying averaging is not only a heuristic method to eliminate random errors but moreover analytically equivalent to the single measurement over the complete time.

3.4.3 Velocity Autocorrelation

When using the above expressions in the context of the previously presented molecular simulation, additional attention needs to be paid to periodic boundary conditions. When a particle crosses a boundary and the variable $\vec{r}_i(t)$ is consequently adjusted, the actual distance travelled is not simply $\vec{r}_i(t)$, but $\vec{r}_i(t) + \vec{l}$, where $|\vec{l}|$ is the box length in the direction of the border crossed. Furthermore, should the particle travel further and cross the box boundary a second (or more general n^{th}) time, the distance becomes $r_i(t) + n_x \vec{l}_x + n_y \vec{l}_y + n_z \vec{l}_z$. This includes the necessity to track the direction of the crossing, as particles going back and forth over the same border do not actually accumulate distance but stay at approximately the same distance. There is a mathematically equivalent approach, foregoing the necessity to keep track of those passages, which is not based on the averaging over distances but integrating over the velocities. This numerically different approach to the calculation of the diffusion coefficient is the so called Velocity Autocorrelation (VAC). We start from the classic equation

$$r(t) = \int_0^t v(\tau) d\tau, \quad (3.38)$$

which we insert into our expression for the diffusion coefficient. We begin by presenting the short derivation for the uncorrected VAC formula before introducing our improvement:

$$D = \frac{1}{6} \frac{\partial}{\partial t} \langle r^2(t) \rangle \quad (3.39)$$

$$= \frac{1}{6} \frac{\partial}{\partial t} \int_0^t \int_0^t \langle v(\tau') v(\tau'') \rangle d\tau' d\tau'' \quad (3.40)$$

$$= \frac{2}{6} \frac{\partial}{\partial t} \int_0^t \int_0^{\tau'} \langle v(\tau') v(\tau'') \rangle d\tau' d\tau'' \quad (3.41)$$

$$= \frac{1}{3} \frac{\partial}{\partial t} \int_0^t \int_0^{\tau'} \langle v(\tau'' - \tau') v(0) \rangle d\tau' d\tau'' \quad (3.42)$$

$$= \frac{1}{3} \int_0^t \langle v(t - \tau) v(0) \rangle d\tau \quad (3.43)$$

Equality (3.42) is a result of the fact that the VAC function as an “equilibrium property is invariant under changes of the time origin” [Fre02] (see also section 2.4.2).

Finally, using the ergodic limit we obtain

$$D = \frac{1}{3} \lim_{t \rightarrow \infty} \int_0^t \langle v(t - \tau) v(0) \rangle d\tau = \frac{1}{3} \int_0^\infty \langle v(\tau) v(0) \rangle d\tau. \quad (3.44)$$

As stated before, this formula does not account for possible convective movement of the atoms. In order to prevent those terms from tainting the results, we derive a convection correction corresponding to the one we have developed for the mean square displacement. Beginning with the respective convection corrected variant, we find that

$$\langle L^2(t) \rangle = \frac{1}{n} \sum_{i=0}^n (r_i(t) - \langle r(t) \rangle)^2 \quad (3.45)$$

$$= \frac{1}{n} \sum_{i=0}^n \left(\int_0^t v_i(\tau) d\tau - \left\langle \int_0^t v d\tau \right\rangle \right)^2 \quad (3.46)$$

$$= \frac{1}{n} \sum_{i=0}^n \left(\int_0^t v_i(\tau) d\tau - \int_0^t \langle v \rangle d\tau \right)^2 \quad (3.47)$$

$$= \frac{1}{n} \sum_{i=0}^n \left(\int_0^t v_i(\tau) - \langle v \rangle d\tau \right)^2 \quad (3.48)$$

$$= \frac{2}{n} \sum_{i=0}^n \int_0^t \int_0^\tau (v_i(\tau)v_i(\tau') - v_i(\tau)\langle v(\tau') \rangle - \langle v(\tau) \rangle v_i(\tau') + \langle v(\tau) \rangle \langle v(\tau') \rangle) d\tau' d\tau \quad (3.49)$$

$$= 2 \int_0^t \int_0^\tau \left(\frac{1}{n} \sum_{i=0}^n [v_i(\tau)v_i(\tau')] - \frac{1}{n} \sum_{i=0}^n [v_i(\tau)\langle v(\tau') \rangle] \right) d\tau' d\tau \quad (3.50)$$

$$- \frac{1}{n} \sum_{i=0}^n [\langle v(\tau) \rangle v_i(\tau')] + \frac{1}{n} \sum_{i=0}^n [\langle v(\tau) \rangle \langle v(\tau') \rangle]) d\tau' d\tau \quad (3.51)$$

$$= 2 \int_0^t \int_0^\tau (\langle v(\tau)v(\tau') \rangle - \langle v(\tau) \rangle \langle v(\tau') \rangle - \langle v(\tau) \rangle \langle v(\tau') \rangle + \langle v(\tau) \rangle \langle v(\tau') \rangle) d\tau' d\tau \quad (3.52)$$

$$= 2 \int_0^t \int_0^\tau (\langle v(\tau)v(\tau') \rangle - \langle v(\tau) \rangle \langle v(\tau') \rangle) d\tau' d\tau. \quad (3.53)$$

We now perform the same shift in the variable as in the original derivation (3.42) and insert the above result in 3.39 to obtain

$$D = \frac{1}{3} \lim_{t \rightarrow \infty} \int_0^t \langle v(t-\tau)v(0) \rangle - \langle v(t-\tau) \rangle \langle v(0) \rangle d\tau, \quad (3.54)$$

which is the complete form of the convection corrected velocity autocorrelation.

3.4.4 Estimates on the Error

In section 3.4.2 we have established that the measure of the mean square distance is expressed as a variance of the displacement, thus we need to consider the confidence interval for the variance estimate resulting from our sampling.

With σ^2 being the variance of the actual probability distribution and s^2 being the variance of our analysed sample, the confidence interval is

$$\frac{s^2}{1 + 1.96\sqrt{\frac{2}{n-1}}} \leq \sigma^2 \leq \frac{s^2}{1 - 1.96\sqrt{\frac{2}{n-1}}} \quad (3.55)$$

$$\Leftrightarrow \left| \sigma^2 - s^2 \right| \leq 1.96 s^2 \sqrt{\frac{2}{n-1}} \quad (3.56)$$

as found in [Sac88], where in our case n is the number of particles over which we sample. Thus, for each time step, we have a quantitative estimate for the local error, which decreases with $\frac{1}{\sqrt{n}}$.

This is the error for the sampling done in each time step. When averaging over the individual time steps as proposed in 3.4.2, one would generally propagate the error following Gauss

$$(\Delta f)^2(x_1, \dots, x_m) = \sum_{i=1}^m \left[\left(\frac{\partial f}{\partial x_i} \right)^2 (\Delta x_i)^2 \right]. \quad (3.57)$$

However, when applying this formula to our averaging,

$$\Delta \langle L^2 \rangle_T = \frac{1}{N} \left[\sum_{i=1}^N (\Delta \langle L^2(t_i) \rangle)^2 \right], \quad (3.58)$$

we note that we only obtain the average of the error of all time steps. Thus, we can not expect the error to decrease by sampling over time for statistical reasons. However, in section 2.4.2 we have described the sampling of the phase space and the ergodic behavior of molecular simulations. Therefore, we do expect the error to decrease further by sampling over time, although we are not able to further quantify its decrease as we can for the one-time measurement.

We would like to point out that, once inside the area of convergence, one can theoretically speed up the convergence beyond any given polynomial degree by the use of a convolution method described in [Can03]. The method makes use of signal filtering functions, constructed from the convolution of the integration interval. However, as the authors point out themselves, while this method improves the convergence of the measurement on the sampled trajectory, it does not increase the amount of phase space from which the measurements are sampled. This is the key consideration for the sampling of complex systems.

3.5 The Convective Term

In the derivation of the flux contributions we established that, aside from the random contributions discussed in the previous section, we encounter convective terms (3.17). Convection of concentration, whether it describes microparticles in a fluid or, as it is the case here, ions, is the result of directed movement imposed on the particles in question, as already implied by the just mentioned equation. It is exactly there that we start, by integrating

$$\frac{1}{|B_r(x)|} \int_{B_r(x)} \sum_{p: x_p \in \Omega} \delta(x - x_p) \langle v \rangle dx \quad (3.59)$$

$$= \frac{1}{|B_r(x)|} \int_{B_r(x)} \sum_{p: x_p \in \Omega} \delta(x - x_p) dx \langle v \rangle \quad (3.60)$$

$$= \frac{1}{|B_r(x)|} \int_{B_r(x)} \tilde{c} dx \langle v \rangle \quad (3.61)$$

$$= c(x) \langle v \rangle. \quad (3.62)$$

While this term is straightforward in its macroscopic representation, the source of the average velocity of all particles is not yet clear. In a system with dynamical behavior of a fluidic carrier material, this movement could very well be the result of convection of the fluid itself, carrying the particles along. In our case however, the solvent is assumed to be stationary and the ions gather their velocity from two other sources which we discuss here.

One source is the electric field induced by the charge distribution, another the chemical potential. While they are quite different in their origin, the prior being the result of a “classical” electrical potential among the charged particles, the other originating from an energy evaluation of the states in the so called partition function¹. They both give rise to an effective force term, from which the *drift velocity* of the ions may be calculated. We will proceed by showing the relation between a force on the ions and their respective convective velocity before turning to the derivations of the two contributions, the electrical field and the change of the chemical potential.

3.5.1 The Einstein-Smoluchowski Relation

In this section we will deal with the relation between a force on the ions and their convective velocity, which will be valid for the two contributions to the ionic migration. From classical motion equations one would expect a force on the ions to result in accelerated movement. Experiments, however, suggest that there is no acceleration, which can be explained by the particle collisions we already described in section 3.4.

The velocity of the particles is generally several magnitudes larger than the velocity change imposed by the acceleration of the particles in the mean free time between collisions [Dem04].

¹ The partition function, which relates system properties to the number of configuration (or states) the system could adopt, is a concept used in statistical mechanics.

Thus, the effect of the force is annihilated by the scattering a particle experiences after a collision so that the effect of the force can be assumed to act on a particle which has no preferred orientation after every collision. Given the conservation of momentum one would now expect the surrounding bulk material to obtain a convective term in the same direction. However, in the physical setting we are considering, we will always find a contribution in the opposite direction as well, which will offset the impulse just described. In anticipation of the next sections, we describe those opposing contributions as the impulse transferred by ions with opposite charge, and the chemical potential/state imbalance created by a particle vacating its previous position. For these reasons it is justified to consider the forces as equilibrated in the bulk material and consider them anew after each collision.

Therefore the velocity imposed on the particle is proportional to the mean free time between collisions,

$$\vec{v}_D = \frac{\vec{F}}{m} \cdot \tau_s, \quad (3.63)$$

with the drift velocity v_D and the mass m of the particle in question. We thus have a linear relation between the drift velocity and the force applied, which we express as

$$\vec{v}_D = \nu \vec{F}, \quad (3.64)$$

where $\nu = \frac{\tau_s}{m}$ is the mobility of the particle in question. The dependence on the mean time between collisions reminds of the diffusion coefficient and indeed there is a direct dependence, the Einstein-Smoluchowski relation [Ein06, Kub66]

$$D = \nu k_B T, \quad (3.65)$$

with the Boltzman constant k_B and the temperature T . We thus obtain our convection velocity by

$$\vec{v}_D = \frac{D}{k_B T} \cdot \vec{F}. \quad (3.66)$$

3.5.2 Convection Induced by the Electric Field

We will now proceed to the derivation of the first contribution to convection, which is induced by the electric field. In essence, we will derive the field from the corresponding electric potential, which turn depends on the concentration of the charged particles of all species not only locally, but in the complete system.

The Electric Field

A particle with electric charge q at position \vec{x} experiences a Coulomb force from a particle with charge Q at position \vec{y}

$$\vec{F}(\vec{x}) = \frac{Qq}{4\pi\epsilon_0|\vec{r}|^2} \hat{r}, \quad (3.67)$$

where we have used the usual notation of $\vec{r} = \vec{x} - \vec{y}$ and $\hat{r} = \frac{\vec{r}}{|\vec{r}|}$. After “normalization” with respect to q [Dem04], this leads to the electric field

$$\vec{E}(\vec{x}) = \frac{Q}{4\pi\epsilon_0|\vec{r}|^2}\hat{r}, \quad (3.68)$$

so that

$$\vec{F} = q \cdot \vec{E}. \quad (3.69)$$

As a result, this force is directly proportional to the charge being carried by the ion. When dealing with multiple charges in a domain, the expression is summed over, yielding

$$\vec{E}(\vec{x}) = \sum_{p: x_p \in \Omega \setminus \{\vec{x}\}} \frac{Q_p}{4\pi\epsilon_0|\vec{r}_p|^2}\hat{r}_p. \quad (3.70)$$

Note that in the above expression we have excluded the evaluation point from the summation ($\Omega \setminus \{\vec{x}\}$), in order to exclude self interaction of a particle.

For dealing with a multitude of charged particles, a quasi-continuous approach is justified, and by our usual averaging approach we substitute the individual charge values Q_p by a continuous charge density function

$$\rho(x) = \frac{1}{|B_r(x)|} \int_{B_r(x)} \sum_{p: x_p \in \Omega \setminus \{\vec{x}\}} Q_p \delta(y - x_p) dy. \quad (3.71)$$

Then, the electric field is expressed by¹

$$\vec{E}(\vec{x}) = \frac{1}{4\pi\epsilon_0} \int_{\Omega} \rho(\vec{y}) \frac{\vec{x} - \vec{y}}{|\vec{x} - \vec{y}|^3} d\vec{y}. \quad (3.72)$$

Even though the above equation is sufficient to compute the value of $E(x)$ throughout the domain, it is not a useful expression in a numerical sense, since each point evaluation would require a separate calculation of the integral on the right hand side. In order to obtain a more suitable function we turn towards the concept of electric potential, which allows a faster evaluation of the function for multiple point values.

The electric field is a conservative one, see introductory works on electrodynamics, for example [Dem04]. Conservative force fields can be expressed as the gradient of a scalar potential function [Bro01] so that

$$\vec{E} = -\nabla\Phi. \quad (3.73)$$

¹ In the reverse direction one can easily compute the discrete formula by separating Ω in subdomains which contain one particle each and exchange summation and integration.

Now we have assembled all pieces using (3.66) in order to obtain

$$\vec{J}_e = \vec{v}_D \cdot c \quad (3.74)$$

$$= \nu \vec{F} \cdot c \quad (3.75)$$

$$= \frac{D}{k_B T} \vec{F} \cdot c \quad (3.76)$$

$$= \frac{D}{k_B T} q \vec{E} \cdot c \quad (3.77)$$

$$= -D \frac{z \cdot e}{k_B T} \nabla \Phi \cdot c \quad (3.78)$$

$$= -D \frac{z \cdot F}{RT} \nabla \Phi \cdot c, \quad (3.79)$$

where z is the charge number of the ionic species in question such that $q = z \cdot e$, F is the Faraday constant and R the ideal gas constant.

The Poisson Equation

In the previous section we have derived the convection contribution in terms of the electrical potential. While we have stated that the latter will depend on the ionic concentration in the system, this remains to be shown. By using the first of the well known Maxwell equations [Dem04] (which is also known as Gauss's law)

$$\operatorname{div} \vec{E} = \frac{\rho}{\varepsilon_0 \varepsilon_r}, \quad (3.80)$$

where ε_0 and ε_r are the dielectric constant and its material dependent correction, respectively, and substituting the electric potential for the electric field ($-\nabla \Phi = \vec{E}$), we establish the Poisson Equation

$$-\Delta \Phi = \frac{\rho}{\varepsilon_0 \varepsilon_r}. \quad (3.81)$$

From here we require an expression for ρ , which is the continuous function obtained by averaging over all charges in the solution. We modify equation (3.71) by referring to different ionic species with charge $q_i = z_i \cdot e$ by the index i :

$$\rho(x) = \sum_i \frac{1}{|B_r(x)|} \int_{B_r(x)} \sum_{p_i: x_{p_i} \in \Omega \setminus \{\bar{x}\}} \delta(x' - x_{p_i}) q_i dx' \quad (3.82)$$

$$= F \sum_i z_i c_i(x) \quad (3.83)$$

This expression allows the calculation of the right hand side of the Poisson Equation by summing up the concentrations of the charged particles. Finding the solution to the Poisson equation is then a standard task, which we will treat in chapter 4.

3.5.3 Convection Induced by the Chemical Potential

This term in the ionic migration is not owed to an actual force on a particle, but is in itself a statistical effect, very much like the diffusion term, resulting in a virtual force. As a consequence attempts have been made to combine both effects into one, by modifying the diffusion coefficient depending on the regional chemical potential [Lec08]. While there is some merit to the idea, since both effects describe a probability of particle displacement, their actual nature is quite different. Whereas the pure diffusion depends on a concentration disparity of the species observed under the same surrounding conditions, the chemical potential introduces the influence of the surrounding (thermodynamical) system. The first subsection will deal with a brief introduction into the thermodynamical concepts required for the definition of the term. Then, the contribution to the ionic flux will be discussed before describing the method to obtain the chemical potential.

Definition of Chemical Potential

Intuitively speaking, the chemical potential is an energy contribution associated with the number of particles of a certain species in a system. When the number of particles is changed, the energy of the system changes proportionally to the number of particles changed. The proportionality constant μ is the chemical potential. For a more formal definition we consider two isolated thermodynamical systems, which are in thermodynamical equilibrium, have a constant volume V and each a different internal energy U_i . This internal energy corresponds to another thermodynamical parameter, the (Helmholtz) free energy, which is defined as

$$F(T, V, N_i) = U - TS, \quad (3.84)$$

where U is the aforementioned internal energy, S is the entropy of the system and T its temperature. When bringing those two systems into contact, allowing particles to be interchanged from one system to the other, the second law of thermodynamics states that the combined energy of the systems decreases towards a minimum¹. Since no heat is exchanged between the two systems (proposed thermodynamical equilibrium) and their volume is constant, the only way to change their combined energy is the exchange of particles, which is formally expressed by

$$F(T, V, N_i) = F_1 + F_2 \quad (3.85)$$

$$\Rightarrow dF = \left(\frac{\partial F_1}{\partial N_1} \right)_{T,V} dN_1 + \left(\frac{\partial F_2}{\partial N_2} \right)_{T,V} dN_2. \quad (3.86)$$

Since the systems are isolated apart from being in contact with each other, it is also known that

$$0 = dN = dN_1 + dN_2, \quad (3.87)$$

¹ The second law of thermodynamics actually states that entropy increases, however this yields a decrease of energy by the fundamental thermodynamic relation in general or equation (3.84) in particular.

so that

$$dF = \left[\left(\frac{\partial F_1}{\partial N_1} \right)_{T,V} - \left(\frac{\partial F_2}{\partial N_2} \right)_{T,V} \right] dN_1 = 0, \quad (3.88)$$

where the zero on the right hand side arises from the requirement that the free energy be minimal. We then define

$$\left(\frac{\partial F}{\partial N_i} \right)_{T,V} = \mu_i(T, V, N_i) \quad (3.89)$$

as the chemical potential. We further say that if $\mu_i = \mu_j$, the systems i and j are in chemical equilibrium. Further details and additional interconnections with other thermodynamic properties can be found in [Kit80].

The Chemical Potential as a Driving Force

We now consider two systems which are not in equilibrium, i.e. there is a difference in chemical potential. Then equation (3.88) will be replaced by

$$dF = \left[\left(\frac{\partial F_1}{\partial N_1} \right)_{T,V} - \left(\frac{\partial F_2}{\partial N_2} \right)_{T,V} \right] dN_1 = (\mu_1 - \mu_2) dN_1. \quad (3.90)$$

With F not at a minimum, the value of dF must be negative. We consider two possible cases:

- $\mu_1 > \mu_2 \Rightarrow dN_1 < 0$, particles flow from system one (with higher chemical potential) to system two,
- $\mu_1 < \mu_2 \Rightarrow dN_1 > 0$, particles flow from system two (with higher chemical potential) to system one.

We thus conclude from the minimum assumption that particles will flow in the direction of the lower chemical potential; that is, they follow the negative gradient of the chemical potential. Moreover, the statistical “force”¹ exerted on the particles is the gradient of the chemical potential [Cra95]. In order to compute the actual flux, we again make use of the Einstein-Smoluchowski relation (3.65). Inserting $-\nabla\mu$ as the force, we obtain the drift velocity

$$\vec{v}_D = -\nabla\mu \cdot \frac{D}{k_B T} \quad (3.91)$$

and thus

$$\vec{J}_{chem} = -\nabla\mu \cdot \frac{D}{k_B T} c \quad (3.92)$$

¹ It cannot be stressed enough that the chemical potential is a thermodynamical and thus statistical parameter only, any individual particle will not be subject to a measurable force, but the bulk of particles behaves as if experiencing a virtual force.

as the transport contribution.

Obtaining the Chemical Potential from Molecular Dynamics

When wishing to extract the chemical potential from molecular dynamics, one faces the challenge that the defining equations of the chemical potential, namely the derivatives of the thermodynamical energy functions with respect to particle numbers, have no direct measurable correspondent in molecular dynamical simulations. Nevertheless, some methods have been developed, of which the Widom test particle method is probably the most well known. It has been designed for Monte Carlo Methods and proceeds by adding a test particle to an accepted system configuration. The resulting change in energy is then used to calculate the chemical potential (for details on this method see [Hab95, Fre02]). Unfortunately, as this method has been designed for use with the Monte Carlo Method, it is in its original form not suitable to be used with molecular dynamics simulations.

Therefore, another approach needs to be found which is compatible with dynamical simulation. Closely following [Hab95], we note that the total differential of the free energy is

$$dF = -SdT - pdV + \mu dN, \quad (3.93)$$

from which we deduce

$$-\left(\frac{\partial p}{\partial N}\right)_{T,V} = \left(\frac{\partial \mu}{\partial V}\right)_{T,N}. \quad (3.94)$$

We then compute the symbolic equivalence,

$$\left(\frac{\partial}{\partial V}\right)_{T,N} = \left(\frac{\partial n}{\partial V}\right)_{T,N} \left(\frac{\partial}{\partial n}\right)_{T,N} = -\frac{N}{V^2} \left(\frac{\partial}{\partial n}\right)_{T,N} \quad (3.95)$$

where we have used the particle density

$$n = \frac{N}{V} \quad (3.96)$$

$$\Rightarrow \frac{\partial n}{\partial V} = -\frac{N}{V^2}. \quad (3.97)$$

Now combining (3.94) and (3.95), we obtain

$$\left(\frac{\partial \mu}{\partial n}\right)_{T,N} = -\frac{V^2}{N} \left(\frac{\partial \mu}{\partial V}\right)_{T,N} = \frac{V}{n} \left(\frac{\partial p}{\partial N}\right)_{T,V} = \frac{1}{n} \left(\frac{\partial p}{\partial n}\right)_{T,N}, \quad (3.98)$$

which after some computations [Hab95] leads to the final equation

$$\frac{\mu}{k_B T} = \ln(n_0 \Lambda^3) + \left(\frac{pV}{Nk_B T} - 1\right) + \int_{n_0}^n \left(\frac{pV}{Nk_B T} - 1\right) \frac{dn'}{n'}, \quad (3.99)$$

where $\Lambda = \left(\frac{2\pi\hbar^2}{mk_bT}\right)^{\frac{1}{2}}$ is the De-Broglie wavelength and n_0 should be a small, albeit non-zero density value, for which μ_0 is known. A good choice for n_0 is a density, for which the ideal gas relations, $\mu_0 = k_B T \ln(n_0 \Lambda^3)$ and $pV = nk_B T$, hold. The values for the different particle densities cannot be obtained from a single simulated trajectory, as this would change the virtual entirety 2.4.2. Instead we start several simulations with the corresponding particle densities, which then provide the required values for the integration (see section 5.2.1).

3.6 Compiling the Extended Nernst-Planck Equation

In the previous sections of this chapter we have established that the change of ionic flux is responsible for the change in ionic concentration. We have further derived the various contributions to the molecular flux and so the remaining task is to combine those contributions and present the complete model equation for the ionic flux. We start with 3.11:

$$\frac{\partial c}{\partial t} = -\nabla \cdot \vec{J} \quad (3.100)$$

$$= -\nabla \cdot \left(\vec{J}_{diff} + \vec{J}_e + \vec{J}_{chem} \right) \quad (3.101)$$

$$= -\nabla \cdot \left(-D\nabla c - D\frac{ze}{k_B T} \nabla \Phi c - \nabla \mu \frac{D}{k_B T} c \right) \quad (3.102)$$

$$= \nabla \cdot \left(D \left(\nabla c + \frac{z \cdot e \nabla \Phi + \nabla \mu}{k_B T} c \right) \right) \quad (3.103)$$

This is the extended Nernst-Planck equation for ion migration. While the unextended form omits the chemical potential μ , this extension is also found with the chemical activity $\ln \gamma$ instead of the chemical potential [Sam99]. However, since the equation makes use of the gradient, both expressions are equivalent up to multiplication with the constant factor RT , since $\mu = \mu_0 + RT \ln \gamma$ [Lec08]. Together with the Poisson Equation

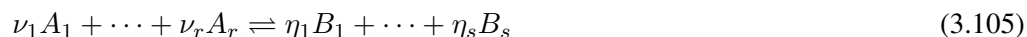
$$-\Delta \Phi = \frac{F}{\epsilon_r \epsilon_0} \sum_i z_i c_i(x) \quad (3.104)$$

we now have the complete, extended Poisson-Nernst-Planck equation system assembled.

3.7 Additional Reactive Contributions

In section 3.3 we have already pointed out that the continuity equation does not account for the addition or subtraction of particles within the averaging sphere. Such changes would be the result of chemical reactions. Although reaction terms are generally not included even in the extended Poisson-Nernst-Planck system, whose coefficients are the main focus of this paper, we will present an approach to include reactive behavior under certain assumptions. First however, we present an overview of other possible treatments. Chemical reactions do not create or destroy particles as physical matter. However, they alter their behavior to a degree such that it is justified to consider the reactants removed from their respective species, whereas

their product will be added to another one. Reactions can generally be described by reaction equations of the form



where A_i and B_i denote the respective molecular species taking part in the reaction, and the *stoichiometric coefficients* ν_i and η_i denote their respective multiplicity. It is generally accepted to use the same shorthands on both sides of the equation, indexing from 1 to $r + s$. One then sets $\nu_{r+i} = -\eta_i$ to denote that those coefficients apply to the backwards reaction. Using the law of mass action [Krä04], reaction rates are then

$$R_i = k_i^f \prod_{j=1, \nu_{ji} > 0}^{r+s} c_j^{\nu_{ji}} - k_i^b \prod_{j=1, \nu_{ji} < 0}^{r+s} c_j^{-\nu_{ji}}, \quad (3.106)$$

where k_i^f and k_i^b are reaction rate coefficients of the forward and backward reaction, respectively. Observing these equations, we notice several challenges. The first is the possibly highly nonlinear dependence of the reaction rate on the present concentration, if the respective stoichiometric coefficients $\nu_i > 1$ or $\eta_i > 1$. The second challenge is to obtain both the forward and backward reaction rate coefficients k_i^f and k_i^b . This is a problem which has not yet been completely solved, although several attempts have been made towards the solution of the subject as far back as 1960. It has been proposed to obtain the *rate of exchange* from quantum statistical computations, observing the forming and dissolving of bonds over time and taking the energy weighted average over the rate of change of the members of the respective species [Yam60]. While the subject has been worked on since, even in modern research computations are still limited to quantum mechanical systems restricted to unimolecular reactions (meaning reactions which have only have a single product type). Attempts to obtain reaction values from a molecular dynamics approach, as described in chapter 2, would face the problem that atoms forming new chemical bonds would undergo a change in their respective electron state, which would require a change in all effective potentials of these atoms. For most systems of interest, such a model has not been developed yet.

A completely different approach is described in [Krä04]. There, the transport equations are extended with the reaction rates, and by building linear combinations, the reaction rates are removed or, respectively, brought to equilibrium. This procedure, however, introduces non-linear and non-physical terms in the transport equations, in essence destroying the physical Poisson-Nernst-Planck model.

In order to retain the correct physical model, we are thus bound to restrict the chemical reactions to those of certain properties so that we can incorporate them into the PNP-system without jeopardizing its physical accuracy. We will present two possible approaches to the incorporation of chemical reactions. The general assumption, required for both methods, is that the reaction is severely imbalanced, that is, the equilibrium is shifted almost completely to either the reactant or the product side of the reaction equation.

Then, the first requirement would be that we deal with unimolecular reactions. In this case, the reaction rate would depend linearly on each species, which would enable us to extend the Nernst-Planck equation by a linear reaction rate to the present diffusion and convection term.

The addition would bring the Nernst-Planck equation into the following form:

$$\nabla \cdot \left[D_i \left(\nabla c_i + \frac{z_i \cdot e \nabla \Phi + \nabla \mu_i}{k_B T} c_i \right) \right] + K_i(x) c_i(x) = \frac{\partial c_i}{\partial t}. \quad (3.107)$$

While we will not use this treatment, it can be perfectly combined with our implicit approach of solving the macroscopic equation, which we present in 4.4.

The second requirement would be that the chemical reaction occurs on a much smaller timescale than the transport of the ions. Since we already demanded that the reactions be imbalanced, we can now simply apply a complete instantaneous reaction between the discretized transport steps. For each point in space we calculate the maximum (weighted by the stoichiometric coefficient) amount of product each species could produce, if the other reactants were supplied in abundance. The minimum of those values will be added to the respective products, whereas all available reactants are reduced by the respective amount, again weighted by their stoichiometric coefficient. Such an approach will be demonstrated by an example in section 5.5.

Chapter 4

The Poisson-Nernst-Planck System

In this chapter we will describe how to determine the discretized solution to the **Poisson-Nernst-Planck** system (PNP) after the coefficient functions have been determined. To achieve this, a **Finite Element Method** (FEM) will be used. Prior to describing our numerical scheme, we will perform a dimensional analysis on the system and describe nondimensionalization, combined with a discussion to what extent such procedures will benefit us. Following this analysis we begin the discussion of the FEM by introducing the required terminology on Sobolev spaces before proceeding to the weak formulation of the Poisson-Nernst-Planck method, which is required for the FE handling. We then present the use of different boundary conditions which arise from physical problems. The core of this section will be the compilation of the complete operator of the Poisson-Nernst-Planck equation system. The ending of this chapter is devoted to a short excursion on error estimation and refinement.

4.1 Nondimensionalization

In all previous sections and chapters we have dealt with the equation in physical units. For mathematical treatment it is sensible to perform a so called nondimensionalization, which means that all quantities are converted to unitless, scalar quantities. This conversion is performed by division with a reference value, which is usually chosen to be a characteristic value of the specific problem. With a “sensible” choice, on which we will comment later, of the following:

- L in [m], the characteristic length of the simulation cell,
- τ in [s], the characteristic time scale of the process,
- \bar{u} in [$\frac{mol}{l}$], the characteristic concentration of the ionic species,
- $\bar{\Phi}$ in [V], the characteristic Voltage of the electric potential
- $\bar{\mu}$ in [J], the characteristic chemical potential
- \bar{K} in [s^{-1}], the characteristic reaction rate of the ions

we define:

$$\begin{aligned}
\vec{x} &= L \cdot \tilde{\vec{x}}, \\
t &= \tau \cdot \tilde{t}, \\
u_i &= \bar{u} \cdot \tilde{u}_i, \\
\Phi &= \bar{\Phi} \cdot \tilde{\Phi}, \\
\mu_i &= \bar{\mu} \cdot \tilde{\mu}_i, \\
K_i &= \bar{K} \cdot \tilde{K}_i,
\end{aligned} \tag{4.1}$$

where $\tilde{\cdot}$ denotes the unitless quantity.

This allows us to rewrite the PNP system (3.103) and (3.104) into the following form:

$$\begin{aligned}
\frac{\bar{u}}{\tau} \frac{\partial \tilde{u}_i}{\partial \tilde{t}} &= \frac{\bar{u}}{L^2} \tilde{\nabla} \cdot \left[D_i \left(\tilde{\nabla} \tilde{u}_i + \frac{z_i \cdot e \bar{\Phi} \tilde{\nabla} \tilde{\Phi} + \bar{\mu} \tilde{\nabla} \tilde{\mu}}{k_B T} \tilde{u}_i \right) \right] + \bar{K} \tilde{K}_i \bar{u} \tilde{u}_i \\
\frac{\bar{\Phi}}{L^2} \tilde{\Delta} \tilde{\Phi} &= \frac{F \bar{u}}{\varepsilon_0 \varepsilon_r} \sum_i z_i \tilde{u}_i
\end{aligned} \tag{4.2}$$

By reorganisation of the constants we obtain the unitless PNP system:

$$\begin{aligned}
\frac{\partial \tilde{u}_i}{\partial \tilde{t}} &= \tilde{\nabla} \cdot \left[\lambda D_i \left(\tilde{\nabla} \tilde{u}_i + p z_i \tilde{\nabla} \tilde{\Phi} + q \tilde{\nabla} \tilde{\mu} \right) \tilde{u}_i \right] + r \tilde{K}_i \tilde{u}_i \\
\tilde{\Delta} \tilde{\Phi} &= \sigma \sum_i z_i \tilde{u}_i
\end{aligned} \tag{4.3}$$

with

$$\begin{aligned}
\sigma &= \frac{F \bar{u} L^2}{\varepsilon_0 \varepsilon_r \bar{\Phi}}, \\
\lambda &= \frac{\tau}{L^2} \\
p &= \frac{e \bar{\Phi}}{k_B T} \\
q &= \frac{\bar{\mu}}{k_B T} \\
r &= \tau \bar{K}
\end{aligned} \tag{4.4}$$

Note that λ and D_i still each have physical units but their product does not. We notice that most of these substitutions have no effect on the general scale of the problem, as they are absorbed into local factors, particularly $\bar{\mu}$ in q and \bar{K} in r . While $\bar{\Phi}$ appears in p and in σ , its choice still does not affect the scale of the problem as it only appears in direct context of its nondimensionalized function $\tilde{\Phi}$. As this localization removes any impact of the choice of these denormalization constants on other characteristic constants of the system, we will not discuss them here further. Nevertheless, they can be useful for analysis of solution behavior in dependence on the relation of these constants, as are Reynolds or Peclet numbers in fluid

dynamics. However, the respective maximum of the values for the electric potential Φ might not always be clear prior to the beginning of the simulation as Φ is dynamically calculated in dependence on the rest of the system. Depending on the constant σ , it may undergo large changes within a simulation.

In our treatment of the situation, we can imagine these constants to be set to a magnitude of 1 of the respective physical unit.

The constants σ and λ are a different matter: While the influence of λ on the scale and progression of the problem seems apparent, σ appears as just another local constant. However, the magnitude of σ has profound impact on the solution of the PNP system. The constant will have the order of magnitude $10^{16} \cdot L^2$, which induces an extremely strong coupling between the charged ionic species. The profound impact of this constant will be discussed in section 5.4. The magnitude of λ is obviously dependent on the choice of L and τ . While the value of L is generally chosen from the length of the model problem, the choice of τ is not as obvious. We have stated above that λ still carries units, namely the inverse units of D_i . Thus, we investigate the product of both factors and find that, in order to have a diffusion coefficient of 1, we would need to choose $\tau = \frac{L^2}{D_i}$. While it is not feasible to scale the NP equations of the different species differently, the diffusion coefficients have a similar order of magnitude. Using this common order of magnitude instead of the individual D_i results in a joint criterion for the choice of the characteristic timescale. However, in addition to the scaling of the mathematical diffusion term, the product λD_i also factors into the convection term. Thus, the magnitude of those terms also needs to be taken into account. Depending on the individual physical setting, one can expect the electric field contribution to be large in comparison to the diffusion. In these cases the time scaling should rather be chosen to accommodate the convection instead of the diffusion. As stated in the discussion of the constants p and q , such instances are not necessarily noticed prior to the beginning of the simulation. Thus, one needs to be vigilant whether the results obtained from the simulation indicate an unexpected dominance of the convection term.

4.2 A Review of System Discretizations

Since our focus will be a solver based on Finite Elements, we will omit a detailed description of either Finite Difference or Finite Volume methods, although those are also used for the treatment of the equation system (e.g. [Pan05, Sch01])

But even when restricting ourselves to a review of finite element based methods, we encounter a variety of different methods. For one we cite [Sam99], to which some later papers make reference, as it contains the extended Poisson-Nernst-Planck system with a completely coupled operator. The non-linearity is treated by a Newton-Raphson method, which works by solving the tangent system for the residual of the operator on the present iteration level. Assembling this tangent system requires substantial effort, as not only the coefficients of the system undergo a change but also the domain of integration. While the calculations presented are restricted to one space dimension, extension of the model to more dimensions are mentioned.

Another one dimensional model can be found in [Kra08]. While the method is almost identical to the one in [Sam99], the Newton iteration method employed to solve the non-linearity requires less computational effort, as it omits the contribution of chemical activity/chemical

potential and also splits the iteration operator so that in each iteration step only the reassembly of a subsystem is required.

In [Lu07] we find a substitution technique put to use which enables the reduction of the system to one of diffusion type. Rewriting the equation

$$\begin{aligned}\frac{\partial u_i}{\partial t} &= \nabla [D_i (\nabla u_i + \beta \nabla q_i \Phi u_i)] \\ &= \nabla [D_i e^{-\beta q_i \Phi} \nabla (e^{\beta q_i \Phi} u_i)]\end{aligned}\tag{4.5}$$

and replacing

$$\begin{aligned}u' &= e^{\beta q_i \Phi} u \\ D' &= D_i e^{-\beta q_i \Phi}\end{aligned}\tag{4.6}$$

one obtains the symmetrized equation

$$\frac{\partial}{\partial t} (u e^{-\beta q_i \Phi}) = \nabla \cdot (D' \nabla u)\tag{4.7}$$

which after being expanded also contains a time derivative of the electrical potential, which the authors expect to be known for each timestep from an unspecified source. The unconditionally stable backwards Euler method is then used to discretize the time. Regarding the steady state case (for which the time derivative of the electrical potential is known to be zero), the use of over- and under-relaxation methods for the iteration between the NP system and the PE is discussed, specifically it was found that under-relaxation is necessary for convergence, while over-relaxation – though reported to be successful in Finite Difference settings – is not applicable in the scheme presented. We also remark that the substitutions, as performed in this paper, prevent the incorporation of additional linear reaction terms, as we permit them in our treatment of the NP system.

4.3 Definitions

In this section we present the mathematical groundwork for the FEM with some definitions. We introduce the notion of weak derivatives of functions which do not need to be continuous, as well as function spaces containing these functions. While there are more possibilities than the presented approach for defining these spaces, we follow the one in [Bra02], which appears to be the most instructive with respect to the method used. Furthermore, we refrain from using the most general form of the definitions in favor of restrictions which will fit the problem we present in this thesis.

Definition 4.3.1 *Let $\Omega \subset \mathbb{R}^n$ be an open, bounded domain with Lipschitz boundary and $u, v \in L^2(\Omega)$. Further, let $\alpha = (\alpha_i)_{i=1}^n$ with $\alpha_i \in \mathbb{N}$ be a multi index. With*

$$\partial^\alpha = \prod_{i=1}^n \frac{\partial^{\alpha_i}}{\partial x_i^{\alpha_i}}\tag{4.8}$$

we define v to be the weak α -derivative of u if the following equality holds for all test functions $\phi \in C_0^\infty(\Omega)$:

$$\int_{\Omega} v \phi \, dx = (-1)^{|\alpha|} \int_{\Omega} u \partial^\alpha \phi \, dx. \quad (4.9)$$

When a function is differentiable in the strong sense, the two notions coincide, that is $\partial^\alpha u = v$, as can be proved by the Fundamental Lemma of variational calculus [Bra02, Bro01]. For this reason we write $\partial^\alpha u$ for the weak derivative of a function as well.

Definition 4.3.2 With Ω as above, we define the Sobolev space $H^m(\Omega)$ to consist of all functions $u \in L^2(\Omega)$ for which the weak derivatives $\partial^\alpha u$ with $|\alpha| = \sum_{i=1}^n |\alpha_i| \leq m$ exists. We define the following set of semi-norms:

$$|u|_k = \sqrt{\sum_{|\alpha|=k} \|\partial^\alpha u\|_{L^2(\Omega)}^2} = \sqrt{\sum_{|\alpha|=k} \int_{\Omega} \partial^\alpha u \partial^\alpha u \, dx}. \quad (4.10)$$

These semi-norms can be summed over in order to obtain a full norm

$$\|u\|_{H^m(\Omega)} = \left(\sum_{|\alpha| \leq m} |u|_\alpha^2 \right)^{\frac{1}{2}}. \quad (4.11)$$

Specifically, for $H^1(\Omega)$ we have

$$\|u\|_{H^1(\Omega)}^2 = \|u\|_{L^2(\Omega)}^2 + \|\nabla u\|_{L^2(\Omega)}^2, \quad (4.12)$$

which we will need later on.

Note that $H^m(\Omega)$ is complete with this norm. As hinted in the introduction, it is possible to define $H^m(\Omega)$ as the completion of $C^m(\bar{\Omega})$ under the norm defined above. Those definitions coincide in our case, since we have made the restriction that the boundary of Ω is Lipschitz smooth [Alt92]. It is for this reason that we can safely demand that Ω be closed, without violating the above definition. Additionally, we follow the convention of denoting the Sobolev space of functions vanishing on the boundary of Ω by $H_0^m(\Omega)$.

4.4 Weak Formulation of the Extended Nernst-Planck Equation

We now turn towards the differential equation. Let L be the differential operator we are interested in, then

$$Lu = f \quad \text{on } \Omega \quad (4.13)$$

$$u = g \quad \text{on } \partial\Omega \quad (4.14)$$

is a strong formulation of the differential equation. With the following definitions

$$a(u, v) = \int_{\Omega} Lu \cdot v \, dx \quad (4.15)$$

$$F(v) = \int_{\Omega} f \cdot v \, dx \quad (4.16)$$

the problem can be rewritten as a weak problem: Find $u \in V$, s.t.

$$a(u, v) = F(v) \quad \forall v \in V, \quad (4.17)$$

where V is a suitable Hilbert space. In this particular formulation, the boundary conditions may be taken care of by the choice of the Hilbert space. By splitting the differential operator L through integration by parts, the space of admissible solutions is extended further. Nevertheless, when the requirements of the Lemma of Lax-Milgram are satisfied, one is guaranteed to obtain a unique solution to the problem - and since the original solution space is included in this extension, one is guaranteed that the strong solution to the equation is found. [Bra02, Gro94]

For the numerical scheme, the function space V is replaced by a discrete subspace $V_h \subset V$ in order to allow handling by a computer. A set of basis functions $\{\phi_k(x)\}_{k=0}^n$ for V_h is given and an approximate solution is constructed in the form

$$u(x) = \sum_{k=0}^n u_k \phi_k(x). \quad (4.18)$$

Since all available test functions would be linear combinations of said basis functions again, it now suffices to test the functional against all basis functions. This results in the following set of equations:

$$a(u, \phi_l) = F(\phi_l) \quad \forall l \quad (4.19)$$

$$\Leftrightarrow a\left(\sum_{k=0}^n u_k \phi_k, \phi_l\right) = F(\phi_l) \quad \forall l \quad (4.20)$$

$$\Leftrightarrow \sum_{k=0}^n u_k a(\phi_k, \phi_l) = F(\phi_l) \quad \forall l, \quad (4.21)$$

which immediately leads to a linear system of equations to be solved. For the problem at hand, the following transformation of the operator is presented: The strong problem of the extended Nernst-Planck equation has the form derived in section 3.6

$$\nabla \cdot \left[D \left(\nabla u_i + \frac{z_i \cdot e \nabla \Phi + \nabla \mu}{k_B T} u_i \right) \right] = \frac{\partial u_i}{\partial t} \quad (4.22)$$

which is a diffusion-convection equation. For the following analysis we extend it by a linear reaction term to obtain a more general result for the existence of the solution, which will hold

for a linear combined diffusion-convection-reaction equation:

$$\nabla \cdot \left[D_i \left(\nabla u_i + \frac{z_i \cdot e \nabla \Phi + \nabla \mu}{k_B T} u_i \right) \right] + K_i(x) u_i(x) = \frac{\partial u_i}{\partial t}, \quad (4.23)$$

which for basisfunctions in $H_0^m(\Omega)$ has the weak equivalent

$$- \int_{\Omega} \left[D_i \left(\nabla u_i + \frac{z_i \cdot e \nabla \Phi + \nabla \mu}{k_B T} u_i \right) \right] \cdot \nabla \phi_l \, dx + \int_{\Omega} K_i(x) u_i(x) \cdot \phi_l \, dx = \int_{\Omega} \frac{\partial u_i}{\partial t} \, dx, \quad (4.24)$$

where both terms have been multiplied by ϕ_l , integrated over the domain Ω and integrated by parts. By choosing $H_0^m(\Omega)$ as the space of test functions, we have for now removed the need to deal with boundary terms, as these will be essentially different for varying physical problems. We will describe these in section 4.4.1 in order to allow for physical solutions which may be non-vanishing on the boundary.

When dealing with a parabolic equation, it is standard procedure to split the solver among the dimensions in order to obtain a second order elliptical problem in one set of dimensions and a first order differential equation in the remaining one. The same approach is followed here, with the time coordinate being the source of parabolicity. Since the boundary conditions can be incorporated independently from the time discretization, we will postpone the presentation of our discretization to section 4.5.

4.4.1 Boundary Conditions for Ionic Migration Problems

In the above section we have ignored the treatment of boundary conditions of the Poisson-Nernst-Planck system, because each physical system yields its own set of conditions. Since we investigate physical ionic migration, we will deal with physical boundary conditions, which we find to be of Dirichlet-type or Robin-type.¹ For the Dirichlet boundary conditions we need our solution to be in a certain function space, whereas for Robin boundary conditions we revisit our integration and notion of flux.

Equilibrated Surroundings: Dirichlet Boundary Conditions

Let us first consider Dirichlet-type boundary conditions. In our model problem, these arise when placing the system, which is to be investigated, in contact with a totally equilibrated ion solution of given concentration with infinite ion supply. In the homogeneous case there is nothing to be done, since our previous handling of the problem would satisfy that situation exactly. In case of nonzero concentration on the boundary we need to ensure that a solution exists which satisfies the partial differential equation on the interior domain and the boundary

¹ The literature does not quite agree on the terminology for the latter. While the name Robin boundary conditions seems to be the most used, we also have encountered the terms mixed boundary conditions or general Neumann-boundary conditions, names which in other works have again different meaning.

condition. Following [Bra02], the problem

$$\begin{aligned} Lu &= f && \text{on } \Omega \\ u &= g && \text{on } \partial\Omega \end{aligned} \quad (4.25)$$

transforms to the weak formulation

$$\begin{aligned} a(u,v) &= F(v) && \forall v \in H_0^m(\Omega) \\ \text{with } u - u_0 &\in H_0^m(\Omega) \end{aligned} \quad (4.26)$$

where u_0 is a function with $u_0|_{\partial\Omega} = g$ and $u_0 \in H^m(\Omega)$. When such a u_0 exists, we find that $w = u - u_0$ satisfies

$$\begin{aligned} Lw &= f' && \text{on } \Omega \\ w &= 0 && \text{on } \partial\Omega \\ f' &= f - Lu_0 \end{aligned} \quad (4.27)$$

Generally, it is not clear whether such a $u_0 \in H^m$ exists to a given boundary function g , and one can construct examples where it is impossible to find such a function. However, our boundary conditions will stem from physical problems, so that we can safely assume the existence of such a u_0 whose singularities (if any) are confined to a set of Lebesgue measure zero in Ω .

Controlled Flux: Robin Boundary Conditions

We now turn to boundary conditions in which we control the flux across the system boundary. In order to make the further reading easier, the convection term will be combined into a single coefficient $\vec{b}_i = \frac{z_i \cdot e \nabla \Phi + \nabla \mu}{k_B T}$. Summarizing the convection terms as in section 4.4, we have found in chapter 3 that the ionic flux is

$$\vec{J}_i = D_i \left(\nabla u_i + \frac{z_i \cdot e \nabla \Phi + \nabla \mu}{k_B T} u_i \right) = D_i \left(\nabla u_i + \vec{b}_i u_i \right) = D_i \nabla u_i + D_i \vec{b}_i u_i, \quad (4.28)$$

the sum of diffusion and convection. However, the ion flux on boundaries is not necessarily subject to the physical interactions which are modeled within the bulk solution. Specifically, in batteries ions would be emitted from a conductive electrode, inside of which the electric potential is constant and respectively the electric field zero. Thus, the ionic flux across the boundary cannot be expected to be under the influence of the electric field as it might arise inside the bulk solution. Those different models give rise to different mathematical formulations with the finite element method. In essence, they dictate whether the partial integration is to be performed for both the diffusion and convection term, or for the diffusion or convection term only. In the following paragraphs we will describe the situations of partial integration for both the diffusion and convection term, and partial integration of the diffusion term only.

When considering diffusive and convective contributions, fixing the flux across the boundary

leads to the following term on the boundary

$$g_i(x) = \vec{J}_{\partial\Omega, i}(x) \cdot \vec{n} = [D_i (\nabla u_i + \vec{b}_i u_i)] \cdot \vec{n}, \quad (4.29)$$

where \vec{n} is the outer normal on the boundary of the domain. We revisit our integration of (4.23) and this time incorporate the boundary integration.

$$\begin{aligned} \int_{\Omega} \nabla \cdot [D_i (\nabla u_i + u_i \vec{b}_i)] \phi_l + K_i(x) u_i(x) \phi_l dx &= \int_{\Omega} \frac{\partial u_i}{\partial t} \phi_l dx \\ \Leftrightarrow - \int_{\Omega} [D_i (\nabla u_i + u_i \vec{b}_i)] \cdot \nabla \phi_l dx + \int_{\Omega} K_i(x) u_i(x) \cdot \phi_l dx & \quad (4.30) \end{aligned}$$

$$\begin{aligned} + \int_{\partial\Omega} \underbrace{[D_i (\nabla u_i + u_i \vec{b}_i)]}_{\vec{J}_{\partial\Omega, i}(x)} \phi_l \cdot \vec{n} &= \int_{\Omega} \frac{\partial u_i}{\partial t} \phi_l dx \end{aligned}$$

$$\Leftrightarrow - \int_{\Omega} [D_i (\nabla u_i + u_i \vec{b}_i)] \cdot \nabla \phi_l dx + \int_{\Omega} K_i(x) u_i(x) \cdot \phi_l dx \quad (4.31)$$

$$\begin{aligned} + \int_{\partial\Omega} g_i \phi_l dx &= \int_{\Omega} \frac{\partial u_i}{\partial t} \phi_l dx \end{aligned}$$

$$\Leftrightarrow - \int_{\Omega} [D_i (\nabla u_i + u_i \vec{b}_i)] \cdot \nabla \phi_l dx + \int_{\Omega} K_i(x) u_i(x) \cdot \phi_l dx \quad (4.32)$$

$$= \int_{\Omega} \frac{\partial u_i}{\partial t} \phi_l dx - \int_{\partial\Omega} g_i \phi_l dx.$$

We have been able to use the boundary conditions to move the boundary integral to the right hand side of the equation, arriving at the problem we have solved previously.

In the case where the model assumes only diffusive transport across the boundary, the boundary term takes the form

$$g_i(x) = \vec{J}_{\partial\Omega, i}(x) \cdot \vec{n} = [D_i \nabla u_i] \cdot \vec{n}. \quad (4.33)$$

Subsequently, we execute the partial integration only on the diffusion term in order to be able

to incorporate our boundary term:

$$\begin{aligned} & \int_{\Omega} \nabla \cdot [D_i (\nabla u_i + u_i \vec{b}_i)] \phi_l + K_i(x) u_i(x) \phi_l dx &= \int_{\Omega} \frac{\partial u_i}{\partial t} \phi_l dx \\ \Leftrightarrow & - \int_{\Omega} [D_i (\nabla u_i)] \cdot \nabla \phi_l dx + \int_{\Omega} \nabla \cdot [D_i u_i \vec{b}_i] \phi_l dx & \end{aligned} \quad (4.34)$$

$$\begin{aligned} & + \int_{\Omega} K_i(x) u_i(x) \cdot \phi_l dx + \int_{\partial \Omega} \underbrace{[D_i (\nabla u_i)]}_{\vec{j}_{\partial \Omega, i}(x)} \phi_l \cdot \vec{n} &= \int_{\Omega} \frac{\partial u_i}{\partial t} \phi_l dx \\ \Leftrightarrow & - \int_{\Omega} [D_i (\nabla u_i)] \cdot \nabla \phi_l dx + \int_{\Omega} \nabla \cdot [D_i u_i \vec{b}_i] \phi_l dx & \end{aligned} \quad (4.35)$$

$$\begin{aligned} & + \int_{\Omega} K_i(x) u_i(x) \cdot \phi_l dx + \int_{\partial \Omega} g_i \phi_l dx &= \int_{\Omega} \frac{\partial u_i}{\partial t} \phi_l dx \\ \Leftrightarrow & - \int_{\Omega} [D_i (\nabla u_i)] \cdot \nabla \phi_l dx + \int_{\Omega} \nabla \cdot [D_i u_i \vec{b}_i] \phi_l dx & \end{aligned} \quad (4.36)$$

$$+ \int_{\Omega} K_i(x) u_i(x) \cdot \phi_l dx = \int_{\Omega} \frac{\partial u_i}{\partial t} \phi_l dx - \int_{\partial \Omega} g_i \phi_l dx.$$

Both types of flux controlling boundary conditions have a direct consequence for the conservation of mass and charge inside the domain. By the continuity equation (3.11) the concentration changes over time when the gradient of the flux is nonzero. In the case of balanced flux conditions we expect to observe conservation of mass when integrating over the complete domain, whereas in the case of unbalanced flux conditions we are bound to observe a change of mass. This aspect will be of relevance in the discussion of the numerical results.

In realistic applications the boundary conditions may be mixed. In these cases we split the boundary into section Γ_D and Γ_R , with the properties

$$\begin{aligned} \Gamma_D \cap \Gamma_R &= \emptyset \\ \Gamma_D \cup \Gamma_R &= \partial \Omega \end{aligned} \quad (4.37)$$

on which Dirichlet or Robin boundary conditions are enforced respectively.

4.5 Time Discretization and the Coupled Poisson-Nernst-Planck System

In section 4.4 we have presented the weak operator of the NP equation up to the time discretization. In order to produce a solver for the coupled Poisson-Nernst-Planck system the solution of the Poisson equation needs to be tied in. This leads to a non-linearity in the equation system. The most direct approach to this non-linearity is to solve the Poisson equation in between the Nernst-Planck steps and use the electric potential of the previous timestep explicitly in the NP solver. Due to the fact that each equation can be solved separately, thus keeping the

linear systems small, this approach promises to be extremely fast. This can be confirmed in numerical experiments. Unfortunately, this approach is generally unstable. While this effect might not be noticed immediately for non physical examples (e.g. with low coupling constants in the Poisson equation) it is extremely pronounced in full physical systems. There it leads to exponential error progression expressed in an increase of the absolute value of the electric field, which leads to non-physical convection and to the violation of conditions placed on the solver by the Lax-Milgram Lemma. In appendix B we will discuss these conditions, which also serve as proof of the systems stability in the non-coupled case.

For the above reasons a different approach is called for. Several examples have been presented in the literature review in section 4.2 at the beginning of this chapter. The cited works on the discrete solution of the PNP all have the use of iteration techniques in common. While such procedures are well suited for obtaining accurate results of nonlinear equations, they require that for each time step numerous iterations need to be performed. [Lu07] reports the necessity of several tens or hundreds of iterations, which have been needed for convergence. From this report we deduce that finding a stable linearization of the problem will extend the accessible time range of the solver considerably. The crucial nonlinear term arises from the coupling of the electric potential Φ and the ionic species u_i , and the product of both quantities in the term

$$\nabla \left[\frac{DF}{RT} (\nabla \Phi) u_i \right]. \quad (4.38)$$

Since the use of an explicit electrical potential and an implicit concentration

$$\nabla \left[\frac{DF}{RT} (\nabla \Phi^n) u_i^{n+1} \right] \quad (4.39)$$

has proved to be unstable, we exchange the explicit and implicit arguments in the above expression to

$$\nabla \left[\frac{DF}{RT} (\nabla \Phi^{n+1}) u_i^n \right]. \quad (4.40)$$

Consequently, the complete (unextended) system, discretized in the time domain, for k ionic species then reads

$$\begin{pmatrix} I - \nabla D_1 \nabla & 0 & \dots & -\frac{z_1 F}{RT} [D u_1^n \Delta + D (\nabla u_1^n) \nabla] \\ \vdots & \ddots & & \vdots \\ 0 & \dots & I - \nabla D_k \nabla & -\frac{z_k F}{RT} [D u_k^n \Delta + D (\nabla u_k^n) \nabla] \\ z_1 Id & \dots & z_k Id & \frac{\varepsilon_0 \varepsilon_r}{F} \Delta \end{pmatrix} \cdot \begin{pmatrix} u_1^{n+1} \\ \vdots \\ u_k^{n+1} \\ \Phi^{n+1} \end{pmatrix} = \begin{pmatrix} u_1^n + g_1 \\ \vdots \\ u_k^n + g_k \\ 0 \end{pmatrix}, \quad (4.41)$$

where the functions g_i represent the respective boundary conditions and I is the identity matrix. With this particular discretization we have removed the unstable behavior of the coupled equations and at the same time abolished the need for an iterative treatment of the

non-linearities. The above formulation does not yet incorporate test functions and partial integrations. Since their incorporation results in a rather large system, we introduce the following shorthands:

$$\mathcal{J}(u, v) = \int_{\Omega} uv \, dx, \quad (4.42)$$

$$\mathcal{D}_i(u, v) = \int_{\Omega} D_i \nabla u \nabla v \, dx, \quad (4.43)$$

$$\mathcal{B}_i(\phi, v) = \int_{\Omega} \frac{z_i F}{RT} [D_i u^n \Delta \phi + D_i (\nabla u^n) \nabla \phi] v \, dx, \quad (4.44)$$

$$\mathcal{P}(\phi, \psi) = \int_{\Omega} \frac{\varepsilon_0 \varepsilon_r}{F} \nabla \phi \nabla \psi \, dx, \quad (4.45)$$

$$\mathcal{F}_i(v) = \int_{\Omega} u_i^n v \, dx, \quad (4.46)$$

$$\mathcal{G}_i(v) = \int_{\partial\Omega} g_i v \, dx. \quad (4.47)$$

Then, the weak form of the above system reads:

$$\begin{aligned} \sum_j \sum_{i=1}^k [(\mathcal{J}(u_i, v_{ij}) + \mathcal{D}_i(u_i, v_{ij}) - \mathcal{B}_i(\Phi, v_{ij}) + z_i \mathcal{J}(u_i, \phi_j)) + \mathcal{P}(\Phi, \phi_j)] \\ = \sum_{i=1}^k \sum_j \mathcal{F}_i(v_{ij}) + \mathcal{G}(v_{ij}) \end{aligned} \quad (4.48)$$

where u_i and Φ are the solution functions for species i and the electric potential at timestep $n + 1$ and v_{ij} and ϕ_j are the respective test functions. The right hand side incorporates both the previous concentration in time as well as possible flux boundary conditions on the ionic species.

4.6 Convergence

Proving the existence of analytical solutions to parabolic equations is in most cases a difficult, if not impossible task, since compatibility requirements of starting and boundary conditions may not meet [Gro94]. The existence of weak solutions has been proved for certain types of equations, and in appendix B we demonstrate that the decoupled Nernst-Planck equation falls under this category. The coupled operator, as it has been derived in the previous section, is an entirely different matter. Since the two coupled equations are of different type (the Poisson Equation is elliptical whereas the NP is parabolic), standard results do not apply. Due to the fact that individual existence of solutions is known, we will henceforth make the assumption

that a solution to the combined problem does exist as well. In the literature this is well accepted, as [Lu07, Kra08, Sam99] contain no analysis of the operator either. The fact that many different numerical schemes produce stable and comparable results support this assumption.

From the question of existence one is immediately led to the question of the quality of the numerical approximation of this solution, since any numerical scheme makes use of a restricted space of functions. Since we have no information about the smoothness of the solution function, we restrict our discussion to the most basic standard results, which we will not describe extensively. But we will outline some follow-up lemmata, while leaving the details of the computations to standard textbooks on the topic of finite elements [Gro94, Bra02]. The most prominent result is

Lemma 4.6.1 (Cea) *Let $a(\cdot, \cdot)$ be a continuous, bounded, V -elliptic bilinear form. Let $u \in V$ be the continuous solution of (4.17) and $u \in V_h$ its respective approximation in the space of basis functions $V_h \subset V$. Then the following estimate is valid:*

$$\|u - u_h\| \leq \frac{c}{c'} \inf_{v_h \in V_h} \|u - v_h\| \quad (4.49)$$

where c and c' are the respective constants of the boundedness (B.3) and ellipticity (B.4) of the Lax-Milgram Lemma.

For careful choices of V_h this Lemma alone can guarantee convergence of the method. In order to obtain this guarantee, we require V_h to be asymptotically dense in V [Gro94]. This means that any function $v \in V$ can be approximated to any desired accuracy by the functions $v_h \in V_h$ if only our discretization h is fine enough. As a consequence we have $\lim_{h \searrow 0} \inf_{v_h \in V_h} \|u - v_h\| = 0$, and by the Cea lemma we then obtain $\lim_{h \searrow 0} \|u - u_h\| = 0$. Nevertheless, the lemma does not provide an order of convergence, e.g. how the convergence depends on h . Obtaining such estimates requires additional properties of the solution function. When the solution is known to be in $H^m(\Omega)$ and the grid used is (quasi-)uniform, one can use the lemma of Bramble-Hilbert, the transformation theorem and other approximation lemmata to obtain the convergence estimate

$$\|u - u_h\|_{H^l(\Omega)} \leq c \inf_{v_h \in V_h} \|u - v_h\|_{H^l(\Omega)} \leq c' \|u - \Pi_h\|_{H^l(\Omega)} \leq c'' h^{k-l} |u|_{H^k(\Omega)}, \quad (4.50)$$

where h is the maximum diameter of the finite elements. Specifically, if we have $u \in H^2(\Omega)$, we obtain

$$\|u - u_h\|_{H^1(\Omega)} \leq ch |u|_{H^2(\Omega)}. \quad (4.51)$$

It should be noted that the above results are of global nature only, that is, they guarantee global convergence of the numerical solution while the local error may still be large. For this reason we will deploy adaptive error estimators which allow us to selectively target those areas of the grid on which the error is largest.

4.6.1 Adaptivity

The convergence results in the previous section are expressed in dependence of the maximum of the element diameter. However, for most problems the error is not spread evenly over the complete domain, but there are regions in which the error is far greater than in others. Most notable examples are singularities in the boundaries or a large local variation in the coefficient functions. In such cases a global refinement of the discretization, while decreasing the error, comes at overboarding costs, since even in cells which had a tolerable error before the finer cell structure requires additional integration to obtain the matrix of the linear system.

The “obvious” solution to this dilemma is to refine the triangulation locally on those cells where the error is larger than average. This measure will increase the accuracy of our solution where it matters, while keeping the computational costs reasonable. This being said, we require an estimate for the local error on the elements which is available at runtime. A naive approach would be to estimate the error by comparing the solution on the current grid with one obtained on a globally refined grid. While this method would certainly allow to estimate where the benefits of additional refinement would be largest, it is also apparent that we would not save ourselves effort, since in order to obtain a “smart” refinement we would proceed with an extensive one first.

In our specific case, where we integrate the same equation over several time steps, one might entertain the question whether such an approach were nevertheless justified, since the extra effort spent on the refinement in the first time step would pay off in all following ones. However, even then this approach would be questionable, since in three (or even two) dimensions the cost of global refinement increases with the third (or second) power, so that the initial error estimate could possibly dominate the whole computational process.

The Kelly Estimator

For the above reasons, we turn to a more sophisticated method of estimating the error, which has been introduced by Kelly, Gago, Zienkiewicz and Babuška in [Kel83]. To be precise, in this context the method should not be referred to as an error estimator, since it is only an actual error estimator for the generalized Poisson equation,

$$-\nabla (a\nabla u) = f \tag{4.52}$$

with Dirichlet- or normal Neumann-boundary conditions¹. Nevertheless, in practical application the method has been found to produce good indications for local refinement for several other finite element problems as well and has been formulated for combined diffusion-convection problems in the original publication. Consequently, the term refinement indicator would be more appropriate and is in use [Banb, Kel83].

For a function $u \in H^1(\Omega)$ we define

$$[u(\vec{x})]_{\vec{y}} = \lim_{h \rightarrow 0} u(\vec{x} + h\vec{y}) - \lim_{h \rightarrow 0} u(\vec{x} - h\vec{y}) \tag{4.53}$$

¹ While we do solve the Poisson equation as well, our primary concern is for the accuracy of the Nernst-Planck equation.

to be the jump of u at the point \vec{x} in direction \vec{y} . We then proceed to define

$$\eta_K^2 = \frac{h}{24} \int_{\partial K} \left[a(\vec{x}) \frac{u_h(\vec{x})}{\partial \vec{n}} \right]_{\vec{n}} d\vec{x}, \quad (4.54)$$

where η_K is the refinement indicator, a is a factor stemming from the problem and h the cell diameter. The division by 24 has been called “esoteric” by some authors [Banb], since it arises from interpolation and stability constants. While those hold for the Poisson problem, this may not be the case for other equations, in fact a variety of factors have been presented in the paper of Kelly.

The estimator also requires one to look out for the finite elements used. Specifically, the estimator depends on discontinuities in the first derivative of the numerical solution, so that it prohibits the use of Hermitian finite elements. Consideration should also go to the degree of the employed polynomials. The formulation is intended to be used with linear finite elements, and while it has been successfully used with higher order elements as well, one should be wary of false indications of superconvergence, as derivatives are likely to approach each other due to higher order interpolation on the cells.

One should also keep in mind that in our specific problem the solution vector not only consists of the ionic species’ concentrations but also the electric field. One may choose to restrict the use of the error indicators to the ionic species’ concentration (or a certain group of species) for the refinement criterion, depending on the specific interests one has in the different solution functions.

Since we solve a finite element system in multiple timesteps, we have the option to use the refinement procedure once at the beginning of the simulation and continue computations with the grid for the total simulation. Other possibilities include the use of the refinement procedure in each timestep, after a series of timesteps or in some other elaborate manner. All options have their merits and flaws, which need to be considered before implementing them in the solver. When implementing a repetitive use of the refinement, one should keep in mind that with traditional use of the refinement criterion, which always increases a fixed ratio of the present cells, the number of cells and degrees of freedom increases exponentially. Thus strategies need to be incorporated, which either stop the refinement process at some threshold or allow for the coarsening of cells as well.

We will present our approach to this matter with the presentation of our implementation using deal.II in the next chapter.

Chapter 5

Numerical Experiments

We will begin by describing the implementation of the FEM, which makes use of several features supplied by the deal.II finite element library. Afterwards we will turn towards the numerical experiments conducted, beginning with those on the molecular domain. We will present the multiscaling results obtained by comparing our improved method for the measurement of diffusion against the traditional method in benchmark tests, before performing simulations on known electrolyte materials and comparing the results to numerical and experimental ones in the literature. We also present results from simulations on a new setup. We then proceed to the New-Poisson-Nernst-Planck solver (NPNP). For the PNP equation system the establishment of benchmark problems to demonstrate the potency of a solver has not yet taken place. Therefore we will present our own choice of problems with increasing difficulty, starting with a decoupled diffusion convection problem. We then proceed to present various simulations in coupled settings and demonstrate the ability of our solver to handle three dimensional problems and regional coefficient changes. We will finish the chapter with the display of computations of more than two species and an incorporated reaction term.

5.1 The Finite Element Library Deal II

The method described above was implemented using the deal.II finite element package [Bana, Banb]. The deal.II package supplies C++ libraries for many of the tasks surrounding the computational implementation of adaptive finite element methods on a computer. In addition to easing the programming burden of grid management, refinement issues and output, the library also provides a choice of numerical methods needed for the integration over the finite elements, integrating boundary conditions into the linear system and finally for solving the linear system.

The library is based on grids of lines, quadrilaterals or hexahedra. Together with local polynomials of variable degree as basis functions of the test function space they define the tensor product Lagrange finite elements. Depending on the dimension of the problem, deal.II does place restrictions on the degree of the basis functions used.

Our implementation allows to choose from the allowed range of finite element degrees and appropriately chooses a Gauss-type integration scheme in order to execute the integration of the test functions over the cell to assemble the matrix and the right hand side. Prior to assembly of the system matrix, the Cuthill-McKee method is used to narrow the bandwidth of

the matrix [Cut69]. The assembly of the matrix is then performed in parallel threads, providing a considerable speed-up to this process.

The assembled sparse matrix is then treated with a **Symmetric Successive Over Relaxation** (SSOR) preconditioner before being solved by **Conjugate Gradient** iteration. Once the integration over the timeline is properly initialized, we benefit tremendously from the previous solutions by using them as the starting vector of the iteration. This significantly reduces the iteration cycles required for convergence from (depending on the spatial refinement) several hundreds to less than 10 iterations.

Prior to calculating the full timeline, the program allows for refinement of the grid, which may be carried out globally or locally. For the latter the deal II library provides an implementation of the Kelly error indicator [Banb, Kel83]. In line with our discussion in 4.6.1 we implemented the following scheme for adaptive refinement: From the starting configuration the solver executes timesteps for a fixed time interval. The Kelly error indicator is used on the ionic species solutions at that point (the electrical potential is ignored for refinement purposes). A fraction, dependent on the users choice, of the cells with highest error indication is refined. Afterwards the whole system is reset to its starting condition and the actual simulation (or, if so chosen, the next refinement step) is carried out on the refined grid. This method allows the indicator to work on sensible solution functions, as the initial state, as well as several timesteps afterwards, may be disturbed by singularities in the differentiation over the cell boundaries.

For the decoupled system (as described in appendix B) we further implemented the use of Petrov Galerkin/streamline upwind-type test functions [Roo96]. A streamline upwind type method for the fully coupled system has not been implemented yet, since the examples of interest do not contain such large convection terms, which demand such a procedure.

5.2 Molecular Dynamics and Multiscaling of Ethylene Carbonate

We begin the tests on the upscaling method by showing that the new proposed method for the calculation of the diffusion coefficient produces virtual identical results to the traditional method without convection correction in systems, from which all convection has been removed prior to the start of the simulation. Following that, we demonstrate the superiority of our corrected method by comparing the results for a system with a strong particle convection. We will then proceed to perform numerical experiments for physical setups, whose results we analyse and compare against published values obtained either by experiment or comparable simulation.

Since our interest is the modelling of batteries, we investigate the behavior of Li^+ and BF_4^- ions. The first setup places them in a pure ethylene carbonate electrolyte, while the second setup investigates the effect of cellulose chains in the same electrolyte.

5.2.1 Configuration of Ethylene Carbonate

We begin by presenting the simulation parameters of **Ethylene Carbonate** (EC). EC is an organic ester with the molecular formula $\text{O}_3\text{H}_4\text{C}_3$. It has a molar mass of $88.06 \frac{\text{g}}{\text{mol}}$ and a

density of $1.3210 \frac{g}{cm^3}$.

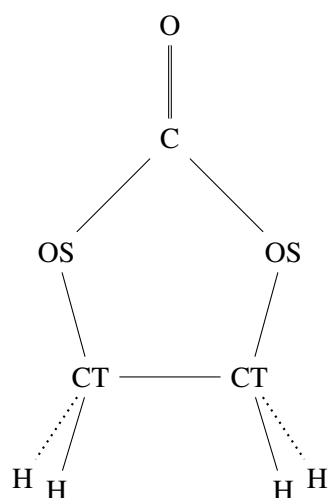


Figure 5.1: Schematic structure of ethylene carbonate; with atom type labels as used by the AMBER force field tables.

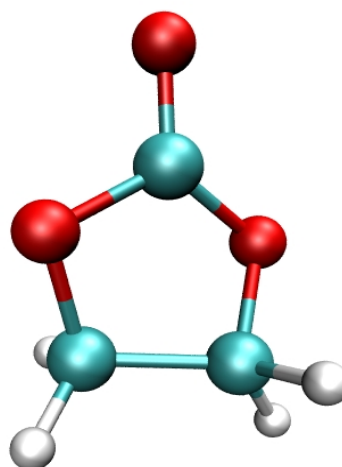


Figure 5.2: Ethylene Carbonate, structure as simulated for single molecule.

Our basic setup consists of 2197 molecules of ethylene carbonate in a simulation box of edge length 62.42 \AA , which corresponds to the density of pure EC. This setup was allowed a 100 pico second equilibration at 323K, before the output was used to create the starting ensembles for the actual computations. Depending on the concentration for which we intend to measure our results, we replaced EC molecules by the conducting ions. We always embedded a pair of Li^+ and BF_4^- , each replacing one EC molecule. For the description of intramolecular forces we will make use of the AMBER force field parameters [Cor95] for the ethylene carbonate molecules and for the inorganic fluoroborate a **united-atom** force field (UA) [Liu06] will be used. Intermolecular interactions will be described by Lennard-Jones and Coulomb potentials, where the Lennard-Jones Potentials will have their cut-off smoothed by a spline function of degree 3, in order to remove force discontinuities as described in section 2.3.3. The Coulomb potential will be calculated using the SPME method [Gri04]. The parameters for the Lennard-Jones and Coulomb potential can be found in table 5.1 and equal the ones used in [JC98]. Since Soetens used a rigid BF_4^- molecule he supplied no LJ-parameters, here the ones from the UA were used [Liu06].

Although we obtained the starting setup from an equilibrated pure EC sample and the mixture should be fairly equilibrated, we performed an optimization of particle positions and box size. The prior is necessary in order to avoid energy singularities (since neither EC nor BF_4^- are exactly tetrahedral), while omitting the latter would still allow for valid simulations, although one should be prepared to allow for longer equilibration time in the main computation.

The simulation will be performed using a second degree Beeman-velocity integration scheme with an NPT ensemble using the Nosé-Hoover thermostat introduced in section 2.3.4 and a Parinello barostat [Gri04]. The calculations are performed using the tremolo software [Gri04]. The use of the NPT ensemble was preferred over the use of the NVT ensemble due to fact that

molecule	atom	$\sigma/\text{\AA}$	$\varepsilon/\frac{\text{kcal}}{\text{mol}}$	q/e
EC	O	2.96	0.210	-0.6452
	OS	3.00	0.170	-0.4684
	C	3.75	0.105	1.0996
	CT	3.5	0.066	0.033
	H1	2.5	0.030	0.1041
Li ⁺		1.46	0.191	1.0
BF ₄ ⁻	B	3.581	0.3975	0.9756
	F	3.118	0.2552	-0.4939

Table 5.1: Van der Waals parameters and partial charges for EC.

the density of the ionic solution can be expected to have a different density than the electrolyte on its own. Since no data on the concentration dependence of the density is available, we could not be sure to fix the proper volume for the solution. On the other hand, fixing the external pressure of one atmosphere allows the solution to equilibrate itself, so that we may expect the solution to be in the physical sensible domain of the phase space. Numerical results validated this expectation, as the domain size expanded during the equilibration phase of the simulation. The temperature of the ensemble was assigned a target value of 323 K and a target pressure of 1 atm. While the electrolyte was equilibrated prior to the insertion of the ions, we expect the presence of the ions to disturb that attained equilibrium. As already mentioned, we specifically expected – and observed – a change in density. Thus we incorporated an equilibration phase of 50 ps prior to the beginning of taking measurements from the system.

The Improved Diffusion Measurement

One of the first test performed compares the measurement of the diffusion coefficient of the improved formula against the traditional measurement by the Einstein-relation in a case where no convection can be found. We plotted measurements of the mean square displacement with the traditional formula and with the convection corrected formula in figure 5.3. The fact that only one line is visible in the plot of both measurements gives testimony of the negligible difference in the results of both methods. In fact, the mean squared distances measured in this example deviate in the order of 10^{-6} , where measurement was taken over 2197 molecules, which were placed in EC structures as described below. (However we only allowed Lennard Jones interaction in between the molecules.) In an example averaging over 214 molecules the deviation was in the order of 10^{-5} . We can conclude that in test cases without convection and reasonable numbers¹ our procedure performs as well as the traditional method.

We proceed to an example for which we have set a strong oriented movement for all particles.

¹ With very few particles the chance increases that the random movement does have a preferred direction. In those cases the error of our method might increase in comparison to the traditional method. Nevertheless it will remain bounded by the error estimates in section 3.4.4

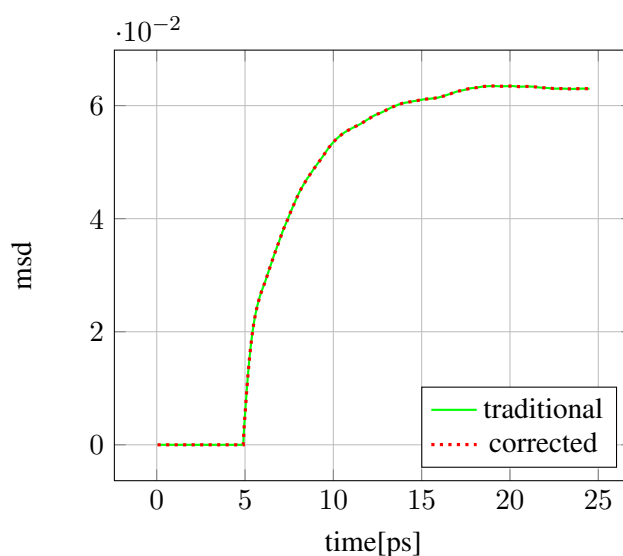


Figure 5.3: Traditional and corrected measurement of mean square displacement in comparison: The fact that the lines cannot be discerned is no error, the difference is in the order of 10^{-6} .

As graph 5.4 clearly shows, the traditional, uncorrected method wrongfully uses the full movement in its calculation for the diffusion coefficient and diverges, while in fact the random movement of the particles is very close to zero. This is correctly computed with our new, improved method. As a result we can confidently report that our new, convection corrected measurement of the diffusion coefficient performs just as well as the traditional method in traditional benchmarking problems and shows superior performance in those problems, for whose characteristics it has been designed.

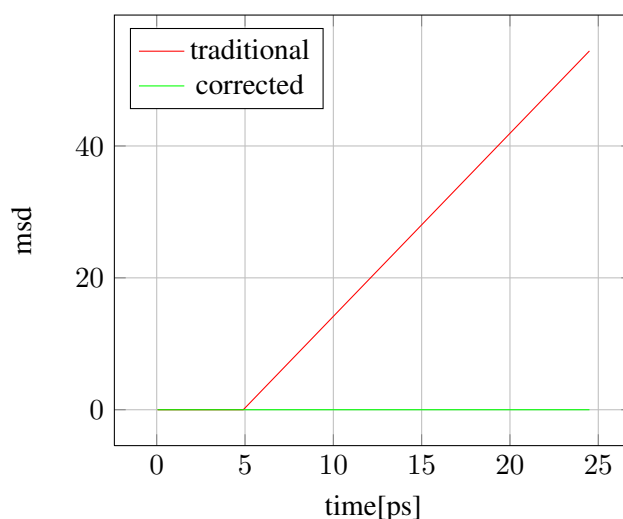


Figure 5.4: Traditional and corrected measurement of mean square displacement in comparison on a sample with convection.

The Diffusion of Li^+ and BF_4^-

Following the proof of concept we turn towards longer simulations with solutions containing ions. In order to determine a dependency of the diffusion coefficient on the concentration of the ions, we simulate several solutions, each with a different number of ions inserted. We display the graphs of the computed diffusion coefficients in figures 5.6, 5.7 and 5.8.

The values computed via the MSD in table 5.2 are generally lower than those found in the numerical simulations published in [JC98], where Li^+ was found to have a diffusion coefficient of $4.7 \cdot 10^{-10} \frac{\text{m}^2}{\text{s}}$ and BF_4^- one of $6.0 \cdot 10^{-10} \frac{\text{m}^2}{\text{s}}$. Measurements were sampled on a single pair of ions over 100 ps. Simulations were carried out using an NVT ensemble, at a temperature of 323K and a Volume corresponding to the density of pure EC. The Pressure was reported to be $1727 \cdot 10^5 \text{ Pa}$, which is approximately 1700 times more than standard atmospheric pressure.

Comparing both results to experimental data in [Hay99], we find that our values are closer to the value of $2.1 \cdot 10^{-10} \frac{\text{m}^2}{\text{s}}$ for Li^+ . We were not able to obtain experimental data for the BF_4^- ion. Further comparing the results for the self diffusion of EC, we come to the conclusion that our values are also below the reported experimental value of $8.0 \cdot 10^{-10} \frac{\text{m}^2}{\text{s}}$ [Hay99].

In order to get an insight into the deviations we witness, we additionally plot the results of the diffusion coefficient of EC for all NPT simulations and NVT simulation. Here we observe that despite the much shorter simulation time, the graph of the NVT simulation is subject to less pronounced oscillations than the graphs of the NPT simulations. Those oscillations could possibly be the result of the oscillation of the simulation domain, as the volume is changed in order to hold a constant pressure. Additionally we observe that the diffusion values of EC are computed to be less than half in magnitude of those, which we computed with the NPT simulations. This may be the result of two contributions. As outlined above, the simulation domain increased from the volume predicted by the physical EC density during the NPT simulation. Thus the NVT ensemble simulates an unnatural density, which can be expected to hinder the movement of the particles. The other contribution could be the domain resizing during the NPT measurement itself, which results in oscillations in the particle conditions.

# Ions	$D_{EC}^{MSD} [10^{-10} \frac{\text{m}^2}{\text{s}}]$	$D_{Li}^{MSD} [10^{-10} \frac{\text{m}^2}{\text{s}}]$	$D_B^{MSD} [10^{-10} \frac{\text{m}^2}{\text{s}}]$
0	2.83	0.00	0.00
6	2.04	0.50	0.58
8	2.24	1.65	2.58
10	2.82	1.40	2.27
12	2.28	0.75	2.39
14	2.03	1.16	1.53

Table 5.2: Diffusion results of MD simulation with ethylene carbonate

In table 5.3 we have also included our computations for the chemical potential of the Li^+ ions. Since the computation of the chemical potential requires the integration over various concentrations as part of the algorithm, the comparison of the results at the different concentration levels does not indicate the quality of the prediction. Furthermore, we have been unable to obtain data (neither experimental nor simulated), which refers to this particular setup of Li^+ ions in an EC electrolyte. In the compilation [DGJ] we have found reference

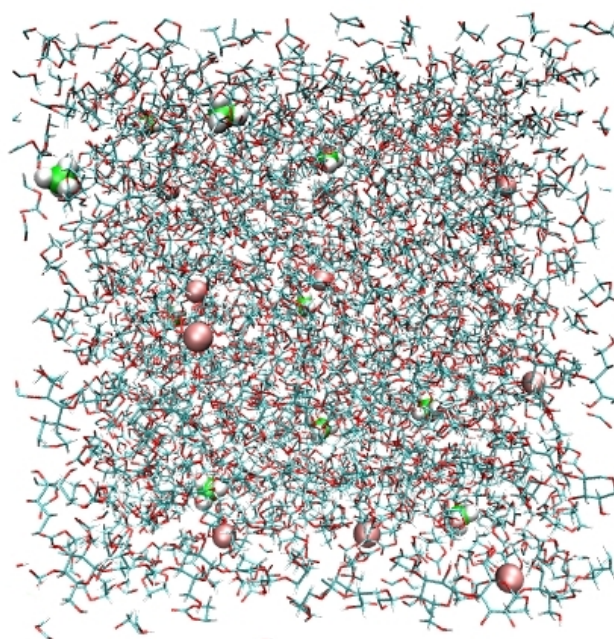


Figure 5.5: Simulation cell with 10 Li^+ and 10 BF_4^-

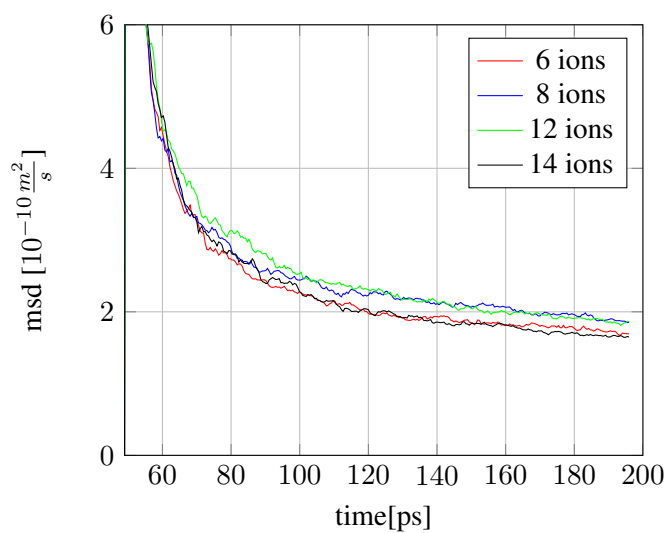


Figure 5.6: Diffusion coefficient of the EC electrolyte.

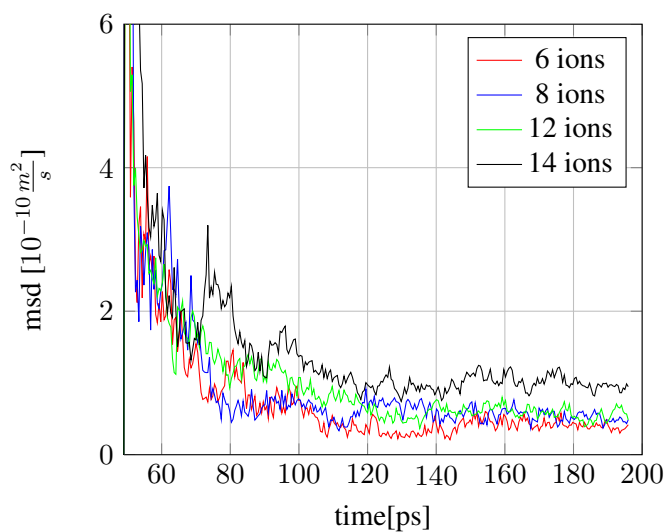


Figure 5.7: Diffusion coefficient of the Li ions.

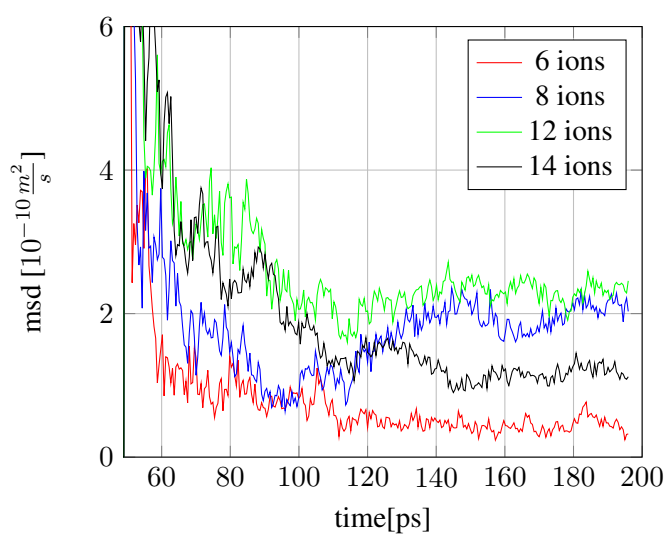


Figure 5.8: Diffusion coefficient of the B ions.

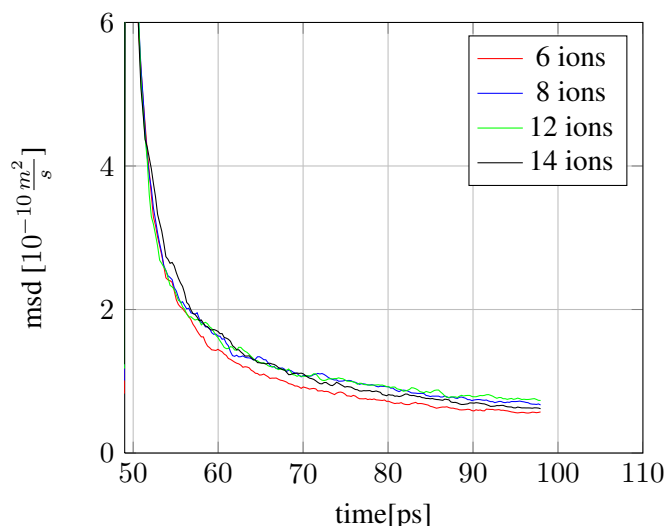


Figure 5.9: Diffusion coefficient of the EC ions.

# Ions	$c[\frac{mol}{l}]$	Volume [m^3]	Pressure [Pa]	chem Pot [$\frac{J}{mol}$]
0	0.00	$2.52 \cdot 10^{-25}$	$4.14 \cdot 10^7$	NaN
6	0.04	$2.51 \cdot 10^{-25}$	$4.15 \cdot 10^7$	$-3.66 \cdot 10^4$
8	0.05	$2.51 \cdot 10^{-25}$	$4.19 \cdot 10^7$	$2.35 \cdot 10^5$
10	0.07	$2.51 \cdot 10^{-25}$	$4.1 \cdot 10^7$	$3.96 \cdot 10^5$
12	0.08	$2.5 \cdot 10^{-25}$	$4.2 \cdot 10^7$	$5.03 \cdot 10^5$
14	0.09	$2.5 \cdot 10^{-25}$	$4.13 \cdot 10^7$	$5.79 \cdot 10^5$

Table 5.3: Chemical potential results of MD simulation with ethylene carbonate

values for Li in various configurations. While our estimate falls in between the values given for aqueous solution and gaseous form we lack comparison to fixed reference values. However, one should note that our method is not required to predict an exact number but only needs to predict the correct change in the chemical potential, as it is only the gradient of the chemical potential, which is used in the PNP. Of the gradient however, we could find no reference values whatsoever.

5.2.2 Cellulose

After having measured the ionic diffusion and chemical potential we turn towards a new material setup. In order to combine membrane with electrolyte properties, we insert strands of cellulose in the ethylene carbonate polymer. The intramolecular forces of the cellulose molecules were also modelled by the AMBER force field parameters [Cor95]. In table 5.4 we present the Lennard-Jones and charge parameters used for the intermolecular field, which mostly correspond to those from table 5.1, with slightly modified charges for OS and CT, in order to preserve electroneutrality for the molecule. For both, ion placement and numerical

simulation, we followed the same procedure as already described in 5.2.1 for the simulation of the ions in EC. Computations were performed with 0 and 10 ions of each species. Subsequently we omitted the computation of the chemical potential, as we lack the required data points for the integration.

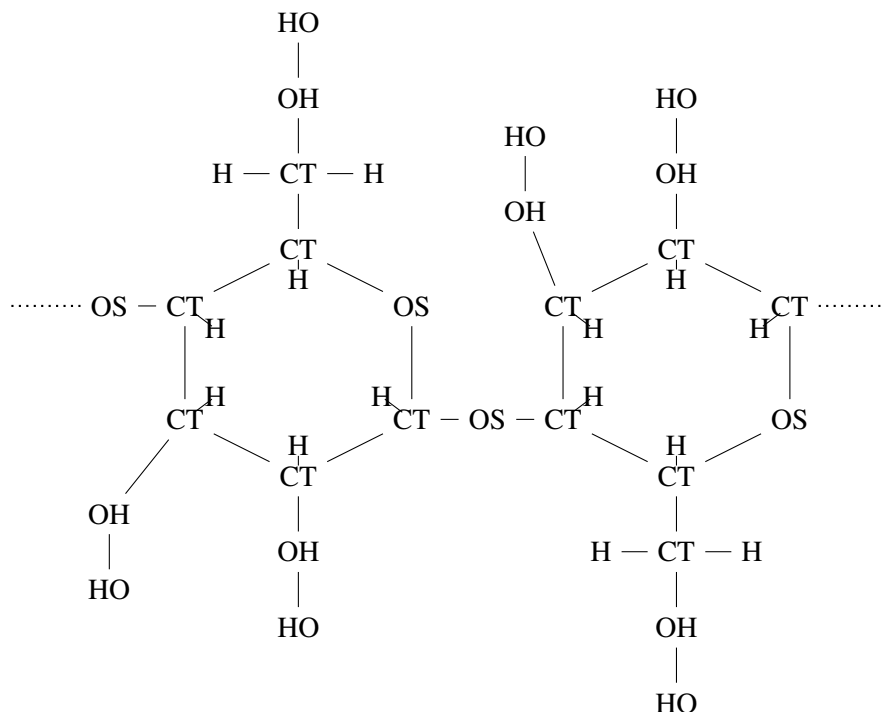


Figure 5.10: Atomic structure of cellulose in beta-1,4 configuration; with atom type labels as used by the AMBER force field tables.

molecule	atom	$\sigma/\text{\AA}$	$\epsilon/\frac{\text{kcal}}{\text{mol}}$	q/e
O	2.96	0.210	-0.6452	
OS	3.00	0.170	-0.46845	
CT	3.5	0.066	0.03305	
H1	2.5	0.030	0.1041	
OH	3.5	0.105	-0.417	
HO	2.5	0.03	0.45	

Table 5.4: Van der Waals parameters and partial charges for cellulose.

The results of the simulation are shown in figure 5.12 and 5.5. From our results we conclude that the cellulose inlay in our simulation cell remains relatively immobile, whereas the electrolyte shows, respecting the error tolerance, the same behavior as before.

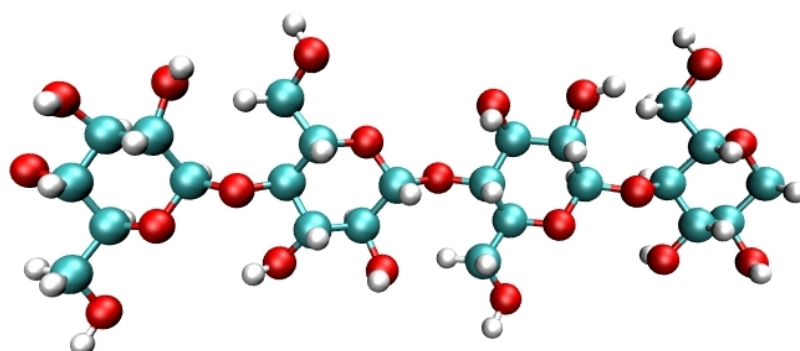


Figure 5.11: Cellulose string; simulated with four basic components in beta-1,4 configuration

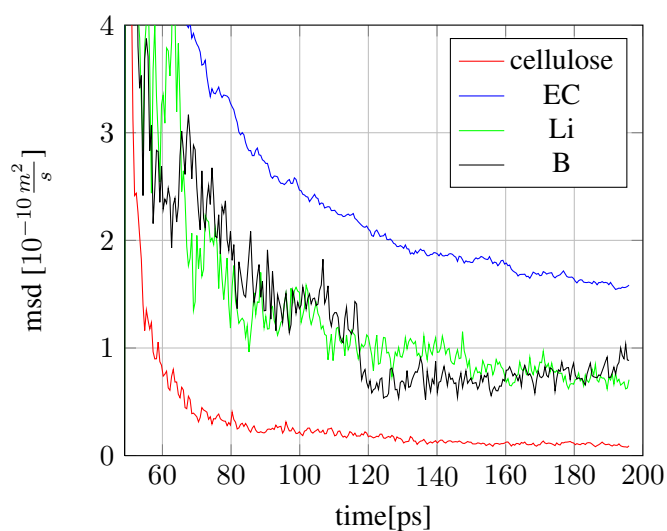


Figure 5.12: Diffusion coefficients with cellulose.

# Ions	$c[\frac{mol}{l}]$	Volume[m ³]	Pressure[Pa]	$D_{EC\ a}^{MSD}$	$D_{Cell\ a}^{MSD}$	$D_{Li\ a}^{MSD}$	$D_{B\ a}^{MSD}$
0	0.00	$1.52 \cdot 10^{-25}$	$4.66 \cdot 10^7$	3.13	0.14	0.00	0.00
10	0.11	$1.51 \cdot 10^{-25}$	$4.65 \cdot 10^7$	2.81	0.12	0.83	0.73

Table 5.5: Results of MD Simulation with cellulose; a: $[10^{-10} \frac{m^2}{s}]$

5.3 Transporting Defects in a Solution

We will now proceed to the discussion of the NPNP solver. As already mentioned, the establishment of benchmark problems for the PNP equation system to demonstrate the potency of a solver has not yet taken place. Therefore we present our own choice of problems with increasing difficulty, starting here with a decoupled diffusion convection problem.

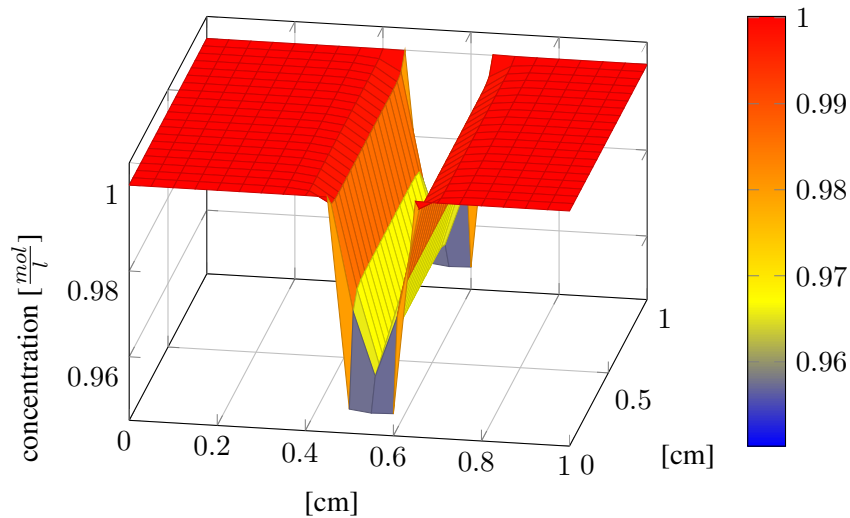


Figure 5.13: Specis A, initial setup

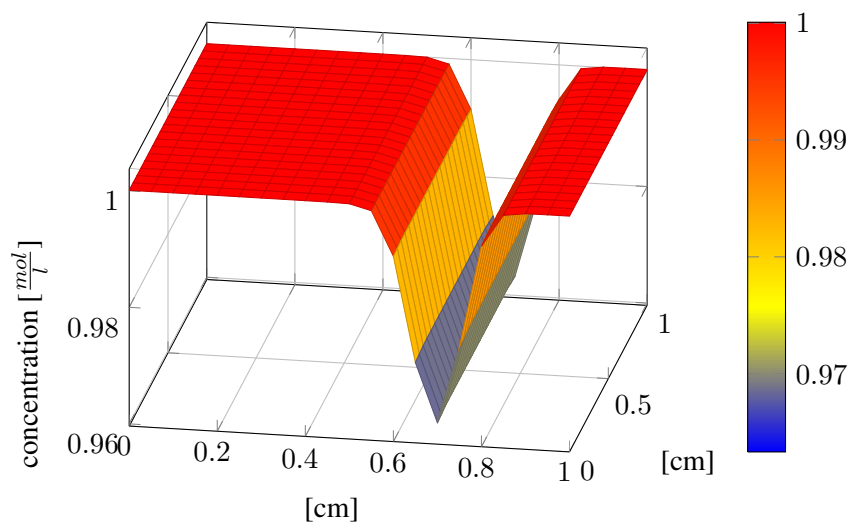


Figure 5.14: Specis A, after 1200 steps

Turning towards the FEM solver of the Nernst-Planck equation, we intend to simulate ion concentration behavior in a solution. As we mentioned in section 4.5, the solution of the coupled system shows a strong dependence on the solution of the Poisson equation. In physical

examples, the coupling between the ionic species is particularly strong, as the constants in the Poisson equation lead to very large constants on the right hand side even after nondimensionalization 4.1. Thus the solutions of a fully coupled example lack the transport characteristics of defects or abundances of concentration. Therefore, we precede our investigations by a trivial, non-coupled (and thus non-physical) example, to exhibit the transport capacity of the solver code. We consider a standard square domain $[0, 1]^2$ of two regions, where we start with two ion concentrations of 1.0 in the bulk of the domain and place a defect of concentration of 0.95 in a central strip $[0.5, 0.6] \times [0, 1]$. Species A is assigned a diffusion coefficient of $2.1e^{-10}$ and a charge of +1, whereas species B is assigned a diffusion coefficient of $4.2e^{-10}$ and a charge of -1. The boundary conditions imposed set the joined flux of diffusion and convection across the boundary to 0, as described in 4.4.1. The starting configuration and the result after 1200 timesteps can be observed in figure 5.14 for species A and in figure 5.16 for species B respectively. As expected, the transport is oriented in opposing directions. We further observe that the defects “smear” out, evidence for the combined effect of diffusion and convection. Both effects show more advancement in species B than in species A, which is expected given that the diffusion coefficient of species B is approximately twice as large as that of species B.

From the above results we conclude that we have mastered the convection and diffusion properties of the decoupled Nernst-Planck equation. The magnitudes of the ionic mobility, as determined by the diffusion coefficient, produce an observable effect as expected prior to the experiment.

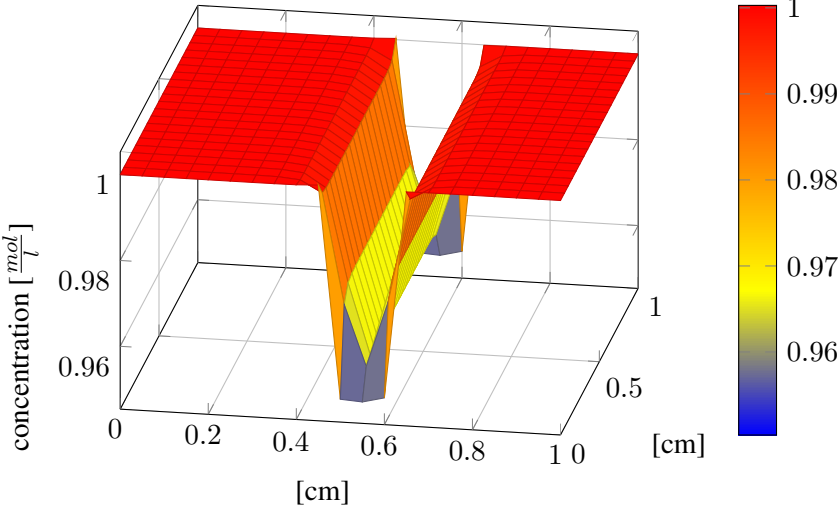


Figure 5.15: Specis B, initial setup

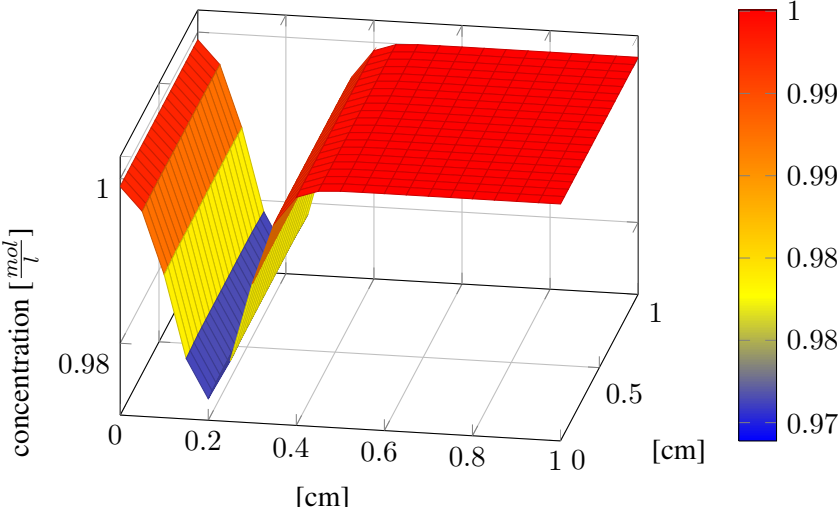


Figure 5.16: Specis B, after 1200 steps

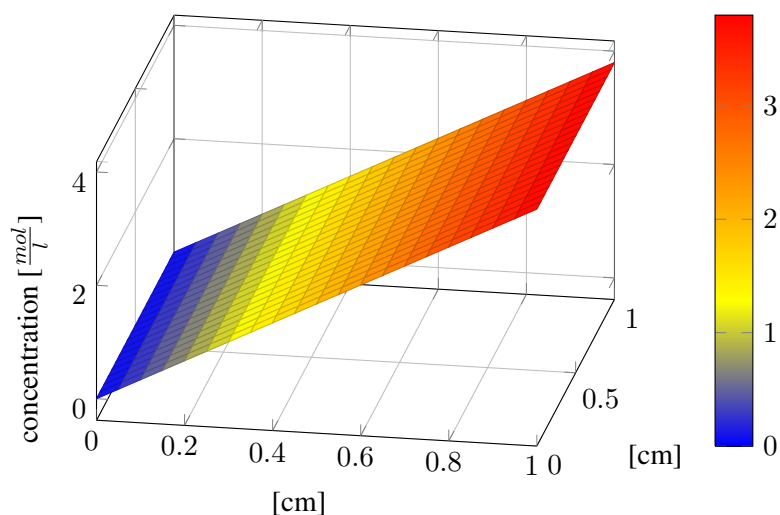


Figure 5.17: Electric potential, initial setup

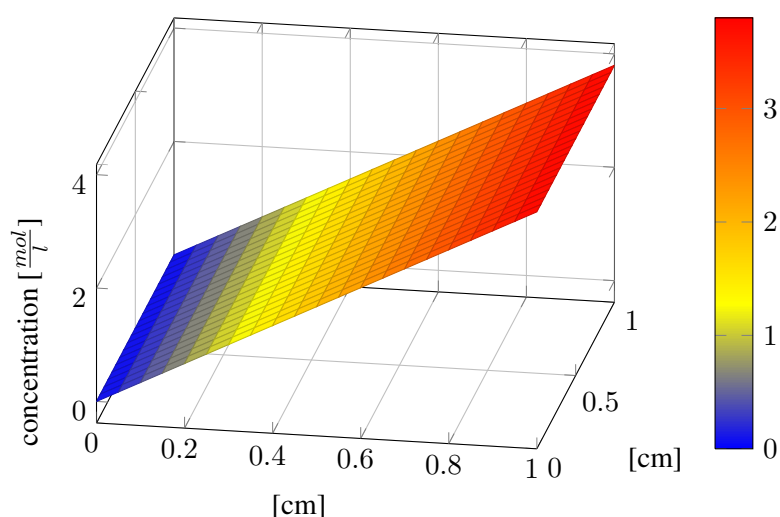


Figure 5.18: Electric potential, after 1200 steps

5.4 Ionic Migration in a Battery System

We now proceed to the fully coupled equation system by simulating the model of a two-species battery. Since we are about to simulate a physical system, we will introduce the boundary conditions defining the properties of this model. They are caused by a concept known as the electro-chemical potential, which is the cause of the net flow which is obtained outside the system. The electrochemical potential is an expression for the difference in chemical potential the electrode material has towards its respective ions. While the electrodes are isolated no reaction can occur, however, when they are placed in contact via a conductor, they exchange

electrons, and the reactions proceed. Thus the current allows for the measurement of the difference of the chemical potential of the electrodes in voltage, that is as a change of electrical potential.

Thus the boundary conditions are implemented as follows:

- For the Poisson Equation Dirichlet boundary conditions are imposed on the electrodes, where each electrode has constant potential (it is a conductor) and the difference between the constants is equivalent to the voltage of the battery. The actual constants are not relevant, as in the NP only derivatives of the potential are computed. Idealizing the battery as a condensator, von-Neumann zero-gradient conditions are imposed on the other boundaries.
- For the NP boundary we set the flux over the electrode boundary to the charging/-discharging current, whereas Robin zero-flux conditions are imposed on the other boundaries. In light of 4.4.1 we have to specify, whether to fix the flux only for the diffusion or for the combined convection-diffusion. This is in essence a modeling question, which should be decided by understanding the ionic behavior on the electrode/electrolyte interface. However, this behavior is far from being understood and the subject of current research. Therefore we have tested both variants. In that process we found that taking the diffusive and convective flux into account yields unphysical results and thus proceed by restricting the integration by parts on the diffusion term.

The magnitude of the ionic flux from the electrodes into the bulk material is another difficult matter, since it is governed by the change in the potential at both electrode-electrolyte interfaces, as this determines the electrons supplied via the conductor. However, we can make use of the formula for electric power P , which enables us to determine the current I via the electrode potential U :

$$P = U \cdot I. \quad (5.1)$$

We then need to calculate the local ionic flux of the species from the electrical current,

$$J_i = \frac{I * \delta t}{A * z_i} \quad (5.2)$$

where A is the interface area and z_i as usual the charge number of the respective ion. While batteries exist, which make use of more than one species reaction (e.g. the Daniell element), each of those reactions is confined to one electrode. Thus, even in those cases where more than one ion participates in the electrochemical reaction, the above model describes the boundary conditions to their full extend.

We simulate a two dimensional lithium-ion battery cell. For the diffusion coefficients we use the average values of our upscaling procedure from table 5.2, namely $1.092e^{-10} \frac{m^2}{s}$ for Li^+ and $1.87e^{-10} \frac{m^2}{s}$ for BF_4^+ . The potential difference is set to 3.8 V, which is the change in energy observed for the $Li \rightarrow Li^+$ reaction. The cell size is set to 1 cm in both axis directions, with discretization intervals of 0.05, the time step is set to 0.05 s. The ionic flux over the electrode boundary is set to 0.5 A for Li^+ and zero for BF_4^+ .

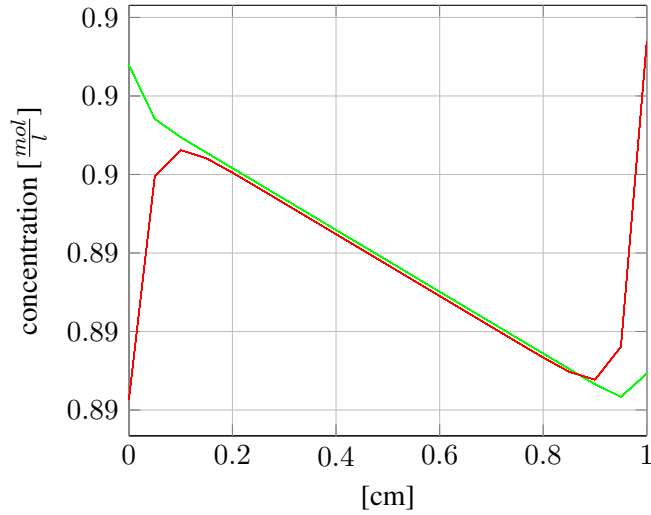


Figure 5.19: Concentration profile 2D battery: Li^+ red, BF_4^- green.

Observing the projection of the ion profile during the discharging procedure, displayed in 5.19, we can confirm the formation of key-characteristics of the solution. Specifically, we observe the bulk of the profile declining in the direction of the ion flux imposed on the boundary, while both concentrations are almost identical. Close to the electrodes, we observe that the profiles separate and cause an increased gradient in the electric potential (see figure 5.20). This behavior is characteristic for the so called Nernst-double layer, which is a model for the ion behavior on the electrode/electrolyte interface. Note that we have not specifically modelled this behavior into our equations, but it arose automatically from our physical treatment. We further observed that in the course of the simulation the gradient of the electric potential in the bulk of the cell tended towards zero, satisfying the boundary conditions by increased gradients in the interface regions. This behavior models the exhaustion of the battery, as the ion transport ceases inside the domain and the flow over the boundary cannot be kept up. With our crude boundary model we were not able to actually reproduce the exhaustion effects on the current, in fact, it is remarkable that we observed this change of the inner potential.

5.4.1 Convergence

In addition comparing qualitative characteristics of our solution function, we will now present convergence results of the solution under grid and time refinement. Since no analytical solutions for our problems are available, we compare the magnitude of the error in successive refinements by the following formula:

$$e_n = \frac{|u_{n+1} - u_n|}{|u_n - u_{n-1}|}. \quad (5.3)$$

In table 5.6 we present the error relation for time refinement. While initially we obtain an excellent indication of first order convergence, we notice that starting with the fourth refinement

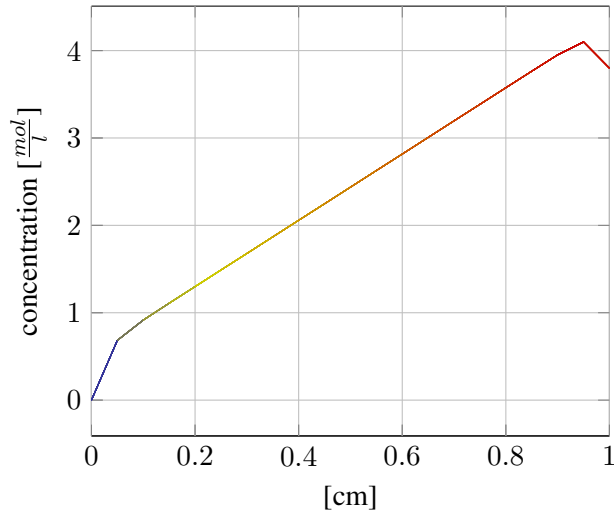


Figure 5.20: Electrical potential of 2D battery.

step, the error in the L^2 and L^∞ norms seems to increase with further time refinement, while the H^1 -error is further reduced. This seemingly odd behavior is the result of numerical loss of mass, investigated in [Mat07]. The electric field is not divergence free, as its source, the charge distribution, is naturally contained inside the simulation domain. As a result, the discretized equation gains an additional term on the right hand side of the equation, leading to the observed loss of mass in every timestep. The rate of loss of mass is constant per timestep made, independent from the time or space discretization. In [Mat07] the loss of mass is also connected to numerical discontinuities in the transport term. While our use of finite elements for the computation of Φ guarantees that Φ itself is not discontinuous, this may not necessarily be true for its gradient, which is our transport term.

In this context we call to attention our very first simulation using the decoupled system. As we can deduce from figures 5.17 and 5.18, the electric field is divergence free, as the gradient of the potential is constant and thus additionally continuous. When observing figures 5.14 and 5.16, we further notice that after 1200 time steps no change of mass has occurred. This result has been confirmed by measurements with other setups using a divergence free convection term.

While the loss of mass hinders the convergence of the function values, their gradient converges. This allows the conclusion, that the transport and diffusion processes, which are primarily dependent on the relative values of the concentration and not the absolute ones, are very well approximated.

time refinement	H^1 -error	L^2 -error	L^∞ -error
2	0.50	0.50	0.50
4	0.50	0.53	0.50
8	0.48	0.79	0.50
16	0.48	1.63	0.81
32	0.46	1.97	2.00

Table 5.6: Convergence rate of NPNP computations, refinement in time.

In table 5.7 we display the error relation for simultaneous time and space refinement. While the numbers in this table hint towards a first order convergence as well, conclusive results can not be drawn, as only four successive refinements could be computed due to limits in computational resources. At this point we remark that the accuracy of the solver is not necessarily the limiting factor regarding the accuracy of the complete method. As we made use of the upscaled values from the MD simulations, the errors made there influence the quality of the results made in the macroscopic solver. Even if our solver were to produce exact analytical solutions to the Poisson-Nernst-Planck system, the solution would still carry the error from the upscaling procedure. Therefore, one needs to consider the relation of the errors of the two methods, as it would be a waste of computational resources if the macroscopic solver were refined to obtain machine epsilon¹, when the error carried from the upscaling method is much larger.

# DoF	H_1 Error	L_2 Error	L_∞ Error
77,763	0.79	0.49	0.56
309,123	0.88	0.55	0.63

Table 5.7: Convergence rate of NPNP computations, refinement in time and space.

5.4.2 3D computation

After our previous example, we now compute the solution to a three dimensional system and introduce regions of changing coefficients. We used the same parameters as for our first example 5.4, with the exception of using the cellulose parameters from 5.5 in the region $[0.9, 1] \times [0, 1]$. Furthermore we reduced the degree of the finite element basis functions to one and keep a grid refinement of 0.1.

In figure 5.21 we have plotted a projection of the 3D result. We observe the same qualitative behavior as in the previous, two-dimensional test.

5.4.3 The Influence of Dendrites

In the above section we have been able to show our competence in PNP computations, however we have not yet demonstrated that our approach opens new areas of investigation, which have previously been inaccessible, since the above examples essentially only show one dimensional

¹ Machine epsilon describes the accuracy of the finite number representations in a computer.

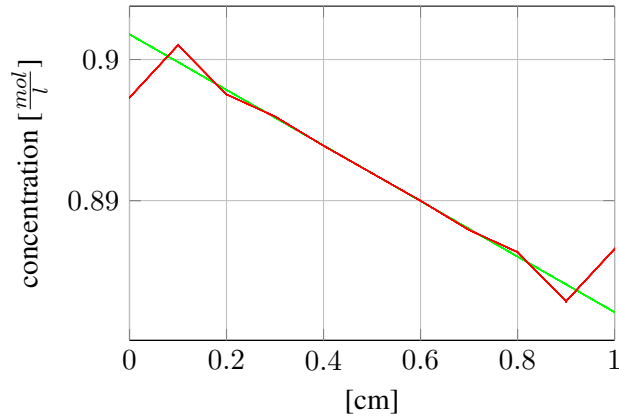


Figure 5.21: Concentration profile 3D battery: Li^+ red, BF_4^- green.

variation of the concentration. We proceed to an example, in which we insert “defective” regions, regions in which the diffusion coefficient varies from the surrounding domain. As we aim towards the simulation of batteries, we have the formation of dendrites in mind, which in real batteries would in the long run lead to short circuiting. The setup is again a two-dimensional cell. For the diffusion coefficients in the bulk electrolyte we use the same average values as before. In the region $[0.9, 1] \times [0, 1]$ we again simulate a cellulose membrane by using the diffusion coefficient displayed in 5.5. Furthermore we specify regions with a diffusion coefficient approximately one order larger of $1.0e^{-9} \frac{\text{m}^2}{\text{s}}$. The potential difference and the length scale are left as in the previous example, as is the spatial refinement. The time step size has been reduced to 0.005 s to cope with the discontinuity in the diffusion coefficient.

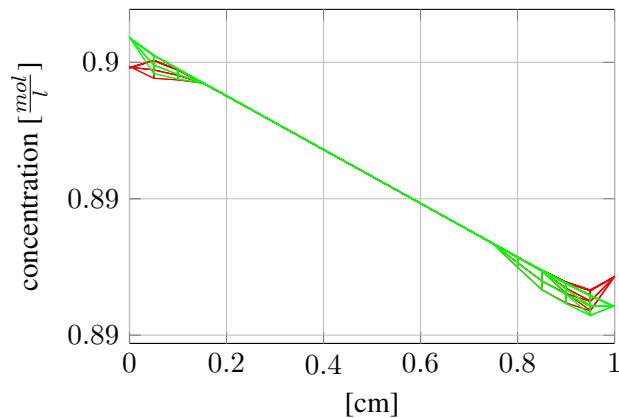


Figure 5.22: Concentration profiles with dendrite regions: Li^+ red, BF_4^- green.

[[IMAGE DISCARDED DUE TO '\tikz/external/mode=list and make']]

Figure 5.23: Concentration profile of Li^+ with dendrite regions.

The resulting concentration profiles are displayed in figure 5.22 and 5.23. The regions which

were assigned a higher ionic mobility feature sinks in the ionic concentrations for either species. At the same time we observe that both double layers at the electrodes are far less pronounced than in both previous examples. While one simulation does not provide enough background data for a rigorous analysis, this result hints towards self-augmentation of dendrite growth. As the existing dendrites conduct the ions faster than the bulk solutions, it seems ions are drawn towards them and thus increase the chance of further dendrite growth.

5.5 Multiple Species with the Incorporation of a Reaction Term

For the following simulation we leave the domain of battery modelling and turn towards the handling of cementitious material. The present simulation does not aim to be quantitative accurate, but a proof of concept. We demonstrate that we are able to model the penetration of a porous material through an ionic solution, have some reaction inside the material and subsequently leach the reaction product out of the domain.

The reaction model used is incorporated as described in section 3.7. The setup consists of an immobile setting of species 0 in a complex geometry. Species 1 and species 2 have identical diffusion coefficients, which are linearly dependent on the concentration c_0 of species 0 according to the formula $D = D_0 + (1 - c_0) \cdot (D_1 - D_0)$, where $D_0 = 1.0e-7$ and $D_1 = 1.0e - 4$. Species 1 was initially set to zero on the complete domain, but boundary condition were set to 0.25, to simulate a totally equilibrated infinite supply on the outside, as outlined in section 4.4.1. Species 2 has an initial concentration of 0 and zero boundary conditions. Species 0 and species 1 react with equal contribution (meaning the stoichiometric coefficients are 1) to form the product species 2. The simulation domain contains some cells which are impenetrable for all of the species. Neither species in this example carries a charge.

The results demonstrate that the species respect the impenetrable domains and only diffuse through the channels. We clearly observe the dissolution of species 0 and the production of species 2. The influence of the reaction on species 1 is harder to discern from the visual results due to the balancing effects of the diffusion and the inflow.

From this numerical experiment we draw several conclusion:

- We have produced further evidence for the ability of the solver to deal with complex geometries, as this time the solver dealt with impenetrable regions.
- We have shown the successful implementation of Dirichlet boundary conditions.
- The direct discretization of the reaction as described in section 3.7 is stable and produces sensible results.
- The concentration dependency of the diffusion coefficient is in working order.
- We observe the effects of the adaptive refinement of the simulation domain.

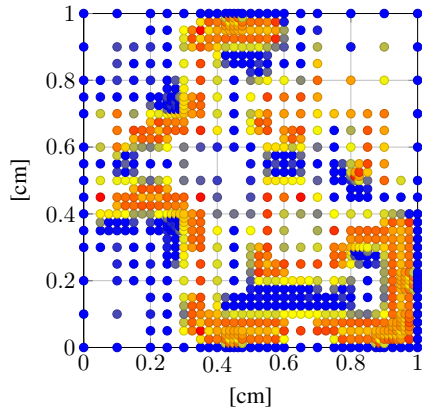


Figure 5.24: Species 0, $t=1$.

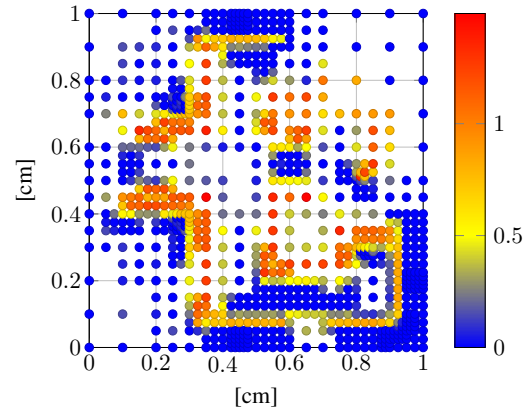


Figure 5.27: Species 0, $t=20$.

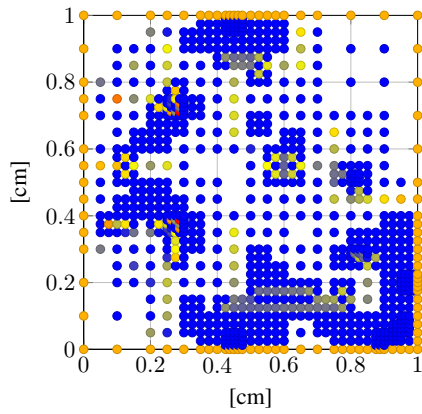


Figure 5.25: Species 1, $t=1$.

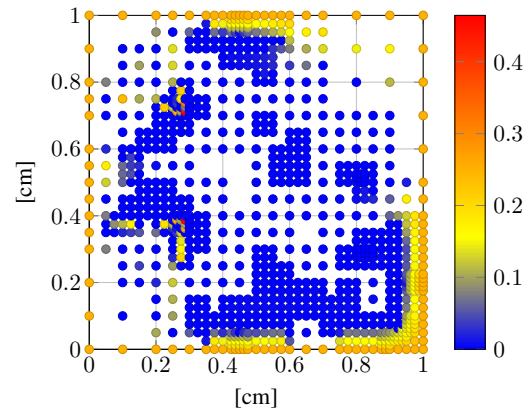


Figure 5.28: Species 1, $t=20$.

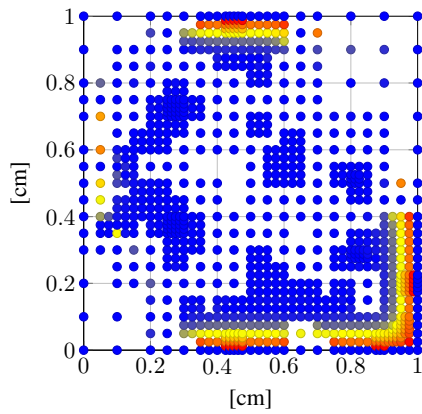


Figure 5.26: Species 2, $t=1$.

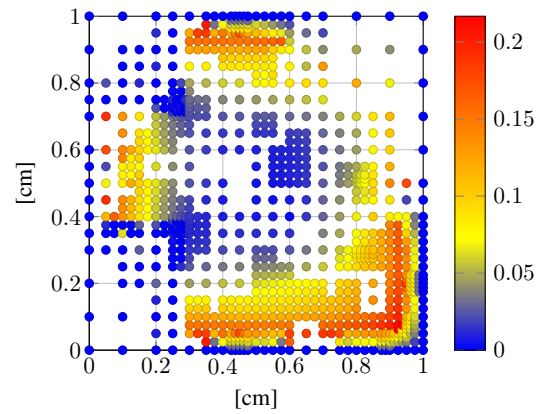


Figure 5.29: species 2, $t=20$.

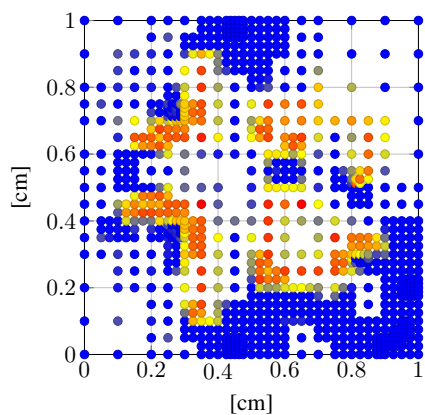


Figure 5.30: Species 0, $t=40$.

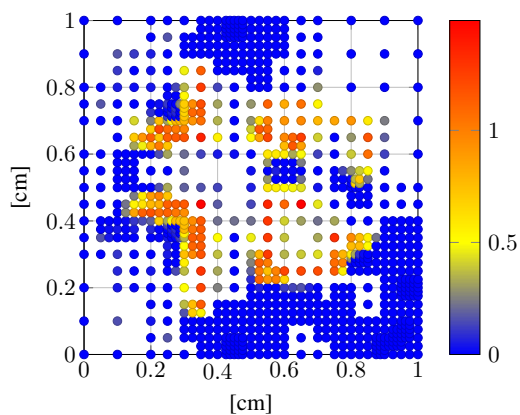


Figure 5.33: Species 0, $t=60$.

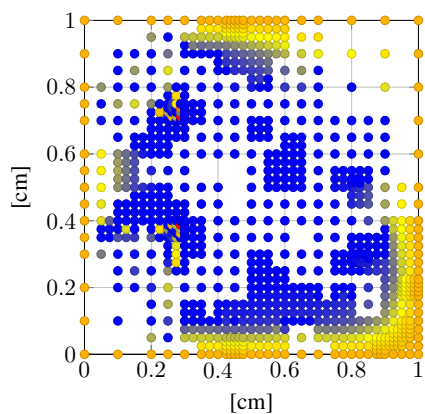


Figure 5.31: Species 1, $t=40$.

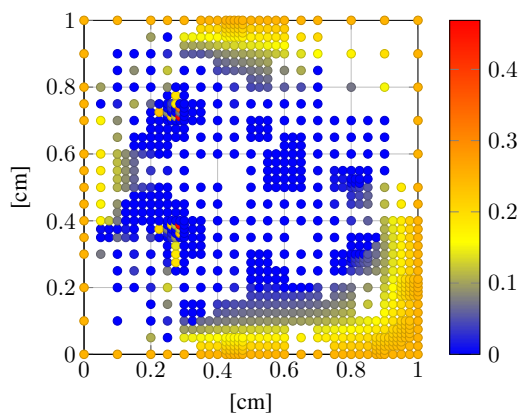


Figure 5.34: Species 1, $t=60$.

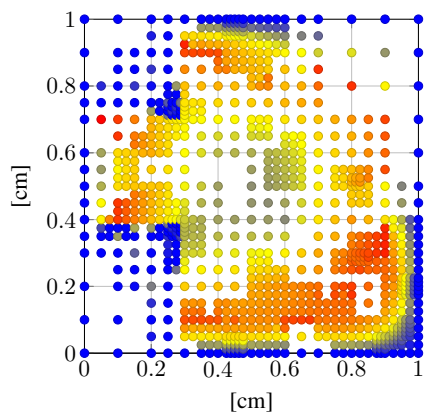


Figure 5.32: Species 2, $t=40$.

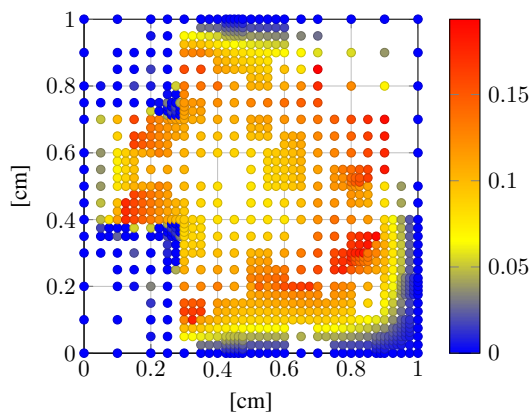


Figure 5.35: Species 2, $t=60$.

Chapter 6

Concluding Remarks

In this work we have established a multiscale treatment for the numerical simulation of ionic motion. We have presented the numerical simulation of atomic systems and analyzed how they relate to the corresponding physical system via the concept of the phase space. By using the method of averaging, we have determined how the atomic and molecular motion affect the ion concentration on the macroscopic scale and we have derived formulas to extract coefficients for the diffusion and convection in the Poisson-Nernst-Planck model. We have developed an improvement to the traditional formula for the diffusion coefficient in order to account for convection effects present in the molecular dynamics simulations. We have further implemented a known method for the calculation of the chemical potential.

The upscaled coefficients have been placed in the Poisson-Nernst-Planck equation, which models the behaviour of the ionic concentration on a macroscopic level. We have compiled an operator for the complete system of equations and developed a linear time discretization, which allows for stable propagation of time steps, despite the strong non-linear coupling induced by the dielectric constant in the Poisson equation.

Using the implemented methods in various testing environments, we have established their success. Specifically, we have confirmed that the convection corrected measurement of the diffusion coefficient is at least equivalent and in some cases superior to the traditional uncorrected measurement. For the measurement of the chemical potential we found that our results fall within the range of other data, while a detailed analysis could not be performed due to the lack of comparable experiments.

While lacking standardized benchmarking scenarios, we have over a series of tests demonstrated the capabilities of the NPNP solver. The calculations have shown expected behaviour in constructed testing scenarios and in more complicated physical setups they were able to reproduce key features of the modeled system, a lithium-ion battery. We were able to expand the accessible geometries and in our prime application, the modeling of batteries, made the simulation of key features possible, which were not accessible before. In addition we have demonstrated that the application of this work is not restricted to one application only, but succeeds in different research areas as demonstrated on the example of the degradation of amorphous material, in which we demonstrated the possible inclusion of reaction effects into our model as well.

In summary we can confidently present the multiscale solver to the PNP as a success on all

involved levels. Our method possesses the potential to make high qualitative predictions for the performance of new materials and structural layouts and thus can contribute to the technological challenges in the fields of batteries and amorphous materials.

6.1 Future Prospects

In our numerical experiments we have shown the strength of our multiscale method. Nevertheless, we have also encountered limitations, which can be discriminated into those due to limitations in the available resources and those which invite further study and improvement on the mathematical model.

The issues experienced in our computations in the molecular domain fall largely into the first category. As we are investigating solutions consisting of bulk material and incorporated ions, the number of molecules in the bulk material is generally large compared to the number of ions within and limits the size of the example which can be calculated within sensible timescales on medium sized computer grids. We have directly seen the impact of those restrictions on the accuracy of our computations, as we compared the fluctuations of averages over several 1000 molecules to those averaging over a dozen particles. Increasing the number of the relevant ion particles into the thousands would result in a respective atom count in the range of several million particles. In addition, the sampling over the full phase space could be very much improved by assembling multiple starting configurations of the same physical system and average over the various trajectories we would obtain. Consequently, larger parallel grid computing structures would make it possible to achieve much more accurate results with the model presented in this paper. We have further outlined the errors introduced in our calculations by either inaccurate knowledge of a system thermodynamical quantities or the error induced into our measurement by numerical occurrences from the use of specific ensembles. Removing the prior issue is a task to be delegated to the physical or chemical sciences. The latter however could be taken into account by modifying the MD simulation software, to account for coordinate changes of the particles due to rescaling and remove those effects from the MSD measurements, much as we have removed the influence of convection.

Another task left to the chemical sciences is the compilation of sufficiently accurate, yet flexible parameters for intramolecular force descriptions. The accuracy of the MD calculations and subsequently the predictions about a material vary with the accuracy with which we model the atomic behaviour.

Pending the resolution of the above issues, another field of study would be the extraction of a diffusion tensor, with the diffusion coefficient varying along different axis in space. This would promise more accurate description of ionic behaviour in oriented structures. With the declared intent to investigate into membrane behaviour for batteries, this advancement might make insights possible, which are currently beyond the scope of any published research.

With our continuous solver we have demonstrated our ability to model time dependent behaviour of ionic migration in different physical settings. While the issues of mass conservation in the coupled system need to be addressed, we were able to reproduce key characteristics of battery systems, despite very crude models on the boundary conditions of the domain. A promising variant seems to be a dependence of the flux and the local potential gradient on

the boundary. Future work should make a reliable model of the boundary a priority. The actual behaviour of ions on the interface between electrode and electrolyte is the subject of current research in physics, chemistry and engineering. As a long-term goal towards the full understanding of battery behaviour, this interface region should also be evaluated with multiscale methods. Since the surface and material of the electrodes have a comparable high influence on the performance of a battery, the ability for accurate predictions in that domain may be expected to be of equal importance as the understanding of the membrane, to which we have already contributed in this thesis.

Appendix A

Homogenization

In this appendix the mathematical technique of homogenization will be presented with respect to a diffusion - convection - reaction problem. All results presented here need to be weighed against the cautions voiced in section 3.2.3

The idea of homogenization is to analyze the solution to a problem with fast oscillating coefficients on a periodic cell structure, and, by analysing its local behaviour on a sample cell, derive non-oscillating, homogenized, effective coefficients for the global problems.

Power Series Ansatz of the Solution Function

Since a dependence on the scale of the periodicity is expected, the solution function u_ε is assumed to have the following dependencies: $u_\varepsilon(x, \frac{x}{\varepsilon}) = u_\varepsilon(x, y)$ with the obvious substitution $y = \frac{x}{\varepsilon}$. Furthermore to start with actual calculations on the expression on the homogenized operator we make an ansatz that the non homogenized solution function can be presented in a power series of the scale of the problem. The function u_ε then takes the following shape:

$$u_\varepsilon(x, y) = \sum_{i=0}^{\infty} \varepsilon^i u_i(x, y) \quad (\text{A.1})$$

Prior to inserting this series into the differential equation we note, that the differential operator ∇ now needs to apply not only to the variable x , but also the variable y , derived from x . With the given substitution it takes the form: $\nabla \rightarrow \nabla_x + \frac{1}{\varepsilon} \nabla_y$.

We further make the substitutions $\frac{ze\nabla\Phi}{k_B T} = b(x)$ and $\frac{\nabla\mu}{k_B T} = v(\frac{x}{\varepsilon}) = v(y) = v_\varepsilon$, accounting for the fact, that the electric field is a result of the concentration of the solution on the whole domain, while the gradient of the chemical potential is obtained locally as is the diffusion coefficient, which is dependent on the fast oscillating variable as well: $D = D(\frac{x}{\varepsilon}) = D(y) = D_\varepsilon$

With the preparations complete it is now possible to insert the series into the differential equation in order to obtain:

$$\frac{\partial u_\varepsilon}{\partial t} = \nabla [D_\varepsilon (\nabla u_\varepsilon + bu_\varepsilon + v_\varepsilon u_\varepsilon)] + Ku_\varepsilon \quad (\text{A.2})$$

$$= \nabla_x \left[D_\varepsilon \left(\nabla_x u_\varepsilon + \frac{1}{\varepsilon} \nabla_y u_\varepsilon + bu_\varepsilon + v_\varepsilon u_\varepsilon \right) \right] \quad (\text{A.3})$$

$$+ \frac{1}{\varepsilon} \nabla_y \left[D_\varepsilon \left(\nabla_x u_\varepsilon + \frac{1}{\varepsilon} \nabla_y u_\varepsilon + bu_\varepsilon + v_\varepsilon u_\varepsilon \right) \right] + Ku_\varepsilon$$

$$= D_\varepsilon \Delta_x u_\varepsilon + \frac{1}{\varepsilon} \nabla_x (D_\varepsilon \nabla_y u_\varepsilon) \quad (\text{A.4})$$

$$+ \frac{1}{\varepsilon} \nabla_y [D_\varepsilon \nabla_x u_\varepsilon] + \frac{1}{\varepsilon^2} \nabla_y [D_\varepsilon \nabla_y u_\varepsilon]$$

$$+ \nabla_x (D_\varepsilon bu_\varepsilon) + \nabla_x (D_\varepsilon v_\varepsilon u_\varepsilon)$$

$$+ \frac{1}{\varepsilon} \nabla_y (D_\varepsilon bu_\varepsilon) + \frac{1}{\varepsilon} \nabla_y (D_\varepsilon v_\varepsilon u_\varepsilon) + Ku_\varepsilon$$

$$= \frac{1}{\varepsilon^2} \nabla_y [D_\varepsilon \nabla_y u_\varepsilon] \quad (\text{A.5})$$

$$+ \frac{1}{\varepsilon} \nabla_x [D_\varepsilon \nabla_y u_\varepsilon] + \frac{1}{\varepsilon} \nabla_y [D_\varepsilon \nabla_x u_\varepsilon]$$

$$+ \frac{1}{\varepsilon} \nabla_y (D_\varepsilon bu_\varepsilon) + \frac{1}{\varepsilon} \nabla_y (D_\varepsilon v_\varepsilon u_\varepsilon)$$

$$+ D_\varepsilon \Delta_x u_\varepsilon$$

$$+ \nabla_x (D_\varepsilon bu_\varepsilon) + \nabla_x (D_\varepsilon v_\varepsilon u_\varepsilon) + Ku_\varepsilon$$

$$= \frac{1}{\varepsilon^2} \nabla_y [D_\varepsilon \nabla_y u_\varepsilon] \quad (\text{A.6})$$

$$+ \frac{1}{\varepsilon} \nabla_x [D_\varepsilon \nabla_y u_\varepsilon] + \frac{1}{\varepsilon} \nabla_y [D_\varepsilon (\nabla_x u_\varepsilon + bu_\varepsilon + v_\varepsilon u_\varepsilon)]$$

$$+ \nabla_x [D_\varepsilon (\nabla_x u_\varepsilon + bu_\varepsilon + v_\varepsilon u_\varepsilon)] + Ku_\varepsilon.$$

By comparison of coefficients with respect to each power of epsilon we can obtain a new set of equations to work with. Note that for any positive power of ε the equations vanishes (under the assumption that the coefficient functions as well as the solution function are bounded), so the evaluation will start with the equation of lowest order. However all required information towards the shape of the homogenized problem can be obtained by looking at the first three equations.

We begin by investigating the equation with the lowest power of ε :

$$O(\varepsilon^{-2}) : \quad \nabla_y [D_\varepsilon \nabla_y u_0] = 0 \quad (\text{A.7})$$

Knowing that the solution is to be periodic in the variable y , it can be deduced from this formula, that u_0 is independent of said variable, thus it is only a function of the macroscopic variable x , e.g. $u_0(x,y) = u_0(x)$. With this knowledge we assemble the equation of the next order of epsilon:

$$O(\varepsilon^{-1}) : 0 = \nabla_y [D_\varepsilon (\nabla_x u_0 + b u_0 + v_\varepsilon u_0)] + \nabla_y [D_\varepsilon \nabla_y u_1] + \nabla_x [D_\varepsilon \nabla_y u_0] \quad (\text{A.8})$$

$$0 = \nabla_y [D_\varepsilon (\nabla_x u_0 + v_\varepsilon u_0)] + \nabla_y [D_\varepsilon \nabla_y u_1] \quad (\text{A.9})$$

where we used the fact that $\nabla_y u_0 = 0$ and $\nabla_y b = 0$. The form of the equation permits the use of a result from functional analysis, the Fredholm Alternative [Alt92], which, when applied to this problem, establishes that there only can be a solution for u_1 , if the following condition is met:

$$\int_Y \nabla_y [D_\varepsilon (\nabla_x u_0 + v_\varepsilon u_0)] dy = 0 \quad (\text{A.10})$$

We make the following ansatz

$$u_1 = \sum_{i=1}^d \left[\frac{\partial u_0}{\partial x_i} \cdot w_i \right] - g u_0 \quad (\text{A.11})$$

where w_i is the solution of the so called cell problem

$$\nabla_y (D_\varepsilon (\nabla_y w_i + e_i)) = 0 \quad (\text{A.12})$$

and g is the solution to the PDE

$$\nabla_y g = v_\varepsilon. \quad (\text{A.13})$$

The solutions to both problems are demanded to be y -periodic.

The validity of the ansatz can be verified by inserting it into (A.8).

Finally we write out the equation in the last non-positive power of ε :

$$\begin{aligned} O(\varepsilon^0) : \quad \frac{\partial u_0}{\partial t} = & \nabla_x [D_\varepsilon \nabla_x u_0 + D_\varepsilon (b + v_\varepsilon) u_0] + K u_0 \\ & + \nabla_x [D_\varepsilon \nabla_y u_1] + \nabla_y [D_\varepsilon \nabla_x u_1 + D_\varepsilon (b + v_\varepsilon) u_1] \\ & + \nabla_y [D_\varepsilon \nabla_y u_2], \end{aligned} \quad (\text{A.14})$$

where we already took the independence of u_0 with respect to y into account. When now

inserting our finding from A.8, we obtain

$$\begin{aligned}
\frac{\partial u_0}{\partial t} &= \nabla_x [D_\varepsilon \nabla_x u_0 + D_\varepsilon (b + v_\varepsilon) u_0] + K u_0 \\
&+ \nabla_x \left[D_\varepsilon \nabla_y \left(\sum_{i=1}^d \left[\frac{\partial u_0}{\partial x_i} \cdot w_i \right] - g u_0 \right) \right] \\
&+ \nabla_y [D_\varepsilon \nabla_x \left(\sum_{i=1}^d \left[\frac{\partial u_0}{\partial x_i} \cdot w_i \right] - g u_0 \right)] \\
&+ D_\varepsilon (b + v_\varepsilon) \left(\sum_{i=1}^d \left[\frac{\partial u_0}{\partial x_i} \cdot w_i \right] - g u_0 \right)] \\
&+ \nabla_y [D_\varepsilon \nabla_y u_2]
\end{aligned} \tag{A.15}$$

$$\begin{aligned}
\Leftrightarrow -\nabla_y [D_\varepsilon \nabla_y u_2] &= \nabla_x [D_\varepsilon \nabla_x u_0 + D_\varepsilon (b + v_\varepsilon) u_0] + K u_0 \\
&+ \nabla_x \left[D_\varepsilon \nabla_y \left(\sum_{i=1}^d \left[\frac{\partial u_0}{\partial x_i} \cdot w_i \right] - g u_0 \right) \right] \\
&+ \nabla_y [D_\varepsilon \nabla_x \left(\sum_{i=1}^d \left[\frac{\partial u_0}{\partial x_i} \cdot w_i \right] - g u_0 \right)] \\
&+ D_\varepsilon (b + v_\varepsilon) \left(\sum_{i=1}^d \left[\frac{\partial u_0}{\partial x_i} \cdot w_i \right] - g u_0 \right)] \\
&- \frac{\partial u_0}{\partial t}
\end{aligned} \tag{A.16}$$

which we integrate over the sample cell. The form of the resulting equation again permits the use of the Fredholm Alternative [Alt92], which, when applied to this problem, establishes that there only can be a solution for u_2 , when the following requirement is met:

$$\begin{aligned}
0 &= \int_{\tilde{Y}} (\nabla_x [D_\varepsilon \nabla_x u_0 + D_\varepsilon (b + v_\varepsilon) u_0] + K u_0 \\
&+ \nabla_x \left[D_\varepsilon \nabla_y \left(\sum_{i=1}^d \left[\frac{\partial u_0}{\partial x_i} \cdot w_i \right] - g u_0 \right) \right] \\
&+ \nabla_y [D_\varepsilon \nabla_x \left(\sum_{i=1}^d \left[\frac{\partial u_0}{\partial x_i} \cdot w_i \right] - g u_0 \right)] \\
&+ D_\varepsilon (b + v_\varepsilon) \left(\sum_{i=1}^d \left[\frac{\partial u_0}{\partial x_i} \cdot w_i \right] - g u_0 \right) - \frac{\partial u_0}{\partial t}) dy.
\end{aligned} \tag{A.17}$$

From there the homogenized equation can be deduced. Collecting the derivatives in x of the

same power we first obtain the homogenized coefficient for the diffusion term, for which we immediately cite the closed expression whose derivation can for example be found in [All07]:

$$\bar{D}_{ij} = \frac{1}{|Y|} \int_Y D_\varepsilon (e_i + \nabla_y w_i) \cdot (e_j + \nabla_y w_j) dy. \quad (\text{A.18})$$

We then collect those which contribute to a convection type term:

$$\nabla_x [D_\varepsilon b u_0] + \nabla_y [D_\varepsilon ((b + v_\varepsilon) \vec{w} - g)] (\nabla_x u_0).$$

Executing the integration we define

$$\begin{aligned} \bar{r}(x) &= \frac{1}{|Y|} \int_Y \nabla_y [D_\varepsilon ((b + v_\varepsilon) \vec{w} - g)] dy, \\ \bar{b}(x) &= \frac{1}{|Y|} \int_Y D_\varepsilon b dy. \end{aligned}$$

And finally those of reaction type:

$$-\nabla_y [D_\varepsilon ((b + v_\varepsilon) g + \nabla_x g)] u_0 + K u_0. \quad (\text{A.19})$$

for which we execute the integration as well

$$\bar{K} = \frac{1}{|Y|} \int_Y K - \nabla_y [D_\varepsilon ((b + v_\varepsilon) g + \nabla_x g)] dy. \quad (\text{A.20})$$

Combining the above definition we present the homogenized equation

$$\frac{\partial u_0}{\partial t} = \nabla_x [\bar{D} \nabla_x u_0 + \bar{b} u_0] + \bar{r} \nabla_x u_0 + \bar{K} u_0. \quad (\text{A.21})$$

Convergence

Having established an expression for our homogenized operator it remains to be shown that the product of the homogenized operator and the solution to the relative problem are indeed the limit of the series of problems which are implicitly given by the series of decreasing ε . However, for our problem such a guarantee is not known to exist, since we are unable to fulfill certain key requirements for the convergence process. One of those conditions is the positivity of D_ε on the whole cell Y . While we can guarantee non negativity on the whole domain, it is conceivable, that in membranes, where the technique of homogenization would be of use (see 3.2.3), the diffusion drops to zero in the bulk material. In that case it is not only the final convergence, but also the operator itself, which cannot be guaranteed any longer, as the equations in the cascade cease to be of Fredholm type. Furthermore, even in cases where the positivity of the diffusion is guaranteed throughout the domain, we encounter problems proving the convergence of our operator in the convection terms. In our formulation the convective

term does not scale with epsilon, nor is it divergence free. (This property is obvious by the computation of the electric field using the Poisson-equation.)

More detailed work on homogenization problems, as well a convergence results for restricted problems can be found in [All07, NR07, NR09, T.G04]

Appendix B

Existence and Uniqueness of a Solution to the decoupled Nernst-Planck Equation

$$\begin{aligned}
 & - \int [D_i (\nabla u_i^{n+1} + u_i^{n+1} \vec{b}_i)] \cdot \nabla \phi_l \, dx + \int K_i(x) u_i^{n+1}(x) \cdot \phi_l \, dx \\
 & = \int \frac{u_i^{n+1} - u_i^n}{\delta t} \phi_l \, dx \tag{B.1}
 \end{aligned}$$

$$\iff \int u_i^{n+1} \phi_l \, dx + \delta t \cdot \left[\int [D_i (\nabla u_i^{n+1} + u_i^{n+1} \vec{b}_i)] \cdot \nabla \phi_l \, dx - \int u_i^n \phi_l \, dx \right] = \int u_i^n \phi_l \, dx. \tag{B.2}$$

One of the most important questions for the solution of the NP system is, whether the equation allows for a solution and if so, whether it is unique. This question has been addressed by the well-known Lemma of Lax-Milgram:

Lemma B.0.1 *Lax-Milgram* The problem 4.17 has a unique solution in V , if

$$\exists c > 0 \quad \text{s.t.} \quad |a(u, v)| < c \|u\|_V \cdot \|v\|_V \quad (\text{bounded}) \tag{B.3}$$

$$\exists c' > 0 \quad \text{s.t.} \quad a(u, u) \geq c' \|u\|_V^2 \quad (V\text{-elliptic}) \tag{B.4}$$

We will now demonstrate that the operator from B.2 indeed satisfies the requirements of the Lax-Milgram Lemma so that a unique solution is guaranteed.

Lemma B.0.2 Let $V = H_0^1(\Omega)$. Then the operator in B.2 is bounded.

Proof We begin our proof by inserting test functions ϕ_l and ϕ_k into the left hand side of (B.3) and reordering the terms:

$$\int \phi_k \phi_l \, dx + \delta t \cdot \left[\int [D_i(x) (\nabla \phi_k + \phi_k \vec{b}_i(x))] \cdot \nabla \phi_l \, dx - \int K_i(x) \phi_k \phi_l \, dx \right] \tag{B.5}$$

$$= (1 - \delta t K_i(x)) \int \phi_k \phi_l \, dx + \delta t D_i(x) \int \nabla \phi_k \cdot \nabla \phi_l \, dx + \delta t D_i(x) \vec{b}_i(x) \cdot \int \phi_k \nabla \phi_l \, dx \tag{B.6}$$

By use of the Hölder inequality we obtain the following estimate for the right hand side:

$$\leq (1 - \delta t K_i) |\phi_k|_{L^2} |\phi_l|_{L^2} + \delta t D_i |\nabla \phi_k|_{L^2} |\nabla \phi_l|_{L^2} + \delta t D_i |\vec{b}_i| |\phi_k|_{L^2} |\nabla \phi_l|_{L^2}. \quad (\text{B.7})$$

We now choose $\alpha := \max \left(1 - \delta t K_i(x), \delta t D_i(x), \delta t D_i(x) |\vec{b}_i(x)| \right)$, which we know to be positive since $\delta t D_i(x)$ is positive on the whole domain. Thus we continue with

$$\leq \alpha (|\phi_k|_{L^2} |\phi_l|_{L^2} + |\nabla \phi_k|_{L^2} |\nabla \phi_l|_{L^2} + |\phi_k|_{L^2} |\nabla \phi_l|_{L^2}), \quad (\text{B.8})$$

from which we obtain the estimate

$$\leq \alpha (c_k |\nabla \phi_k|_{L^2} c_l |\nabla \phi_l|_{L^2} + |\nabla \phi_k|_{L^2} |\nabla \phi_l|_{L^2} + c_k |\nabla \phi_k|_{L^2} |\nabla \phi_l|_{L^2}) \quad (\text{B.9})$$

by using the Poincaré inequality (see [Buc, Alt92]) on each of the summands as needed, where c_k and c_l depend on the domain Ω as required by the inequality.

In order to obtain the Sobolev norms required for (B.3), we square the inequality:

$$a(\phi_k, \phi_l)^2 < \alpha^2 (c_k c_l + 1 + c_k)^2 |\nabla \phi_k|_{L^2}^2 |\nabla \phi_l|_{L^2}^2 \quad (\text{B.10})$$

$$= \alpha^2 (c_k c_l + 1 + c_k)^2 |\nabla \phi_k|_{L^2}^2 |\nabla \phi_l|_{L^2}^2 \quad (\text{B.11})$$

Now the product of the squares of the L^2 is missing only positive terms to the respective Sobolev norm, so the inequality will not be harmed

$$\leq \alpha^2 (c_k c_l + 1 + c_k)^2 \left[\|\phi_k\|_{H^2}^2 \|\phi_l\|_{H^2}^2 \right] \quad (\text{B.12})$$

subsequently taking the square root results in the originally desired inequality. □

Lemma B.0.3 *Let $V = H_0^1(\Omega)$. Then the operator in (B.2) is elliptic.*

Proof Inserting a test function ϕ_l into the operator, we obtain

$$\int \phi_l \phi_l \, dx + \delta t \cdot \left[\int \left[D_i(x) \left(\nabla \phi_l + \phi_l \vec{b}_i(x) \right) \right] \cdot \nabla \phi_l \, dx - \int K_i(x) \phi_l \cdot \phi_l \, dx \right] \quad (\text{B.13})$$

$$= (1 - \delta t K_i(x)) \int \phi_l \phi_l \, dx + \delta t D_i(x) \int \nabla \phi_l \nabla \phi_l \, dx + \delta t D_i(x) \vec{b}_i(x) \int \phi_l \nabla \phi_l \, dx. \quad (\text{B.14})$$

We focus our attention on the mixed term in order to arrive at a Sobolev norm:

$$\int_{\Omega} \phi_l \nabla \phi_l \, dx = \int_{\partial \Omega} \phi_l \phi_l \vec{n} \, dx - \int_{\Omega} \nabla \phi_l \phi_l \, dx \quad (\text{B.15})$$

$$\Leftrightarrow 2 \int_{\Omega} \phi_l \nabla \phi_l \, dx = \int_{\partial \Omega} \phi_l \phi_l \vec{n} \, dx \quad (\text{B.16})$$

which, when inserted into the complete operator, yields:

$$(1 - \delta t K_i) \int_{\Omega} \phi_l \phi_l dx + \delta t D_i \int_{\Omega} \nabla \phi_l \nabla \phi_l dx + \delta t D_i \vec{b}_i \frac{1}{2} \int_{\partial \Omega} \phi_l \phi_l \vec{n} dx. \quad (\text{B.17})$$

In the case

$$\vec{b}_i(x) \vec{n} > 0 \quad \text{on } \partial \Omega$$

we can continue with our estimate straightforwardly from (B.17):

$$\geq (1 - \delta t K_i) \int_{\Omega} \phi_l \phi_l dx + \delta t D_i \int_{\Omega} \nabla \phi_l \nabla \phi_l dx \quad (\text{B.18})$$

$$\geq (1 - \delta t K_i) |\phi_l|_{L^2} + \delta t D_i |\nabla \phi_l|_{L^2} \quad (\text{B.19})$$

$$\geq \min(1 - \delta t K_i, \delta t D_i) (|\phi_l|_{L^2} + |\nabla \phi_l|_{L^2}) \quad (\text{B.20})$$

$$= \min(1 - \delta t K_i, \delta t D_i) \|\phi_l\|_{H^2}, \quad (\text{B.21})$$

with the additional constraint that

$$\delta t < \min_i \min_{x \in \Omega \text{ s.t. } K_i(x) < 0} \left| \frac{1}{K_i(x)} \right|. \quad (\text{B.22})$$

Note that here and in the following estimate all coefficient functions used in this model equation are bounded and the domain Ω is closed, therefore the minimum and maximum of the function are assumed, respectively. Incidentally, should the maximum be zero and the respective minimum be infinity, the proposed method has a unique solution independently of the time discretization δt .

If, on the other hand, $\vec{b}_i(x) \vec{n} < 0$ holds somewhere on $\partial \Omega$, we have to introduce a more elaborate requirement on the time discretization. To achieve ellipticity we require that

$$(1 - \delta t K_i(x)) \int_{\Omega} \phi_l \phi_l dx + \frac{\delta t}{2} D_i(x) \vec{b}_i(x) \int_{\partial \Omega} \phi_l \phi_l \vec{n} dx > c \int_{\Omega} \phi_l \phi_l dx \quad (\text{B.23})$$

In order to achieve this, we set

$$\delta t < \min_i \min_{x \in \Omega \text{ s.t. } K_i(x) < 0 \text{ or } \vec{b}_i(x) < 0} \left| \frac{1}{-K_i + D_i \vec{b}_i \frac{\int_{\partial \Omega} \phi_l \phi_l \vec{n} dx}{\int_{\Omega} \phi_l \phi_l dx}} \right| \quad (\text{B.24})$$

$$= \frac{1}{\max_i \max_{x \in \Omega \text{ s.t. } K_i(x) < 0 \text{ or } \vec{b}_i(x) < 0} \left| -K_i + D_i \vec{b}_i \frac{\int_{\partial \Omega} \phi_l \phi_l \vec{n} dx}{\int_{\Omega} \phi_l \phi_l dx} \right|}. \quad (\text{B.25})$$

We now use the above defined δt in our operator:

$$(1 - \delta t K_i) \int_{\Omega} \phi_l \phi_l dx + \frac{\delta t}{2} D_i \vec{b}_i \int_{\partial\Omega} \phi_l \phi_l \vec{n} dx \quad (\text{B.26})$$

$$> \int_{\Omega} \phi_l \phi_l dx + \left(\frac{1}{\max \left| -K_i + D_i \vec{b}_i \frac{\int_{\partial\Omega} \phi_l \phi_l \vec{n} dx}{\int_{\Omega} \phi_l \phi_l dx} \right|} \right) \left(-K_i \int_{\Omega} \phi_l \phi_l dx + D_i \vec{b}_i \frac{1}{2} \int_{\partial\Omega} \phi_l \phi_l \vec{n} dx \right) \quad (\text{B.27})$$

$$= \int_{\Omega} \phi_l \phi_l dx + \frac{-K_i \int_{\Omega} \phi_l \phi_l dx + D_i \vec{b}_i \frac{1}{2} \int_{\partial\Omega} \phi_l \phi_l \vec{n} dx}{\max \left| -K_i + D_i \vec{b}_i \frac{\int_{\partial\Omega} \phi_l \phi_l \vec{n} dx}{\int_{\Omega} \phi_l \phi_l dx} \right|} \quad (\text{B.28})$$

$$= \int_{\Omega} \phi_l \phi_l dx + \frac{-K_i + D_i \vec{b}_i \frac{\int_{\partial\Omega} \phi_l \phi_l \vec{n} dx}{\int_{\Omega} \phi_l \phi_l dx}}{\max \left| -K_i + D_i \vec{b}_i \frac{\int_{\partial\Omega} \phi_l \phi_l \vec{n} dx}{\int_{\Omega} \phi_l \phi_l dx} \right|} \int_{\Omega} \phi_l \phi_l dx \quad (\text{B.29})$$

$$\geq \tilde{c} |\phi_l|_{L^2}, \quad (\text{B.30})$$

where $\tilde{c} \geq 0$, and the maximum is applied under the conditions of (B.24). By the inequality in (B.27) we thus have proved (B.23).

We regroup (B.17) accordingly and then continue

$$(1 - \delta t K_i) \int_{\Omega} \phi_l \phi_l dx + \frac{\delta}{2} t D_i \vec{b}_i \int_{\partial\Omega} \phi_l \phi_l dx + \delta t D_i \int_{\Omega} \nabla \phi_l \nabla \phi_l dx \quad (\text{B.31})$$

$$\geq c |\phi_l|_{L^2} + \delta t D_i |\nabla \phi_l|_{L^2} \quad (\text{B.32})$$

$$\geq \min(c, \delta t D_i) (|\phi_l|_{L^2} + |\nabla \phi_l|_{L^2}) \quad (\text{B.33})$$

$$= \min(c, \delta t D_i) \|\phi_l\|_{H^2}, \quad (\text{B.34})$$

proving the claim. □

We would like to point out that this result is completely independent of the space discretization for test function in H_0^m as assumed in the beginning. The proof will extend to testfunctions which do not vanish on the boundary without additional effort, when we manage to move boundary integral to the right hand side. This can be seen in section 4.4.1. There we observe an indirect dependence on the space discretization on the boundary by the estimate in (B.25). However we call attention to the fact that the factor \vec{b} generally includes the electric field, which is coupled to the concentrations by the Poisson equation. Treating the NP and Poisson system separately leads to an explicit treatment of the electric field, which causes the whole system to become unstable. Besides non-physical flow and oscillation effects, after some time the magnitude of the electric field has been found to increase exponentially thus violating the

condition we have established on the operator. To remove this instability, the coupling Poisson equation needs to be implicitly included in the computations of the NP equations, leading to a combined operator which we discussed in section 4.5.

Bibliography

- [All07] ALLAIR, G. und RAPHAEL, A.-L.: Homogenization of a convection-diffusion model with reaction in a porous medium. *C.R.Acad.Sci. Paris* (2007), (344):S. 523–528 (Cited on pages 105 and 106)
- [Alt92] ALT, H.W.: *Lineare Funktionalanalysis - Eine Anwendungsorientierte Einführung*, Springer, 2 Aufl. (1992) (Cited on pages 61, 103, 104, and 108)
- [Bana] BANGERTH, W.; HARTMANN, R. und KANSCHAT, G.: deal.II — a general-purpose object-oriented finite element library. *ACM Trans. Math. Softw.*, Bd. 33(4) (Cited on page 73)
- [Banb] BANGERTH, W.; HARTMANN, R. und KANSCHAT, G.: deal.II *Differential Equations Analysis Library, Technical Reference*, URL <http://www.dealii.org>, <http://www.dealii.org> (Cited on pages 70, 71, 73, and 74)
- [Ber84] BERENDSEN, H.J.C.; POSTMA, J.P.M.; VAN GUNSTEREN, W.F.; DINOLA, A. und HAAK, J.R.: Molecular dynamics with coupling to an external bath. *J. Chem. Phys.* (1984), Bd. 81(8) (Cited on page 27)
- [Bra02] BRAESS, D.: *Finite Elemente*, Springer, 3 Aufl. (2002) (Cited on pages 60, 61, 62, 64, and 69)
- [Bro01] BRONSTEIN, I.N.; SEMENDJAJEW, K.A.; MUSIOL, G. und MÜLIG, H.: *Taschenbuch der Mathematik*, Verlag Harri Deutsch, 5. Aufl. (2001) (Cited on pages 49 and 61)
- [Buc] BUCKLEY, S. M.: Sobolov spaces: A short course (Cited on page 108)
- [Can03] CANCES, E.; CASTELLA, F.; CHARTIER, P.; FAOU, E.; LE BRIS, C.; LEGOLL, F. und G., Turinici: High-order averaging schemes with error bounds for thermodynamical properties calculations by MD calculations. *INRIA Research Report* (2003), (4875) (Cited on page 46)
- [Carhr] CARUS, Titus Lucretius: *De Rerum Natura* (55 v.Chr.) (Cited on page 40)
- [Cho09] CHOI, Yong Seok und KIM, Sung Jin: Electrokinetic flow-induced currents in silica nanofluidic channels. *Journal of Colloid and Interface Science* (2009), (333):S. 672–678 (Cited on page 34)

- [Cor95] CORNELL, W.D.; CIEPLAK, P.; BAYLY, C.I.; GOULD, I.R.; MERZ, K.M.; FERGUSON, D.M.; D.C.SPELLMEYER; FOX, T.; J.W.CALDWELL und KOLLMAN, P.A.: A Second Generation Force Field for the Simulation of Proteins, Nucleic Acids, and Organic Molecules. *J. Am. Chem. Soc.* (1995), Bd. 117:S. 5179–5197 (Cited on pages 75 and 81)
- [Cra95] CRACKNELL, Roger F.; NICHOLSON, David und QUIRKE, Nicholas: Direct Molecular Dynamics Simulation of Flow Down a Chemical Potential Gradient in a Slit-Shaped Micropore. *Phys. Rev. Lett.* (1995), Bd. 74(13):S. 2463–2466 (Cited on page 52)
- [Cut69] CUTHILL, E. und MCKEE, J.: Reducing the bandwidth of sparse symmetric matrices, in: *ACM '69: Proceedings of the 1969 24th national conference*, ACM, S. 157–172 (Cited on page 74)
- [Dem04] DEMTRÖDER, W.: *Experimentalphysik 2 - Elektrizität und Optik*, Springer, 3. Aufl. (2004) (Cited on pages 47, 49, and 50)
- [DGJ] DR. GEORG JOB, Hrsg.: *Tabelle chemischer Potenziale. Eduard-Job-Stiftung* (Cited on page 78)
- [Dre08] DREHER, M. und TANG, S.: Time history interfacial conditions in multiscale computations of lattice oscillations. *Comput. Mech.* (2008), Bd. 41:S. 683–698 (Cited on page 36)
- [Ein06] EINSTEIN, A.: Neue Bestimmung der Moleküldimension. *Annalen der Physik* (1906), Bd. 19:S. 289–306 (Cited on pages 40 and 48)
- [Far07] FARRELL, D. E.; PARK, H. S. und LIU, W. K.: Implementation aspects of the bridging scale method and application to intersonic crack propagation. *International Journal for Numerical Methods in Engineering* (2007), Bd. 71:S. 583–605 (Cited on page 36)
- [Fre02] FRENKEL, Daan und SMIT, Berend: *Understanding Molecular Simulation*, Academic Press, 2. Aufl. (2002) (Cited on pages 17, 25, 44, and 53)
- [Gil77] GILLESPIE, D. T.: Exact stochastic simulation of coupled chemical reactions. *The Journal of Physical Chemistry* (1977), Bd. 81(25):S. 2340–2361 (Cited on page 35)
- [Gri04] GRIEBEL, M.; KNAPEK, S.; ZUMBUSCH, G. und CAGLAR, A.: *Numerische Simulation in der Moleküldynamik*, Springer (2004) (Cited on pages 17, 25, 29, 31, and 75)
- [Gro94] GROSSMANN, C. und ROOS, H.-G.: *Numerik partieller Differentialgleichungen*, Teubner, 2 Aufl. (1994) (Cited on pages 62, 68, and 69)
- [Hab95] HABERLANDT, R.; FRITZSCHE, S.; PEINEL, G. und HEINZIGER, K.: *Molekulardynamik*, vieweg (1995) (Cited on pages 17, 31, and 53)

- [Hay99] HAYAMIZU, K.; AIHARA, Y.; ARAI, S. und MARTINEZ, C.G.: Pulse-Gradient Spin-Echo H , Li , and F NMR Diffusion and Ionic Conductivity Measurements of 14 Organic Electrolytes Containing $LiN(SO_2CF_3)_2$. *H. Phys. Chem. B* (1999), Bd. 103(3):S. 519–524 (Cited on page 78)
- [JC98] J.-C., Soetens; C., Millot und B., Maigret: Molecular Dynamics Simulation of $Li^+BF_4^-$ in Ethylene Carbonate, Propylene Carbonate, and Dimethyl Carbonate Solvents. *The Journal of Physical Chemistry* (1998), Bd. 102 (Cited on pages 75 and 78)
- [Kel83] KELLY, D. W.; GAGO, J. P.; ZIENKIEWICZ, O.C. und BABUSKA, I.: A posteriori error analysis and adaptive processes in the finite element method: Part I - Error analysis. *International Journal for Numerical Methods in Engineering* (1983), Bd. 19 (Cited on pages 70 and 74)
- [Kit80] KITTEL, C. und KROEMER, H.: *Thermal Physics*, Freeman, 2 Aufl. (1980) (Cited on page 52)
- [Krä04] KRÄUTLE, S. und KNABNER, P.: A new numerical reduction scheme for fully coupled multicomponent transport-reaction problems in porous media. *Preprint Series of the Inst. for Appl. Math., Erlangen* (2004), (306) (Cited on page 55)
- [Kra08] KRABBENHØFT, K. und KRABBENHØFT, J.: Application of the Poisson-Nernst-Planck equations to the migration test. *Cement and Concrete Research* (2008), (38):S. 77–88 (Cited on pages 34, 59, and 69)
- [Kub66] KUBO, R.: The fluctuation-dissipation theorem. *Reports on Progress in Physics* (1966), Bd. 29(1):S. 255–284 (Cited on page 48)
- [Lec08] LECCA, Paola; DEMATTÉ, Lorenzo und PRIAMI, Corrado: Modeling and simulating reaction-diffusion systems with state dependent diffusion coefficients. *Proceedings of World Academy of Science, Engineering and Technology* (2008), Bd. 34 (Cited on pages 51 and 54)
- [Liu] LIU, W. K.; ZHANG, L. T.; KARPOV, E. G.; KADOWAKI, H. und PARK, H.: Bridging Scale Particle and Finite Element Methods (Cited on page 36)
- [Liu06] LIU, Zhiping; WU, Wixaoping und WANG, Wenchuan: A novel united-atom force field for imidazolium-based ionic liquids. *Phys. Chem. Chem. Phys.* (2006), Bd. 117(8):S. 1096–1104 (Cited on page 75)
- [Lu07] LU, B.; ZHOU, Y.C.; HUBER, G.A.; BOND, S.D.; HOLST, M.J. und MCCOMMON, J.A.: Electrodifusion: a continuum modelling framework for biomolecular systems with realistic spatiotemporal resolution. *The Journal of Chemical Physics* (2007), Bd. 127 (Cited on pages 60, 67, and 69)
- [Mat07] MATTHIES, G. und TOBISKA, L.: Mass conservation of finite element methods for coupled flow-transport problems. *Intern. J. Comput. Sci. Math* (2007), Bd. 1(2-4):S. 293–307 (Cited on page 90)

- [Nos07] NOSKOV, A.V.; LILIN, S.A. und PARFENYUK, V.I.: Simulation of ion mass transfer processes with allowance for the concentration dependence of diffusion coefficients. *Russian Chemical Bulletin, International Edition* (2007), Bd. 55(4):S. 661–665 (Cited on page 34)
- [NR07] NEUSS-RADU, Maria und JÄGER, Willi: Effektive transmission conditions for reaction-diffusion processes in domains separated by an interface. *SIAM J. MATH. ANAL.* (2007), Bd. 39(3):S. 687–720 (Cited on page 106)
- [NR09] NEUSS-RADU, M. und ET AL.: Multiscale analysis and simulation of a reaction-diffusion problem with transmission conditions. *Nonlinear Analysis: Real World Applications* (2009) (Cited on page 106)
- [Pan05] PANHUIS, Peter IN 'T: Li-ion Battery Modelling. *Master's Thesis TECHNISCHE UNIVERSITEIT EINDHOVEN* (2005) (Cited on pages 34 and 59)
- [Pra05] PRAPROTNIK, Matej; DELLE SITE, Luigi und KREMER, Kurt: *J. Chem. Phys.* (2005), Bd. 123 (Cited on page 36)
- [Pra06] PRAPROTNIK, Matej; DELLE SITE, Luigi und KREMER, Kurt: Adaptive resolution scheme for efficient hybrid atomistic-mesoscale molecular dynamics simulations of dense liquids. *Phys. Rev. E* (2006), Bd. 73(6):S. 066701 (Cited on page 36)
- [Roo96] ROOS, H.-G.; STYNES, M. und TOBISKA, L.: *Numerical Methods for Singularly Perturbed Differential Equations — Convection-Diffusion and Flow Problems*, Bd. 24 von *Springer Series in Computational Mathematics*, Springer-Verlag, Berlin (1996) (Cited on page 74)
- [Sac88] SACHS, L.: *Statistische Methoden: Planung und Auswertung*, Springer-verlag, 6. Aufl. (1988) (Cited on page 46)
- [Sal98] SALMON, R.: *Lectures on Geophysical Fluid Dynamics*, Oxford University Press (1998) (Cited on page 37)
- [Sam99] SAMSON, E. und MARCHAND, J.: Numerical Solution of the Extended Nernst-Planck Model. *Journal of Colloid and Interface Science* (1999), Bd. 215:S. 1–8 (Cited on pages 54, 59, and 69)
- [Sch] SCHWABEL, F.: *Quantenmechanik*, Springer (Cited on pages 17 and 19)
- [Sch01] SCHUSS, Z.; NADLER, B. und EISENBERG, R.S.: Derivation of Poisson and Nernst-Planck equations in a bath and channel from a molecular model. *Physical Review* (2001), Bd. 64 (Cited on pages 35 and 59)
- [Tan06] TANG, S.; HOU, T. Y. und LIU, W. K.: A mathematical framework of the bridging scale method. *International Journal for Numerical Methods in Engineering* (2006), Bd. 65:S. 1688–1713 (Cited on page 36)

- [T.G04] T.GOUDON und POUPAUD, F.: Homogenization of transport equations; weak mean field approximation. *SIAM Journal of Mathematical Analysis* (2004) (Cited on page 106)
- [Tuc99] TUCKERMAN, M. E. und ET AL: *Europhys. Lett.* (1999), Bd. 45(149) (Cited on page 31)
- [Woo57] WOOD, W. W. und PARKER, F. R.: Monte Carlo Equation of State of Molecules Interacting with the Lennard-Jones Potential. I. A Supercritical Isotherm at about Twice the Critical Temperature. *Journal of Chemical Physics* (1957), Bd. 27:S. 720–733 (Cited on page 24)
- [Yam60] YAMAMOTO, T.: Quantum Statistical Mechanical Theory of the Rate of Exchange Chemical Reactions in the Gas Phase. *The Journal of Chemical Physics* (1960), Bd. 33(1) (Cited on page 55)

List of Figures

2.1	Periodic cells.	23
3.1	Exemplification of a diffusion process.	41
5.1	Schematic structure of ethylene carbonate	75
5.2	Ethylene Carbonate	75
5.3	Comparison traditional and improved MSD measurement	77
5.4	Comparison traditional and improved MSD measurement with convection	77
5.5	Simulation cell	79
5.6	Diffusion coefficient of EC	79
5.7	Diffusion coefficient of Li	80
5.8	Diffusion coefficient of B	80
5.9	Diffusion coefficient of EC from NVT ensemble	81
5.10	Cellulose structure in beta-1,4 configuration	82
5.11	Cellulose in beta-1,4 configuration	83
5.12	Diffusion coefficients with cellulose	83
5.13	Specis A, initial setup	84
5.14	Specis A, after 1200 steps	84
5.15	Specis B, initial setup	86
5.16	Specis B, after 1200 steps	86
5.17	Electric potential, initial setup	87
5.18	Electric potential, after 1200 steps	87
5.19	Concentration profile of Li^+ and BF_4^- in 2D battery	89
5.20	Electrical potential of 2D battery.	90
5.21	Concentration profile of 3D battery.	92
5.22	Concentration profiles of Li^+ and BF_4^- with dendrite regions	92
5.23	Concentration profile of Li^+ with dendrite regions.	92
5.24	Reaction, species 0, timestep 1	94
5.25	Reaction, species 1, timestep 1	94
5.26	Reaction, species 2, timestep 1	94
5.27	Reaction, species 0, timestep 20	94
5.28	Reaction, species 1, timestep 20.	94
5.29	Reaction, species 2, timestep 20	94

5.30	Reaction, species 0, timestep 40	95
5.31	Reaction, species 1, timestep 40	95
5.32	Reaction, species 2, timestep 40.	95
5.33	Reaction, species 0, timestep 60	95
5.34	Reaction, species 1, timestep 60	95
5.35	Reaction, species 2, timestep 60	95

List of Tables

5.1	Van der Waals parameters and partial charges for EC.	76
5.2	Diffusion results with EC	78
5.3	Chemical potential results with EC	81
5.4	Van der Waals parameters and partial charges for cellulose.	82
5.5	MD results with cellulose	83
5.6	Convergence rate of NPNP computations, refinement in time.	91
5.7	Convergence rate of NPNP computations, refinement in time and space.	91